

UC Riverside

UC Riverside Electronic Theses and Dissertations

Title

WUSCHEL Mediated Bifunctional Transcriptional Regulation of CLAVATA3 Levels and Spatial Pattern in Arabidopsis thaliana

Permalink

<https://escholarship.org/uc/item/61h2x729>

Author

Rodriguez, Kevin Wilfredo

Publication Date

2017

Copyright Information

This work is made available under the terms of a Creative Commons Attribution License, available at <https://creativecommons.org/licenses/by/4.0/>

Peer reviewed|Thesis/dissertation

UNIVERSITY OF CALIFORNIA
RIVERSIDE

WUSCHEL Mediated Bifunctional Transcriptional Regulation of *CLAVATA3* Levels and
Spatial Pattern in *Arabidopsis thaliana*

A Dissertation submitted in partial satisfaction
of the requirements for the degree of

Doctor of Philosophy

in

Cell, Molecular and Developmental Biology

by

Kevin Wilfredo Rodriguez

September 2017

Dissertation Committee:
Dr. Venugopala Reddy Gonehal, Chairperson
Dr. Patricia Springer
Dr. Li Fan

Copyright by
Kevin Wilfredo Rodriguez
2017

The Dissertation of Kevin Wilfredo Rodriguez is approved:

Committee Chairperson

University of California, Riverside

Acknowledgements

I would like to express my gratitude to my supporters in achieving this degree. I would like to thank Dr. Venu Gonehal for providing me with such amazing projects and a diverse education in multiple levels of plant biology. The training through a broad approach of molecular, genetics, developmental and biochemistry allowed us to tackle research from every angle. I would also like to thank Dr. Mariano Perales for all the training and guidance to help mold me as the researcher that I am. I would also like to thank my research committee for all their advice. In summation, everyone's advice, mentorship, patience, friendship and immense discussions were invaluable.

I would like to also thank all my past and current lab members Andy Snipes, Aaron Devries, Alex Plong and Albert Do for their support in experimental techniques and useful discussions. I would also like to thank all the undergraduate researchers Jackie Le, John Voung, Denny Chang, Andy Chen, Frank Somoano, Vanessa Ceja, Dariush Neja, Valery Franco, So Hang, Maria Isabel Gutierrez Topez, Kyle Hill and Paul Rubiro for all their support.

Parts of this dissertation were published in *PNAS* with co-author Dr. Mariano Perales. The text of chapter 2 in this dissertation, in whole, is a reprint of the material as it appears in: Perales M, **Rodriguez K**, Snipes S, Yadav R, Diaz-Mendoza M, and Reddy GV. (2016) Threshold-dependent transcriptional discrimination underlies stem cell homeostasis. *Proc Natl Acad Sci USA* 113:E6298-E6306. The co-author Reddy GV. listed in that publication directed and supervised the research which forms the basis for this dissertation.

The text of chapter 4 in this dissertation, in whole, is a reprint of the material as it appears in: **Rodriguez K**, Perales M, Snipes S, Yadav R, Diaz-Mendoza M, and Reddy GV. (2016) DNA-dependent homodimerization, sub-cellular partitioning, and destabilization control WUSCHEL levels and spatial patterning. Proc Natl Acad Sci USA 113:E6307-E6315. The co-author Reddy GV. listed in that publication directed and supervised the research which forms the basis for this dissertation.

Dedication

I would like to dedicate this thesis to my whole family [too many to list] to thank them for all their support, inspiration and love through all the years. (Los quiero mucho). I can't express the gratitude for the hard work, courage and inspiration from both my father and mother. I would like to thank both of my sisters, Jennifer and Keiry, for supporting me in every way imaginable. I would also like to thank my nephew, Aaron S. "es" Lindo, for being awesome and allowing me to act like a little kid, when I needed a break from being an adult.

I would like to thank all my brothers, including but not limited to: Marvo, Lunch-Box, Kevin, Lucho, Dairy and Medina. Thank you all for always supporting me and pushing me to be the best. I could not have made it this far without you guys.

Finally, I would like to thank my best friend and partner in crime. Claire, you are the Bonney to my Clyde. Thanks for all the words of encouragement and support even through my vices. Also, thank you for forcing me to smile, to enjoy the little things in life and for calling me on my faults. Love you, most of the time!

ABSTRACT OF THE DISSERTATION

WUSCHEL Mediated Bifunctional Transcriptional Regulation of *CLAVATA3* Levels and Spatial Pattern in *Arabidopsis thaliana*

by

Kevin Wilfredo Rodriguez

Doctor of Philosophy, Graduate Program in
Cell, Molecular and Developmental Biology
University of California, Riverside, September 2017
Dr. Venugopala Reddy Gonehal

The balance between self-renewing stem cell divisions and differentiation of stem cell progeny in Shoot Apical Meristems (SAMs) is crucial for the development of all the above-ground organs. This is regulated by self-sustaining feedback loop between WUSCHEL(WUS) and CLAVATA (CLV) genes. WUS, a homeodomain transcription factor expressed in the rib-meristem (RM), migrates into overlying stem cell domain, also referred to as the central zone (CZ). In the CZ, WUS represses a set of differentiation promoting transcription factors to prevent premature differentiation of stem cell progeny and also activates its own negative regulator *CLV3*. *CLV3*, a secreted peptide, negatively regulates *WUS* expression through *CLV1* and related transmembrane receptors. This process is critical for the homeostasis of the stem cell population. The transcriptional mechanisms underlying the *CLV3* activation and repression of differentiation factors in stem cells are not known. It is also not known how *WUS* protein levels are regulated. The structure-function analysis of the *WUS* protein has led to the identification of the last 63 amino acid region that is both sufficient and necessary to maintain higher *WUS* in the RM and lower *WUS* in the CZ. This region contains information for subcellular partitioning, stability and transcriptional activity of *WUS*.

Analysis of the *CLV3* promoter uncovered 5 closely spaced cis-elements that bind WUS, referred to as the cis-regulatory module (CRM). The in vivo cis element deletion analysis shows that the collective activity of all 5 cis elements is required for activation of *CLV3* in the CZ and repression in the RM. Biochemical analysis of the WUS-binding behavior to *CLV3* elements uncovered a concentration dependent switch from monomeric to dimeric/higher molecular weight complex. Taken together, it led to a model where WUS activates and represses *CLV3* at lower and higher WUS, respectively. The manipulation of WUS levels and the affinity of cis elements largely agreed with the concentration dependent switch in *CLV3* regulation. While determining the contribution of the number of cis elements and affinity of cis elements to *CLV3* regulation, we found that the expression data from mutant *CLV3* promoters could only be explained by a model based on cooperativity between elements. These new findings show that the cis-element grammar (number, affinity and possibly spacing) may be crucial in interpreting local differences in WUS levels in regulating *CLV3* levels and spatial pattern.

Table of Contents

Title page	
Copyright Page.....	
Signature Approval Page.....	
Acknowledgements	iv
Dedication	vi
Abstract.....	vii
Table of Contents	ix
CHAPTER 1: Introduction.....	1
1.1 Introduction to plant development.....	2
1.2 Organization of the shoot meristem	2
1.3 Molecular mechanism of regulation in the SAM	3
1.5 Objectives (aims of the study).....	10
CHAPTER 2: Threshold-dependent transcriptional discrimination underlies stem cell homeostasis.	17
2.1 Abstract.....	18
2.2 Introduction.....	18
2.3 Results	21
2.4 Discussion.....	31
CHAPTER 3: Reciprocal interaction among cis elements within a WUSCHEL-binding homotypic cis-regulatory module regulate CLAVATA3 levels and spatial pattern.	57
3.1 Abstract.....	58
3.2 Introduction.....	59
3.3 Results	64

3.4 Discussion	70
CHAPTER 4: DNA-dependent homodimerization, sub-cellular partitioning, and protein destabilization control WUSCHEL levels and spatial patterning.....	87
4.1 Abstract	88
4.2 Introduction.....	89
4.3 Results	93
4.4 Discussion	103
CHAPTER 5: Concluding discussion and future research.....	123
Materials and methods	134
References	148

List of figures

Fig. 1.1. Stages in the development of <i>Arabidopsis thaliana</i>	11
Fig. 1.2. The shoot apical meristem.....	12
Fig. 1.3. The regulators of the shoot apical meristem maintenance.	13
Fig. 2.1. A CRM regulates <i>CLV3</i> expression.....	35
Fig. 2.2. Characterization of the WUS-binding <i>cis</i> elements in <i>CLV3</i>	37
Fig. 2.3. Complementation analysis with <i>pCLV3</i> mutant promoters.	39
Fig. 2.4. The same <i>cis</i> elements mediate activation and repression of <i>CLV3</i> expression.	40
Fig. 2.5. Estimation of the binding affinities of WUS to the five <i>cis</i> elements in the CRM and to the higher-affinity (970-M4) mutant <i>cis</i> element.	42
Fig. 2.6. The effect of <i>cis</i> -element deletions on <i>CLV3</i> expression.....	44
Fig. 2.7. DNA promotes homodimerization of WUS.	46
Fig. 2.8. The DNA promotes homodimerization of WUS.	48
Fig. 2.9. Nucleotides within and outside the TAAT core modulate WUS binding.....	50
Fig. 2.10. Increasing the <i>cis</i> -element affinity lowers the dimerization threshold, leading to <i>CLV3</i> repression.....	51
Fig. 2.11. The <i>CLV3</i> promoter is sensitive to WUS dosage.	53
Fig. 2.12. <i>pCLV3</i> is sensitive to WUS dosage.....	55
Fig. 2.13. The mutant <i>CLV3</i> promoters are repressed in the inner layers and are activated in the outer layers of <i>clv3-2</i> mutants.	56
Fig. 3.1. The CRM context determines the <i>cis</i> -elements ability to interpret the WUS dependent transcriptional discrimination.....	77
Fig. 3.2. Model of interaction among elements in <i>CLV3</i> CRM.....	79
Fig. 3.3. Affinity and integrated signaling from all elements determine expression level and domain.	80

Fig. 3.4. Complementation analysis of <i>clv3-2</i> with mutant constructs.....	81
Fig. 3.5. Complementation of <i>clv3-2</i> with mutant <i>pCLV3</i> construct.	82
Fig. 3.6. Expression of reporters upon ubiquitous overexpression of <i>WUS</i> protein.	83
Fig. 3.7. Expression of reporters from 10071 mutant promoter in <i>clv3-2</i> background.....	85
Fig. 3.8. <i>WUS</i> and <i>CLV3</i> regulatory loops.	86
Fig. 4.1. The C terminus of <i>WUS</i> is sufficient for the spatial patterning of <i>WUS</i> protein.	107
Fig. 4.2. The stability of <i>WUS</i> is determined by a 63-aa region in the C terminus.	109
Fig. 4.3. The EAR-like domain influences nuclear accumulation of <i>WUS</i>	111
Fig. 4.4. The transcriptional regulatory domains influence the subcellular localization of <i>WUS</i>	113
Fig. 4.5. The DNA binding and dimerization of <i>WUS</i> restrict its spatial localization.....	115
Fig. 4.6. <i>WUS</i> contains two homodimerization domains.	117
Fig. 4.7. The two homodimerization domains are required for <i>WUS</i> function.	119
Fig. 4.8. Ectopic overexpression of <i>WUS</i> destabilizes <i>WUS</i> protein.	120
Fig. 4.9. Characterization of a Dex-inducible eGFP- <i>WUS</i> system.....	121
Fig. 4.10. A sketch illustrating the control of <i>WUSCHEL</i> levels and spatial patterning in IMs.	122
Fig. 5.1. Functions of domains within the <i>WUS</i> protein.....	133

List of Abbreviations

AA	Amino acid
AD	Acidic region
Amp	Ampicillin
BiFC	Bimolecular Fluorescence Complementation
bp	Base pair
CLV	CLAVATA
CRM	Cis-Regulatory Module
CZ	Central Zone
Da	Dalton
DAI	Days after induction
DBD	DNA-Binding Domain
Dex	Dexamethasone
DNA	Deoxyribonucleic acid
dNTP	Deoxyribonucleoside 5'-triphosphate
<i>E. coli</i>	<i>Escherichia coli</i>
eGFP	enhanced Green Fluorescent Protein
EMSA	Electromobility Shift Assay
EAR-like	Ethylene-responsive element binding factor-associated amphiphilic repression
GAL4-AD	GAL4 activation domain
GAL4-BD	GAL4 binding domain
Gent	Gentamycin
GR	<i>Rattus</i> Glucocorticoid Receptor
AtHAM	<i>Arabidopsis thaliana</i> HAIRY MERISTEM orthologs
HOD	Homodimerization Domain
Hyg	Hygromycin
Kan	Kanamycin
Kb	Kilobase pair
kDa	Kilodalton
Lb	Luria-Bertani media
Ler	Landsberg <i>erecta</i>
M	molar
mg	milligram
ml	millilitre
mm	millimeter
mM	millimolar
MS	Murashige and Skoog media
M.W.	Molecular weight
mYFP	modified Yellow Fluorescent Protein
ng	nanogram
nm	nanometer
nM	nanomolar
OZ	Organizing Center
PAGE	Polyacrylamide gel electrophoresis
PCR	Polymerase Chain Reaction

PZ	Peripheral Zone
Rif	Rifampicin
RM	Rib Meristem
RNA	Ribonucleic acid
RT	room temperature
SAM	Shoot Apical Meristem
SDS	Sodium dodecyl sulfate
Spec	Spectinomycin
STM	SHOOT MERISTEMLESS
Taq	<i>Thermus aquaticus</i>
Tet	Tetracycline
v/v	volume per volume
w/v	weight per volume
WUS	WUSCHEL
WUS-box	Conserved domain in WUS-related family members
WT	Wild-type
Y2H	yeast two-hybrid
µg	microgram
µl	microliter
µm	micrometer
µM	micromolar

CHAPTER 1:

Introduction

Introduction to plant development.

Organogenesis in plant development is a continuous process that occurs throughout the life of the plant. Unlike animals where most of the body patterning occurs at embryogenesis, plant embryo development contributes to the specification of the shoot and the root apical meristems (SAMs and RAMs), which harbor pluripotent stem cells that form the basis for the development of the shoots and the roots (Kaufmann et al., 2010) (Fig. 1.1). During germination, the SAM activity resumes to produce leaves, flowers, branches and the stem while also maintaining a constant set of stem cells (Fig. 1.1). During the vegetative phase of development rosette leaves are produced in a specific spatio-temporal pattern. During the subsequent reproductive phase, the SAM switches to producing floral meristems. Floral meristems are determinate structures that produce four sepals, four petals, six stamens and two carpels before terminating. The organs are produced sequentially as the floral meristem is sub-divided into four different concentric whorls (Fig. 1.1). RAMs sustain growth of the root, contributing to the uptake of water and nutrients, nutrient storage and respiration.

Organization of the shoot apical meristem.

The *Arabidopsis* SAM is composed of 3 clonally distinct cell layers and functional zones (Fig 1.2). The outermost cell layer (L1, contributing to the epidermis) forms a monolayer that is restricted to a single cell layer as cells divide in anticlinal planes, only undergoing cell divisions perpendicular to the cell surface. The cells contributing to the sub-epidermal layer (L2) also divide anticlinally and form a monolayer. The cells beneath the L2 layer divide in both anticlinal and periclinal orientations, undergoing cell division perpendicular and parallel to cell surface, to form multiple layers. The L1 and L2 together

compose the tunica while the apical L3 and basal L3 compose the corpus. Overlapping with the layered organization of cells, there exists different functional zones in the SAM (Fig. 1.2 B). The central zone (CZ) is at the tip of the SAM and it harbors stem cells. The Organizing center (OC), located within the Rib-meristem (RM) and beneath the CZ , provides cues for stem cell specification in the CZ. The stem cells located in all three layers in the CZ divide relatively slowly when compared to their daughters which are pushed into the adjacent peripheral zone (PZ). The CZ harbors a small population of stem cells across L1-L3. The slowly dividing stem cells are maintained throughout the life of the plant, producing additional stem cells that remain in the CZ and daughter cells that are displaced laterally into the Peripheral Zone (PZ). In the PZ, a sub-set of cells differentiate in a specific spatio-temporal pattern, as organ primordia. The staggered initiation of organ primordia, which are arranged in a spiral phyllotactic pattern at approximately 137° from the previous organ (Fig. 1.2C) occurs as a result of auxin accumulation (Vernoux et al., 2010; Reinhardt et al., 2000).

Molecular mechanism of regulation in the SAM.

Multiple factors regulate a combination of gene expression and growth patterns to mediate maintenance of the SAM. SAM maintenance results from a critical balancing act of the appropriate number of stem cells through self-renewing divisions and differentiation of daughter cells. The stem cell population within the SAM is maintained fairly consistently throughout the life of the plant. This requires the appropriate rate of cell division, as increased cell division rates would lead to overproliferation of the SAM while reduced cell division rates would lead to collapse of the stem cell population. Organ formation in the SAM occurs as a result of recruitment of cells in specific locations in the PZ. Selecting

cells in multiple regions or different number of cells would result in aberrant organ formation, thus affecting SAM homeostasis. A number of signaling molecules and transcription factors have been implicated in SAM homeostasis (Meyerowitz 1997; Lenhard and Laux, 1999; Barton, 2010). This introduction will focus on main regulators involved in regulating the homeostatic balance between stem cells and differentiating stem cell daughters.

Analysis of loss-of-function mutants for a number of factors that function in the meristem have revealed their roles at various levels of meristem initiation and maintenance. Meristem promoting factors are expressed in a spatially restricted pattern in such a fashion such that they are coexpressed within the SAM and function for SAM endurance. While meristem negative factors are spatially-temporally restricted, leading to the formation of organ primordia and fleeting of the SAM. Spatial restriction of factors has allowed us to understand how some factors have been shown to have similar roles while others have opposing and yet all can function to achieve meristem proliferation. The question is how all these factors are properly balanced to maintain a fairly consistent SAM size.

During early embryonic development, at the two-cell stage, the plant hormone auxin is produced in the basal cell and is transported to the apical cell by the action of PINFORMED (PIN). This directed auxin transport specifies the apical cell. (Friml et al., 2003; Muller and Sheen, 2008; Moller and Weijers, 2009; Bejamins and Scheres, 2008). The apical cell, predecessor of the pro-embryo, is enriched with auxin in comparison to the basal cell, predecessor of the suspensor (Mansfield and Briarty, 1991; Laux and

Jurgens, 1997). At the 16 cell stage, auxin accumulates throughout the pro-embryo and the central 4 cells begin to express WUSCHEL (discussed in next section). Auxin enrichment and antagonist interaction with another plant hormone-cytokinin (discussed in next section), in later stages of embryo development specifies the hypophysis and organization of the root stem cell niche. At the heart stage, auxin becomes enriched at the tip of the cotyledons while depleted in the region between the two cotyledons which will be specified as the SAM.

The initiation of the SAM depends on transcription factors and the interaction between auxin and cytokinin (Endrizzi et al., 1996; Long et al., 1996; Kerstetter et al., 1997; Jasinski et al., 2005; Yanai et al., 2005). Initiation of the SAM occurs in later stages of embryo development in a place located between the two developing cotyledons (Fig. 1.1). The transcription factors-WUSCHEL(WUS), SHOOTMERISTEMLESS (STM) , CUP-SHAPED COTYLEDON (CUC) and AINTEGUMENTA(ANT) have been implicated in this process. WUS, a homeodomain transcription factor is first detected at the 16-cell stage (Mayer et al., 1998). As embryonic development continues, ANT, an APETALA2 DNA-binding motif transcription factor involved in cell proliferation, is expressed in developing cotyledons (Mizukami and Fischer, 2000). STM, a homeodomain transcription factor, is expressed initially in a small stripe of cells located between the two cotyledons and finally assumes a circular shape encompassing cells of the SAM (Aida et al., 1999). CUC1/2, NAC DNA binding domain transcription factors, initially expressed in the SAM, later become restricted to a narrow stripe of cells located between the two cotyledons but excluded from the STM domain (Aida et al., 1997; Aida et al., 1999). CUC1/2 are implicated in the specification of organ boundaries and SAM establishment. The

localization of WUS and STM and their function establish the meristem identity, as mutations in either result in plants that lack shoot meristems.

In addition to the transcription factors discussed above, the plant hormone pathways have been implicated in SAM maintenance (Fig 1.3A). 1) Cytokinin is a plant hormone involved in cell division and higher cytokinin levels have been shown to enlarge SAMs (Werner et al., 2003; Higuchi et al., 2004; Werner and Schmulling, 2009). 2) Auxin is a plant hormone whose enrichment in the PZ of the SAM leads to organ initiation (Benkova et al., 2003; Reinhardt et al., 2003). Cytokinin is critical to regulating the SAM as depletion reduces the size and activity of the SAM (Werner et al., 2003; Higuchi et al., 2004; Werner and Schmulling, 2009). Cytokinin signaling, mediated by a family of three plasma-membrane bound receptors, activates both of the Type A- Arabidopsis Response Regulators (ARRs) and the Type-B ARRs. Type-B ARRs, contain a DNA binding domain and upon phosphorylation activate the expression of Type A-ARRs, which do not contain a DNA binding domain. The activity of Type-A ARRs block the function of B-ARRs through an unknown mechanism. Thus, the activation of Type-A ARRs forms a self-regulating feedback to restrict the activity of Type-B ARRs, which activate cytokinin regulated genes. A fluorescent marker that reports the responsiveness of cells to cytokinin, Two Component output Sensor (TCS), containing B-TYPE ARR binding sites and minimal promoter driving GFP (*pTCS::mGFP5-ER*) allows visualization of cytokinin sensitivity of cells *in planta*. In *Arabidopsis* SAMs, the *pTCS::mGFP5-ER* expression overlaps with the *WUS* expression domain (Muller and Sheen, 2008; Gordon et al., 2009). Higher levels of exogenous application of cytokinin has been shown to activate *WUS* transcription (Gordon et al., 2009).

There is also evidence that cytokinin functions in positive feedback loops with both WUS and STM, reinforcing cytokinin as a positive stem cell signal. Cytokinin promotes expression of the Class I Knotted-like homeobox (*KNOXI*) genes, including STM. STM in turn activates cytokinin biosynthesis through activation of *ADENOSINE PHOSPHATE-ISOPENTENYL TRANSFERASE (IPT7)*, which encodes a key biosynthetic enzyme (Rupp et al., 1999; Jasinski et al., 2005; Yanai et al., 2005). On the other hand, although, auxin is produced in the SAM by the rate limiting enzymes, YUCCA1/4 (Zhao, 2008; Cheng et al 2007), cells in the central parts of the SAM fail to respond to auxin. Instead the auxin concentrates, through directed transport mediated by PIN1, in organ primordia in the PZ (Reinhardt et al., 2003). Auxin signaling functions through degradation of negative regulators-[AUXIN/INDOLE-3_ACETIC ACID (Aux/IAA)] leading to the activation of transcription factors-[AUXIN RESPONSE FACTORS (ARFs) proteins] that determine auxin transcriptional regulation (Liscum and Reed, 2002; Quint and Gray, 2006). Auxin functions to represses Type A- ARR (*ARR7/ARR15*) and possibly *STM* expression to counter cytokinin signaling (Zhao et al., 2010; Furutani et al., 2004; Yanai et al., 2005). Thus, the localized accumulation of cytokinin signaling functions to maintain the stem cell population while localized concentration of auxin at primordia initiation sites leads to organ initiation. In a very simplistic view, the mutual antagonism between auxin and cytokinin contributes to some extent to SAM maintenance.

In addition to the feedback between transcription factors and plant hormones, SHOOTMERISTEMLESS (*STM*), a homeobox containing transcription factor, is involved in proliferation and inhibits cellular differentiation (Endrizzi et al., 1996; Long et al., 1996; Scofield et al., 2013). *STM* is expressed throughout the SAM, excluding the leaf primordia

(Fig. 1.3A) (Endrizzi et al., 1996; Long et al., 1996; Kerstetter et al., 1997; Jasinski et al., 2005; Yanai et al., 2005). *stm* mutants fail to maintain a meristem as a combined effect of decreased cell proliferation and premature differentiation of stem cells causing depletion of stem cell population (Endrizzi et al., 1996; Scofield et al., 2014). Treatment of *stm* loss-of-function mutant with cytokinin or expression of IPT, a cytokinin biosynthetic gene from *STM* promoter, suppresses the *stm* mutant phenotype (Jasinski et al., 2005). On the other hand, overexpression of *STM*, leads to ectopic meristem formation and it also leads to an increase in expression of Cytokinin biosynthesis genes (Sinha et al., 1993; Yanai et al., 2005; Jasinski et al., 2005). It has also been shown that cytokinin biosynthesis enzyme (rice gene *LONELY GUY*) is required for the accumulation of *KNOX* transcripts (Kurakawa et al., 2007). It would seem that the *KNOX* and cytokinin could function in a positive feedback loop which is established after the initiation of the *STM* promoter at the heart stage. (Rupp et al., 1999, Muller and Sheen, 2008). Taken together, the higher cytokinin environment generated by *KNOX* activity may promote cell proliferation. In parallel, *STM* has been shown to repress *ASYMMETRIC LEAVES1 (AS1)*. *AS1* is a MYB domain TF (Byrne et al., 2002; Byrne et al., 2000) which has been implicated in aspects of leaf differentiation. Thus *KNOX* family members may also play a role in repression of differentiation factors.

It has been shown that *WUS* negatively regulates the A-type-ARRs (Leibfried et al., 2005). Since the A-type ARR inhibits the function of the B-type ARR, *WUS*-mediated direct repression is expected to create a higher cytokinin environment (Reviewed in Muller and Sheen, 2007). The requirement of inhibition of A-type-ARRs in SAMs is further supported by mutations in the *ABPHYL* gene, which encodes a A-type ARR in maize,

which cause an enlarged SAM similar to what is observed upon exogenous application of cytokinin (Giulini et al., 2004). An additional factor that implicates cytokinin in regulating SAM maintenance is ALTERED MERISTEM PROGRAM1 (AMP1), a predicted carboxypeptidase with a yet unknown substrate. Mutations in *AMP1* lead to an increase in cytokinin levels and SAM size (Helliwell et al., 2001). These results together show intimate relationship between transcriptional regulators, hormones and differentiation factors which act in concert to regulate SAM homeostasis.

One of the central most pathway in stem cell maintenance and focus of this dissertation is the WUS and CLAVATA3 feedback system. WUS, a homeodomain transcription factor that is expressed in the L3, migrates to the outer layers to specify stem cells in the CZ [Fig. 1.3B] (Mayer et al., 1998, Schoof at al., 2000; Yadav et al., 2011). The *wus* loss-of-function mutants cause early termination of the SAM and cause only a partial production of floral organs, which at most can produce a single stamen but no carpel (Laux et al., 1996; Mayer et al., 1998). WUS not only specifies stem cell fate in the CZ but also activates its own negative regulator-*CLV3*. *CLV3* is a small secreted peptide that signals through several transmembrane receptors of the *CLV1* family, to negatively regulate *WUS* expression (Fletcher et al., 1999; Brand et al., 2000; Clark et al., 1997; Ogawa et al., 2008). Silencing of *CLV3* leads to expansion of *WUS* expression and overproliferation of the SAM (Mayer et al., 1998; Reddy and Meyerowitz, 2005). On the other hand, Increasing *CLV3* leads to the decrease in the *WUS* levels and a reduction of the SAM (Brand et al., Science 2000; Mullet et al., Plant Cell 2006; Yadav et al., 2010). Thus WUS-mediated activation of *CLV3* in the CZ is critical for stem cell maintenance. In addition, WUS also promotes stem cell maintenance by repressing differentiation promoting factors

presumably through a direct transcriptional regulation (Yadav et al., 2013). A direct binding of WUS to the promoter of only four differentiation promoting TFs-*KANADI1*, *KANADI2*, *YABBY3* and *AS2* has been documented (Yadav et al., 2013). These results shown that WUS can directly activate and repress transcription of target genes in the same cells. How WUS can discriminate between transcriptional activation and repression in same cells is not known. It is also not known how WUS, which is present both in the RM and the CZ can only activate *CLV3* in the CZ. It is also not known how WUS protein levels are regulated such that it leads to a higher accumulation in the RM and lower accumulation in the CZ.

Objectives (aims of the study).

WUS and *CLV3* are two critical factors in regulating stem cell maintenance in the shoot apical meristem. The molecular mechanisms of how these two factors are regulated to maintain a proper balance is largely unknown. The goals of this dissertation are focused on understanding the following aspects:

- Identification and characterization of the regulatory regions in the *CLV3* gene required for its expression.
- Determining the cis-regulatory mechanisms underlying the concentration-dependent transcriptional activation and repression mediated by WUS.
- The mechanisms involved in regulating the WUS protein concentration.

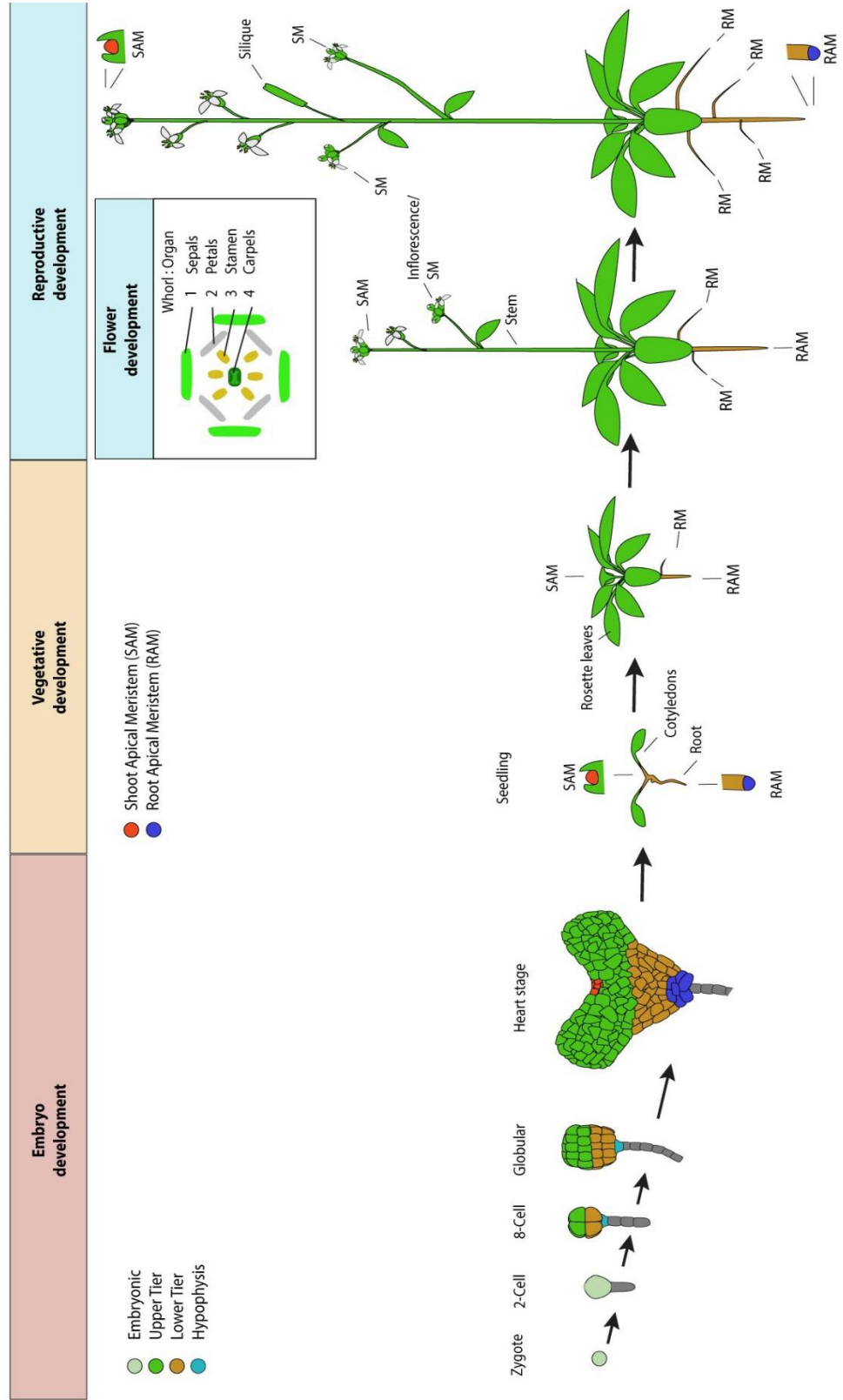
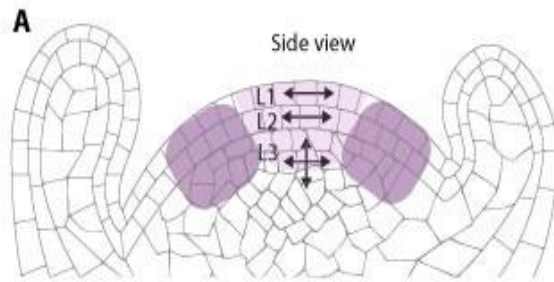


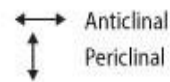
Fig. 1.1. Stages in the development of *Arabidopsis thaliana*. Embryo development begins with apical-basal patterning. The pro-embryo can be divided into the upper tier and lower tier cells. The upper tier develops into SAM, hypocotyl and cotyledons, whereas the lower tier develops into the primary root. The shoot and root meristems are established during the development of the embryo. WUS is initially expressed at the 16 cell stage to specify the organizing center of the shoot meristem. The hypophysis gives rise to the organizing center of the root meristem. During the post-embryonic vegetative stage, the SAM activity sustains the development of rosette leaves that are organized in a spiral pattern around the SAM. Transition of the SAM from the vegetative to the inflorescence meristem leads to the production of floral meristem (FMs) which develop into flowers. The FM sequentially produces 4 different type of floral organs. The outer two organs, sepal and petal, serve to protect the interior reproductive organs, stamen and carpel. Completion of the development of floral organs leads to the termination of the stem cell activity in the floral meristems. The root apical meristem meristem (RAM) sustains the development of roots. Figure adapted from (ten Hove et al., 2015).



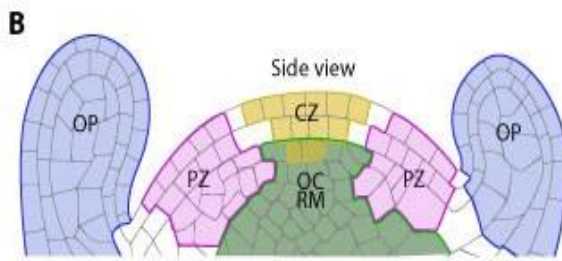
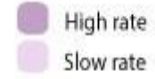
Cell Layers

L1	Layer 1	Epidermal	} Tunica
L2	Layer 2	Subepidermal	
L3	Layer 3	Corpus	

Cell division orientation

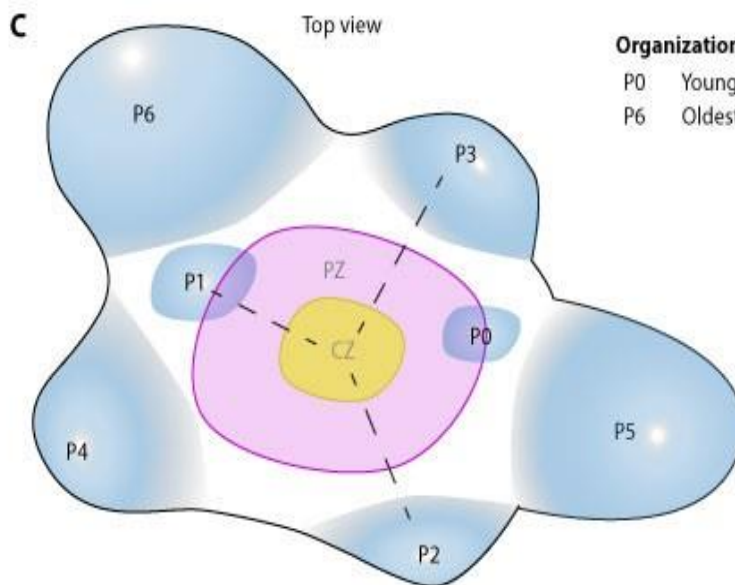


Cell division Rates



Domains of the SAM

CZ	Central Zone
PZ	Peripheral Zone
RM	Rib Meristem
OC	Organizing Center
OP	Organ Primordia



Organization of Primordia

P0	Youngest Primordia
P6	Oldest primordia

Fig. 1.2 The shoot apical meristem. (A-B) Graphic representation of cellular organization of SAMs as seen in side view (A). Cell walls are shown in grey. The outer two layers (L1 and L2), referred to as the tunica, undergo anticlinal cell divisions (perpendicular to the surface). The inner layer (L3) undergoes both anticlinal and periclinal cell divisions producing a multi-layer tissue, referred to as the corpus. Cell division rates in the SAM are regulated; in the central part of the SAM (light purple region), the cell cycle duration varies between 36-72 hours, while in the PZ (dark purple regions), cell cycle duration varies between 18-36 hours (Reddy et al., 2004). (B) The SAM can also be sub-divided into functional domains. The central zone (CZ; yellow) is at the tip of the SAM and harbors stem cells in all three layers. The Rib meristem (RM)/organizing center (OC; green) located beneath the CZ provides signals for stem cell maintenance. The peripheral zone (PZ) surrounds the CZ and OC. In the PZ organ primordia (OP) initiate in a specific spatio-temporal pattern. The cells beneath the OC/RM differentiate into stem. (C) Graphic representation of the top view of the shoot apical meristem. Organ primordia (blue) are arranged in a spiral around the SAM. The organ primordia at different stages of development are labeled P0-P6 with P0 being the youngest.

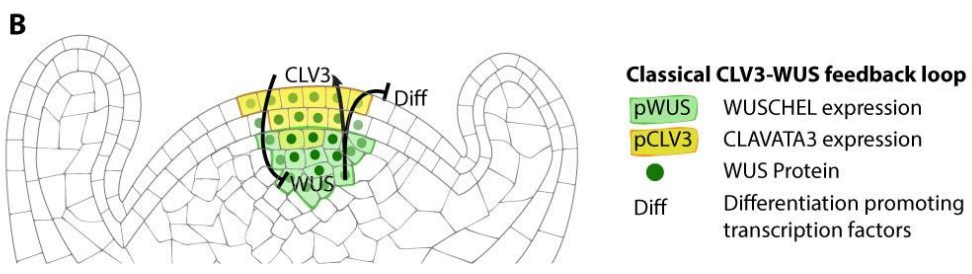
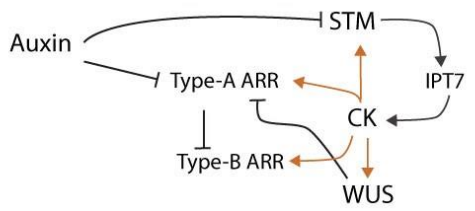
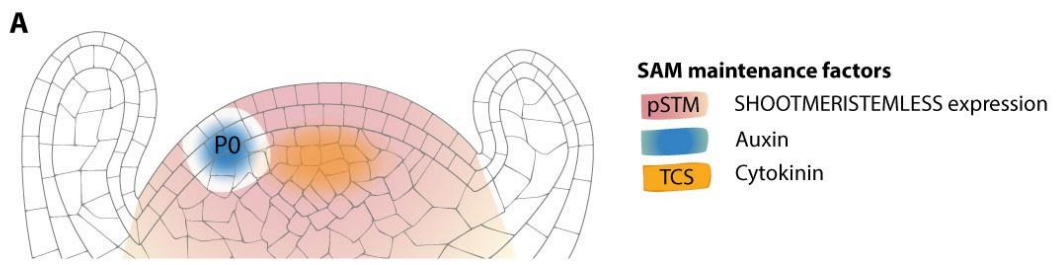


Fig. 1.3 The regulators of the shoot apical meristem maintenance.

(A-B) Graphic representation of cellular organization of SAM shown in side view. Cell walls are shown in grey. Auxin is enriched at the sites for the future primordia (blue). Auxin functions to repress *STM* expression and downregulates the Type-A ARR (ARR7, ARR15). Cytokinin signaling (orange) activates both Type-A and Type-B ARR and possibly *STM* and *WUS*. *STM* produces a positive feedback loop by activating expression of *ADENOSINE PHOSPHATE ISOPENTENYL TRANSFERASE (IPT7)* which is an enzyme that catalyzes cytokinin production. *WUS* also functions in a positive feedback loop with cytokinin as *WUS* represses the cytokinin negative regulators, Type-A ARR. (B) The classical feedback loop regulating SAM maintenance involving *WUSCHEL (WUS)* and *CLAVATA3 (CLV3)*. *WUS* is expressed in the OC (green cell wall) and the *WUS* protein (green circles) migrates to the CZ where it accumulates at lower levels. *WUS* directly activates *CLV3* in the CZ which in turn signals back to repress *WUS* expression. The negative feedback loop functions to regulate the *WUS* levels which is critical for stem cell maintenance.

CHAPTER 2:

Threshold-dependent transcriptional discrimination underlies stem cell homeostasis.

The text of chapter 2 in this dissertation, in whole, is a reprint of the material as it appears in: Perales M, **Rodriguez K**, Snipes S, Yadav R, Diaz-Mendoza M, and Reddy GV. (2016) Threshold-dependent transcriptional discrimination underlies stem cell homeostasis. Proc Natl Acad Sci USA 113:E6298-E6306. The co-author Reddy GV. listed in that publication directed and supervised the research which forms the basis for this dissertation.

Abstract:

Transcriptional mechanisms that underlie the dose-dependent regulation of gene expression in animal development have been studied extensively. However, the mechanisms of dose-dependent transcriptional regulation in plant development have not been understood. In *Arabidopsis* shoot apical meristems, WUSCHEL (WUS), a stem cell-promoting transcription factor, accumulates at a higher level in the rib meristem and at a lower level in the central zone where it activates its own negative regulator, *CLAVATA3* (*CLV3*). How WUS regulates *CLV3* levels has not been understood. Here we show that WUS binds a group of *cis*-elements, *cis*-regulatory module, in the *CLV3*-regulatory region, with different affinities and conformations, consisting of monomers at lower concentration and as dimers at a higher level. By deleting *cis* elements, manipulating the WUS-binding affinity and the homodimerization threshold of *cis* elements, and manipulating WUS levels, we show that the same *cis* elements mediate both the activation and repression of *CLV3* at lower and higher WUS levels, respectively. The concentration-dependent transcriptional discrimination provides a mechanistic framework to explain the regulation of *CLV3* levels that is critical for stem cell homeostasis.

Introduction:

Various mechanisms have been proposed to explain dose-dependent transcriptional regulation mediated by morphogen gradients in animal development (Rogers et al., 2011). Transcriptional mechanisms that underlie dose-dependent modulation of gene expression in plant development have not been discovered, but cell-fate specification is known to rely heavily on positional cues (Bhalerao et al., 2003). Shoot apical meristems (SAMs) contain a set of pluripotent stem cells in the central zone (CZ);

the stem cell descendants that are displaced into the adjacent peripheral zone (PZ) differentiate as lateral organs (Steeves et al., 1989), and the stem cell descendants that are displaced into the rib meristem (RM), located beneath the CZ, differentiate and become part of the stem (Steeves et al., 1989). In *Arabidopsis* SAMs, WUSCHEL (WUS), a homeodomain transcription factor that is expressed in the RM, has been shown to provide cues for stem cell maintenance (Laux et al., 1996; Mayer et al., 1998). WUS synthesized in few cells of the RM has been shown to migrate into adjacent cells where it accumulates at a lower level than in the RM (Yadav et al., 2011). WUS has been shown to activate *CLAVATA3 (CLV3)* expression (Schoof et al., 2000). CLV3 is a secreted peptide that activates a receptor kinase pathway to restrict *WUS* transcription (Fletcher et al., 1999; Clark et al., 1997; Brand et al., 2000; Kondo et al., 2006). Earlier studies have shown that a precise regulation of *CLV3* level is critical to control *WUS* transcription (Lenhard et al., 2003; Reddy et al., 2005). However, the mechanisms underlying transcriptional regulation of *CLV3* have remained elusive.

WUS has been shown to bind the regulatory regions of type A ARABIDOPSIS RESPONSE REGULATORS (ARRs), negative regulators of cytokinin signaling, and repress their transcription (Leibfried et al., 2005). The function of at least two type A ARR, *ARR7* and *ARR15*, have been shown to be critical for activating *CLV3* expression (Zhao et al., 2010). Because the type A ARR lack the DNA-binding domain, they might play an indirect role in *CLV3* activation. EMSAs have shown that WUS binds the regulatory sequences in *CLV3*, and transient transfection studies in *Arabidopsis* leaf protoplasts have shown that these regulatory sequences activate *CLV3* transcription (Yadav et al., 2011). However, further studies are required to understand the in vivo significance of WUS

binding in transcriptional regulation of *CLV3*. It also is not known how *CLV3* is transcribed in only a few cells of the CZ despite the presence of the WUS protein in a much broader spatial domain (Yadav et al., 2011). WUS has been shown to interact with HAIRY MERISTEM (HAM) family proteins HAM1 and HAM2, which are expressed in the RM and lateral edges of the PZ (Schulze et al., 2010; Zhou et al., 2015). Perhaps HAM proteins may provide a spatial context for expression of *CLV3* in the CZ.

Several studies have shown that WUS also represses the transcription of many genes (Leibfried et al., 2005; Busch et al., 2010; Yadav et al., 2013), including several differentiation-promoting transcription factors, thus preventing premature differentiation of stem cell descendants (Yadav et al., 2013). The transient transcriptional assays in *Arabidopsis* leaf protoplasts have shown that WUS can function as both an activator and a repressor (Ikeda et al., 2009). WUS has been shown to bind the transcriptional corepressor proteins TOPLESS (TPL) and -TOPLESS RELATED (TPR) (Kieffer et al., 2006; Dolzblasz et al., 2016). The TPL and TPR proteins also have been shown to interact with HISTONE DEACETYLASE19 (HDA19) to form a transcriptional repression complex (Szemenyei et al., 2008). These studies suggest that WUS may exist in different protein complexes that allow it to function both as a repressor and as an activator; however, the association of WUS with the components of a transcriptional activation complex has not been established. Furthermore, WUS has been shown to bind *cis* elements containing TAAT core sequences in the regulatory regions of activated target genes *CLV3* (Yadav et al., 2011) and *AGAMOUS* (Lohmann et al., 2001) as well as in the regulatory regions of repressed target genes (Leibfried et al., 2005; Busch et al., 2010; Yadav et al., 2013). However, the mechanisms through which WUS can discriminate between transcriptional

activation and repression by using similar *cis* elements are not understood. Here we used in vivo assays and biochemical analysis to investigate WUS-mediated regulation of *CLV3* transcription. Our analysis shows that WUS functions as an activator at lower concentrations and as a repressor at higher concentrations. Our finding that WUS binds the same *cis* elements as a monomer at lower concentrations and as a dimer at higher concentrations suggests that WUS-mediated transcriptional discrimination may involve changes in the binding behavior of WUS to DNA. Moreover, we find that WUS binds a collection of closely spaced *cis* elements with different affinities that may buffer variations in WUS levels to maintain *CLV3* transcription. Finally, we discuss the significance of concentration-dependent transcriptional regulation in the context of stem cell homeostasis and the mechanisms of transcriptional regulation.

Results:

A WUS-Binding *cis*-Regulatory Module Regulates *CLV3* Expression and Stem Cell Homeostasis. Our efforts to understand the regulation of the transcriptional control of *CLV3* led to the identification of six WUS-binding *cis* elements. Five of these elements, 950, 970, 997, 1007, and 1060 (the numbers represent the position of *cis* elements measured in base pairs from the start codon) (Fig. 2.1A and Fig. 2.2 A–D) were clustered within 110 bp in the 3' region, collectively referred to as the “*cis*-regulatory module” (CRM). To understand the in vivo significance of the CRM, we generated a deletion by removing the CRM in the *CLV3* regulatory region (hereafter referred to as “*pCLV3*”) driving the *Histone2B-modified YFP* (*H2B-mYFP*) reporter (Boisnard-Lorig et al., 2001). The mutations in the WUS-binding *cis* element –1080 located upstream of the start codon identified in an earlier study (Yadav et al., 2011) did not influence *pCLV3* expression

(Fig. 2.2E). The deletion of the CRM led to low levels of expression of the reporter in the L1 and the L2 cell layers and the RM, showing that the WUS-binding CRM is required for activating *CLV3* (Fig. 2.1B). The mutant *pCLV3-ΔCRM* promoter lacking the CRM failed to complement fully the overproliferated *clv3-2* mutant SAMs and the overproliferated floral meristems (FMs), as revealed by the presence of a higher number of carpels (Fig. 2.1 C and D and Fig. 2.3). These results show that the WUS-binding CRM is required for maintaining the *CLV3* level needed for SAM and FM maintenance.

To understand the significance of the five *cis* elements in the CRM in *CLV3* regulation (Fig. 2.4A and Fig. 2.5), we introduced mutations that abolish WUS binding (Fig. 2.4 B–F and Fig. 2.2 A–D) and that also contained a point mutation in the upstream –1080 *cis* element ($n = 15$) (Fig. 2.2E) into the *pCLV3::H2B-mYFP* reporter (Fig. 2.4 G and H). The mutations in the highest-affinity *cis* element 970 (the double mutant *pCLV3-DM*) led to a decrease in reporter fluorescence in the L1 and the L2 layers and an increase in the L4 layer (Fig. 2.4 C, I, and J and Fig. 2.6 A–C) ($n = 12$). The mutation in intermediate-affinity *cis* element 997 (Fig. 2.4D) did not significantly alter *CLV3* expression (Fig. 2.2E). However, mutations in the 970 and the 997 elements (the triple mutant *pCLV3-TM*) resulted in a decrease in expression levels in the L1 and the L2 layers along with a significant increase in expression in layers 4–6 (Fig. 2.4 K and L and Fig. 2.6 A–E) ($n = 16$). The *pCLV3-TM* also revealed a higher number of cells that expressed the mutant reporter, some of which showed reporter expression at extremely low levels even in the L1 and L2 layers (Fig. 2.4 K and L). An increase in the number of cells expressing *pCLV3-TM* and higher levels of the mutant reporter in deeper layers suggest that the higher-affinity *cis* elements 970 and 997 may inhibit lower-affinity *cis* elements from activating

CLV3. Additional mutations in the lower-affinity *cis* elements 950 (Fig. 2.4B) and 1060 (Fig. 2.4F) were introduced to create a quintuple mutant promoter, *pCLV3-QM*, which led to a severe decrease in expression in the L1 layer and higher expression in the L4 layer (Fig. 2.4 M and N and Fig. 2.6 A–C). An overall reduction in the number of *pCLV3*-expressing cells was observed in all cell layers (Fig. 2.4 M and N and Fig. 2.6 E–F) ($n = 12$). A decrease in the number of cells in *pCLV3-QM* suggests that the lower-affinity *cis* elements 950 and 1060 can activate *CLV3* transcription in a broader spatial domain. The mutation in the final lower-affinity *cis* element 1007 (Fig. 2.4E) was introduced to generate a sextuple mutant, *pCLV3-SM*. The *pCLV3-SM* revealed a severe reduction in *pCLV3* expression (Fig. 2.4 O and P) that was comparable to the reporter expression observed upon deletion of the entire CRM (Fig. 2.1B). Taken together these results show that WUS uses the same *cis* elements to activate and repress *CLV3* expression. Furthermore, these results show that higher-affinity *cis* elements may repress transcription from the lower-affinity *cis* elements to prevent misexpression of *CLV3* in deeper cell layers and thus suggest interactions among *cis* elements.

WUS Binds to *cis* Elements in a Concentration-Dependent Manner. The misexpression of the *cis*-element mutant promoters of *CLV3* observed in the previous section suggests that WUS may repress *CLV3* transcription in the RM, where it accumulates at a higher level, and activate in the L1 and the L2 cell layers, where it accumulates at a lower level (Yadav et al., 2011). To understand the biochemical basis by which WUS can mediate both transcriptional activation and repression by binding the same *cis* elements, we tested the binding behavior of *cis* elements at increasing concentrations of the WUS protein. Five *cis* elements formed a low molecular weight complex at lower WUS levels and a higher molecular weight complex with increasing WUS

concentrations (Fig. 2.7 A–E and Fig. 2.8 P–S). We tested whether the concentration-dependent switch is caused by the dimerization of WUS, which was found to be critical for WUS function. WUS contains two homodimerization domains, homodimerization domain1 (HOD1) and homodimerization domain2 (HOD2). HOD1 consists of a single amino acid residue located within the loop that connects the second and third α -helices of the homeodomain. HOD2 consists of a 74-aa region (amino acids 134–208) in the central part of the protein (Rodriguez et al., 2016). A truncated form of WUS (amino acids 1–134) lacking HOD2 bound *CLV3 cis* elements with affinity comparable to that of the full-length protein. However, the truncated form required about four times higher WUS levels to produce a higher molecular weight complex, revealing that HOD1 alone is sufficient to dimerize at higher WUS levels (Fig. 2.7 F–H). A WUS mutant protein lacking both HOD1 and HOD2, WUS (amino acids 1–134:G77E), bound *cis* elements with lower affinity but failed to produce a higher molecular weight complex (Fig. 2.7I). The HOD1 mutant version with the intact HOD2, WUS (amino acids 1–208:G77E), was unable to bind DNA (Fig. 2.7J), unlike with the HOD1 mutant lacking the HOD2, WUS (amino acids 1–134:G77E). The severe loss of binding of the HOD1 single mutant with an intact HOD2 may be caused by the predominance of intermolecular interactions between WUS–WUS homodimers that might have outcompeted the DNA–WUS interactions. Alternately, the intact HOD2 might have inhibited the mutated HOD1 from binding DNA through a drastic conformational change in the homeodomain or by enhancing steric hindrance. In summary, these results show that the two HOD domains are required for dimerization of WUS at higher concentrations and that HOD1 also is necessary for DNA binding.

Decreasing the Homodimerization Threshold of *cis* Elements Leads to *CLV3*

Repression. The results from the analysis of *cis* element deletion suggested that WUS may activate *CLV3* transcription at lower concentrations and repress *CLV3* transcription at higher levels. The biochemical analysis revealed that the same *cis* elements could bind WUS as monomers at lower concentrations and as dimers at higher levels. The EMSA experiments also show that WUS formed dimers at lower WUS concentrations in interactions with the higher-affinity *cis* elements than in interactions with the lower-affinity *cis* elements (Fig. 2.7 A–E and Fig. 2.8 A–D). Thus the affinity and the dimerization thresholds are inversely correlated. These experiments also suggest that the WUS-binding sequence contains information that determines WUS-binding affinity and homodimerization thresholds. Taken together, these observations suggested that WUS may repress *CLV3* transcription by forming homodimers at higher concentrations. Such a model predicts that decreasing the homodimerization threshold of *cis* elements should lead to repression of *CLV3* in the CZ, where WUS is present at a lower level.

To test further the importance of the WUS-binding sequence in promoting WUS homodimerization, we analyzed the self-association behavior of WUS in solution (without DNA) by using size-exclusion chromatography (SEC) at WUS concentrations ranging from 0.3 to 15 μM . The SEC analysis revealed that even a 50-fold increase in WUS concentration was unable to convert the monomeric pool into dimeric or higher-order complexes (Fig. 2.7 K–M and Fig. 2.8 E–S). However, in the presence of DNA, a mere two- to fourfold increase in WUS concentration was sufficient to switch the monomeric WUS–DNA complex completely into a dimeric WUS–DNA complex (Fig. 2.7 A–E and Fig. 2.8 A–D). Taken together, these results show that the WUS-binding sequence promotes

homodimerization or multimerization of WUS (EMSA experiments may not have distinguished dimeric complexes from multimeric complexes) and that the homodimerization threshold is inversely correlated to *cis*-element affinity.

Based on the biochemical analysis presented in the previous section, we hypothesized that a much higher-affinity *cis* element might dimerize WUS at lower concentrations in the CZ and repress *CLV3*. As part of our efforts to understand DNA features that determine affinities and dimerization thresholds, we systematically mutated each base pair within and outside the TAAT core of the high-affinity *cis* element 970, which contains two tandem TAAT cores. Nucleotides both within and outside the TAAT core either increased or decreased affinity to WUS, suggesting that a higher-order structure may influence binding affinities (Fig. 2.9). Earlier studies have shown that the homeodomain proteins can bind sequences that deviate slightly from the canonical TAAT core-containing sequences (Noyes et al., 2008; Berger et al., 2008). To take advantage of this ability of homeodomain proteins to bind noncanonical TAAT core sequences, we considered two of these mutant *cis* elements, 970-M4 and 970-M1, for further analysis with respect to WUS binding. Estimation of the binding affinity revealed that 970-M4 bound WUS at an affinity approximately three times higher ($K_d = 0.05830 \mu\text{M}$) (Fig. 2.5G) than that of the wild-type 970 *cis* element (Fig. 2.5B). The 970-M1 mutant also bound WUS at a concentration range comparable to that of 970-M4 (Fig. 2.10 A and B). The WUS protein that contained only HOD1 was able to dimerize with 970-M1 and 970-M4 (Fig. 2.10 A and B) at much lower levels than with the wild-type 970 (Fig. 2.4C). Moreover, the full-length WUS protein dimerized with 970-M4 at lower levels than with the wild-type 970 *cis* element (Fig. 2.10 C and D). Taken together, these results show that the two higher-affinity *cis* elements also exhibited lower dimerization thresholds.

In our efforts to understand the role of dimerization in *CLV3* regulation, we analyzed higher-affinity mutant reporters and *CLV3* genomic constructs. Introduction of the 970-M4 and 970-M1 mutations into the *pCLV3::H2B-mYFP* reporter resulted in a dramatic decrease in the reporter expression except in deeper cell layers, where it was expressed at lower levels (Fig. 2.10 E–G and Fig. 2.6 B and C) ($n = 12$) that were comparable to the expression detected upon deletion of the CRM (Fig. 2.1B). Consistent with the lower levels of the reporter, complementation assays using the 970-M4 and 970-M1 mutant promoters expressing the *CLV3* genomic region failed to complement fully the SAM and the FM defects of *clv3-2* mutants (Fig. 2.1 C and D and Fig. 2.3). To test further whether the repression is *WUS* dependent, we introduced the mutant reporters into *clv3-2* mutants that accumulate *WUS* at extremely low levels in the L1 layer despite its higher synthesis in deeper layers (Fig. 2.10 K and L) (Daum et al., 2014). Both 970-M4 and 970-M1 were reactivated in the L1 layer of *clv3-2* SAMs (Fig. 2.10 I and J). The recovery of expression of the 970-M4 and 970-M1 reporters suggests that the repression caused by higher-affinity binding could be alleviated by decreasing the *WUS* concentration. Taken together these results show that increasing the *cis*-element affinity decreases the dimerization threshold and is sufficient to repress *CLV3*.

CLV3 Expression Is Sensitive to WUS Dosage. The *cis* element manipulation analysis reveals that *WUS* activates *CLV3* transcription at lower concentrations and represses *CLV3* transcription at higher concentrations. Earlier studies have shown that ectopic overexpression of *WUS* leads to activation of *CLV3*, a result that is not consistent with higher *WUS* levels leading to *CLV3* repression (Yadav et al., 2010; Müller et al., 2006). However, these studies only analyzed *WUS* mRNA patterns and did not analyze

WUS protein distribution patterns following ectopic activation. The results presented in the companion article in this issue (Rodriguez et al., 2016) show that ectopic overexpression of WUS leads to protein destabilization. eGFP-WUS expressed from a CZ-specific promoter (*pCLV3::LhG4;6XOP::eGFP-WUS*) accumulated at much lower level ($n = 20$) (Fig. 2.11B) than eGFP-WUS expressed from the *pWUS* (Fig. 2.11A). These SAMs also revealed higher levels of *pCLV3* ($n = 5$) (Fig. 2.11 D and E and Fig. 2.12 A and B), in agreement with earlier studies (Yadav et al., 2010; Müller et al., 2006). The ubiquitous overexpression of WUS using a dexamethasone (Dex)-inducible system (*35S::eGFP-WUS-GR*) also destabilized WUS protein (Rodriguez et al., 2016). Specifically, within 6 h of Dex application, the protein became unstable in cells located in the CZ. The region of lower protein accumulation expanded radially into adjacent PZ cells within 12 h of Dex treatment and reached outer edge of the PZ within 24 h of Dex treatment (Rodriguez et al., 2016). We also monitored the *pCLV3* response to the induction of *35S::eGFP-WUS-GR* and found an increase in *pCLV3* levels within 12 h of Dex treatment and subsequent radial expansion of the reporter expression into adjacent PZ cells within 24 h of Dex treatment (Fig. 2.11 G–I). These results reveal that *CLV3* activation correlates with a reduction in WUS levels.

A close spatiotemporal correlation between the dilution of WUS levels and the increase in *pCLV3* expression suggested that lower WUS levels may activate *CLV3* transcription. We tested this hypothesis by transiently depleting WUS using a Dex-inducible two-component system to activate an artificial microRNA (amiRNA) directed against WUS (Fig. 2.11P). Within 4 d of Dex treatment, a dramatic increase in *pCLV3* along with radial expansion of the reporter was observed, and continued treatment with

Dex for 8 d led to lower *pCLV3* expression (Fig. 2.11 J–O) ($n = 12$). The *wus-1* heterozygous mutants also expressed *pCLV3* at higher level, whereas homozygous mutants failed to express *pCLV3* at a detectable level (Fig. 2.11 Q–S and Fig. 2.12 D and E). The radial expansion of the *pCLV3* upon partial depletion of WUS could be caused by the overpopulation of the monomeric form of WUS, which has been shown to diffuse farther in inflorescence meristems (Rodriguez et al., 2016; Daum et al., 2014), showing that the regulation of transcription and protein distribution are coupled. Taken together, these experiments show that the decrease in WUS levels leads to the activation of *CLV3* expression until WUS levels fall below a certain threshold.

Because a decrease in WUS level led to *CLV3* activation, we next tested whether an increase in WUS level can repress *CLV3*. Expression of WUS carrying a strong nuclear localization signal, *NLS-eGFP-WUS*, by using the *pCLV3::LHG4* driver revealed an intense fluorescence in the nuclei of a few cells, showing that an enhanced nuclear accumulation improves WUS protein stability (Fig. 2.11 C) ($n = 20$). These SAMs revealed a severe decrease in *pCLV3* expression ($n = 5$) (Fig. 2.11 F and Fig. 2.12 C), showing that higher WUS levels repress *CLV3*. We cannot rule out the possibility that the repression could be indirect; however, the results from the manipulation of *cis* elements and WUS levels in tandem show that *CLV3* transcription is maintained over a window of WUS levels bound by the activation and the repression thresholds.

The *CLV3* promoter lacking the CRM, *pCLV3(ΔCRM)*, partially complemented the enlarged SAM (Fig. 2.1C) and FM (Fig. 2.1D) phenotypes of *clv3-2* mutants. An earlier study has shown that at 16% of wild-type levels the *CLV3* mutant promoter was able to complement partially *clv3-2* mutant phenotypes (Müller et al., 2006), indicating that the meristem maintenance requires only a small amount of *CLV3*. A relatively better floral meristem rescue (based on carpel number) was observed with the *pCLV3-SM* mutant than with the higher-affinity mutants *pCLV3(970-M1)* and *pCLV3(970-M4)* and with the mutant promoter lacking the entire CRM, suggesting that *pCLV3-SM* may contain relatively higher *CLV3* levels (Fig. 2.1D). EMSA shows that the nucleotides outside the TAAT core also can influence *WUS* binding (Fig. 2.9) and that *WUS* also can bind a partially mutated *cis* element (Fig. 2.2D). These observations suggest that at higher levels *WUS* may still bind the mutant *cis* elements or elements elsewhere within the CRM and can explain the higher levels of *CLV3* in the *pCLV3-SM* mutant than seen with the deletion of the CRM. Therefore, a collective *WUS* binding to the CRM may be important in regulating *CLV3* transcription. In *clv3-2* mutants the expression of the mutant reporter *pCLV3(TM)* was decreased in the inner layers, where *WUS* accumulates at higher levels, and was increased in the L1 layer, where *WUS* accumulates at lower levels (Fig. 2.13), suggesting that the remaining *cis* elements respond to *WUS* levels. A similar resetting of the *pCLV3(SM)* in *clv3-2* mutants suggests that the remaining regulatory elements located within and outside the CRM may also respond to *WUS* levels. The resetting of the mutant promoters in *clv3-2* also suggests that the dosage sensitivity of *CLV3* depends partly on the CRM.

Discussion

Our work shows that WUS mediates the activation and repression of *CLV3* by using the same set of *cis* elements within the CRM. WUS levels vary not only among cells located in different cell layers but also between adjacent cells of a given cell layer (Fig. 2.6F). The observation that WUS binds each *cis* element within the CRM with different affinities may provide a mechanism to buffer these variations in maintaining *CLV3* transcription that, in turn, has been shown to regulate *WUS* transcription in the RM (Schoof et al., 2000; Brand et al., 2000). The higher levels of WUS repressing *CLV3* and lower levels activating *CLV3*, as proposed here, may not be able to produce a stable system if a strict linear relationship exists between levels of *WUS* transcription and the amount of WUS protein. However, we have observed lower levels of WUS in the L1 layer of *clv3-2* mutants despite higher synthesis in the RM, suggesting additional tiers of WUS regulation. Earlier studies have shown that *CLV3* promoter is highly active in the L1 layer of *clv* mutants (Brand et al., 2000), as is consistent with lower levels of WUS activating *CLV3* transcription. The lower levels of WUS protein accumulation in the L1 layer of *clv3-2* mutants could be caused by a direct role of *CLV3*-mediated signaling in posttranslational regulation of WUS. Alternately it might be an indirect consequence of higher protein synthesis resulting from enhanced transcription, because our work shows that overexpression of *WUS* leads to protein instability (Rodriguez et al., 2016). In either scenario, higher levels of WUS-repressing *CLV3* will destabilize WUS, leading to *CLV3* activation, which in turn stabilizes the WUS protein and leads to *CLV3* repression, thus forming a feedback loop that connects concentration-dependent transcriptional regulation of *CLV3* to the regulation of WUS protein levels. The *cis* element manipulation analysis also suggests interactions among *cis* elements. Perhaps higher WUS levels might induce

cooperative interactions among *cis* elements, as shown in the case of BICOID binding to the HUNCHBACK CRM (Ma et al., 1996); these cooperative interactions could lead to enhanced dimerization and transcriptional repression. Biochemical analysis of the collective WUS-binding behavior to the CRM, along with the in vivo analysis of the importance of spacing between *cis* elements and relative orientations of *cis* elements, may provide further insights into the nature of interaction among *cis* elements.

Several alternate models can explain WUS-mediated concentration-dependent transcriptional regulation. The WUS-mediated repression of *CLV3* may involve the quenching of an independent activator of *CLV3* by the WUS homodimers. Such a mechanism would lead to higher levels of *CLV3* upon WUS removal or deletion of WUS-binding *cis* elements. We have observed *CLV3* up-regulation upon partial depletion of WUS, which can explain the quenching mechanism. However, *wus* null mutants do not express *CLV3*, which is not consistent with the quenching mechanism. The quenching mechanism also fails to explain the decrease in *CLV3* expression observed upon mutating WUS-binding *cis* elements unless the independent activator also binds the same *cis* elements. Alternately, spatially localized coactivators in the CZ or corepressors in the RM could mediate the localized activation of *CLV3*. Biochemical studies have shown that the HAM proteins expressed in both the RM and the PZ interact with WUS (Schulze et al., 2010; Zhou et al., 2015). The genetic analysis revealed that HAM proteins require WUS function in regulating SAM maintenance (Zhou et al., 2015). At present we do not understand the mechanisms by which HAM proteins promote SAM maintenance; however, the *CLV3* repression observed in the L1 and the L2 layers of higher-affinity *cis* element mutants presented here shows that WUS can repress *CLV3* in a HAM-

independent fashion. Perhaps HAM proteins may provide an additional layer of regulation in potentiating the WUS-mediated repression in inner layers, either by increasing the binding affinity of WUS to *cis* elements or by promoting homodimerization of the WUS protein. Moreover, the switch in *CLV3* expression observed in *cis*-element mutation analysis cannot support the CZ-localized coactivator model.

We suggest that WUS might function with an activation complex and a repression complex present in both the CZ and the RM. At lower concentrations, WUS could bind as a monomer or as a heterodimer that could recruit activation machinery. At higher concentrations, WUS homodimers may fail to engage an activation complex, may favor recruitment of ubiquitously expressed corepressor complex, or may prevent the CRM located in the 3' region from engaging with the proximal promoter. Future work on both transcriptional coregulators and understanding the importance of the location of the CRM may lead to further insights into the concentration-dependent modulation of gene expression.

Acknowledgements

We thank Thomas Laux for sharing driver lines and *wus* mutants; Jacqueline Le for supporting experimental work; Araceli Diaz Perales and Maria Garrido Arandia of the Centro de Biotecnología y Genómica de Plantas, Universidad Politécnica de Madrid-Instituto Nacional de Investigación y Tecnología Agraria y Alimentaria (INIA) for providing advice and the equipment used in the SEC experiments; and members of the G.V.R. laboratory and Patricia Springer for comments on the manuscript. This work was supported by National Science Foundation Grant IOS-1456725 (to G.V.R.).

Footnotes

M.P. and K.R. contributed equally to this work.

M.P. and M.D.-M. Present address: Centro de Biotecnología y Genómica de Plantas, Universidad Politécnica de Madrid (UPM)–Instituto Nacional de Investigación y Tecnología Agraria y Alimentaria (INIA) Campus Montegancedo UPM, Pozuelo de Alarcón, Madrid, 28223, Spain.

R.K.Y. Present address: Department of Biological Sciences, Indian Institute of Science Education and Research, Mohali, 140306, India

Author contributions: M.P. and G.V.R. designed research; M.P., K.R., S.S., R.K.Y., M.D.-M., and G.V.R. performed research; M.P., K.R., M.D.-M., and G.V.R. analyzed data; and M.P., K.R., and G.V.R. wrote the paper.

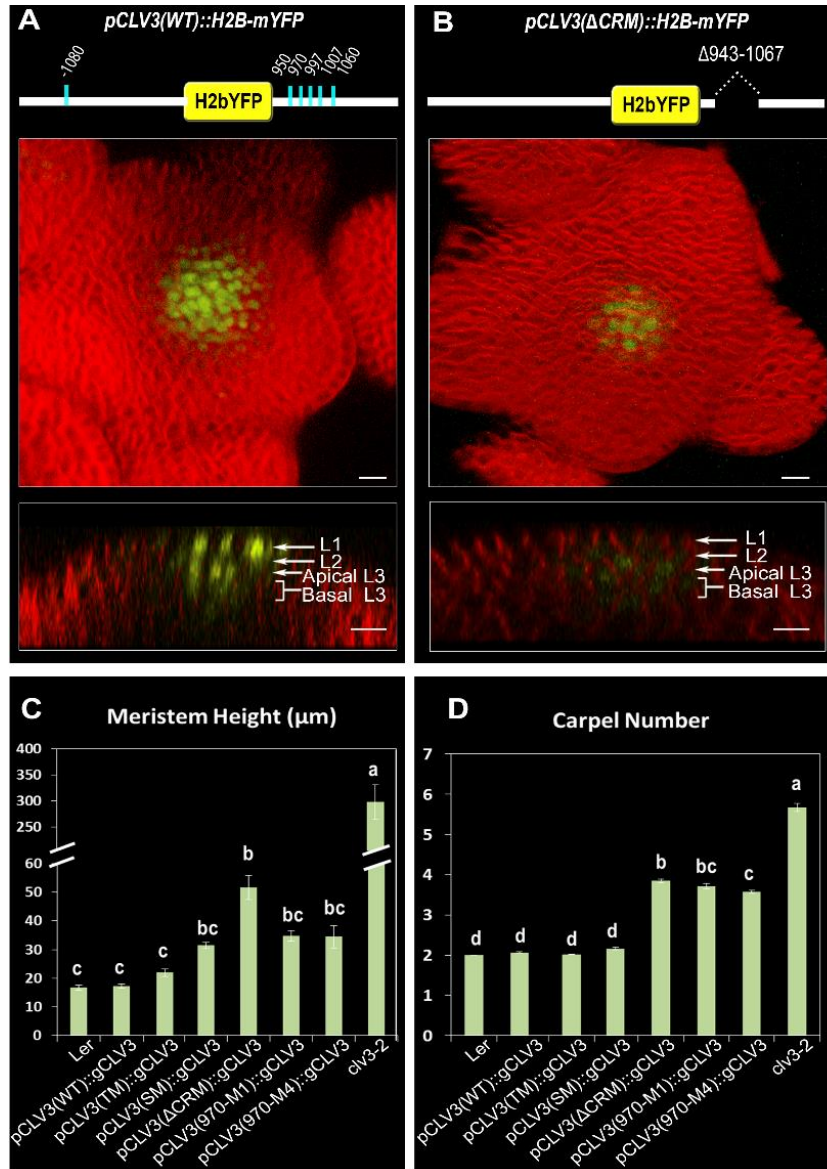


Fig. 2.1. A CRM regulates *CLV3* expression. (A and B) 3D-reconstructed top and side views of inflorescence meristems showing wild-type *pCLV3::H2B-mYFP* (A) and deletion of the CRM (nucleotides 943–1067), also referred to as “*pCLV3-ΔCRM*” (B). H2B-mYFP expression is shown in yellow; FM4-64 labeling is shown in red. The white arrows indicate different cell layers. (Scale bars: 10 μm.) (C and D) The phenotypic complementation analysis with the *CLV3* genomic region containing the mutated WUS-binding *cis* elements. The inflorescence meristem height (C) and the number of carpels (D) in *clv3-2* plants transformed with the wild-type *pCLV3* and various *CLV3* mutant promoters: *pCLV3-TM* (970 and 997 double mutant); *pCLV3-SM* (950, 970, 997, 1007, and 1060 quintuple mutant); *pCLV3-ΔCRM* (nucleotides 943–1067 deletion); and the two higher-affinity mutants *pCLV3-970-M1* and *pCLV3-970-M4* expressing the *CLV3* genomic region. In all *CLV3* promoters, the upstream –1080 *cis* element is mutated. The error bars represent SE. Different letters indicate statistical differences between *cis* lines ($P < 0.001$) as determined by Tukey’s Honest Significant Difference (HSD) tests.

A

CLV3 -1080	GGCTCATATAAATCAATTTATG	GGCTCATATGATCCATTCAATTTATG
CLV3 1060	GTCGGTTAAATTTATCCTTCCCA	GTCGGTTGGCCTTATCCTTCCCA
CLV3 1007	ACATACAATAATAAAATGATGATG	ACATACAAGGGGAAAAATGATGATG
CLV3 997	TTATTGTATGTTTAAATGTGACTAT	TTATTGTATGTTCCATTGTGACTAT
CLV3 970	CACATCCATAATTTATTTGCATTGACAATTG	CACATCCATGGGGTATTTGCATTGACAATTG
CLV3 950	AACGTACTAATAAAATTTCCCAACGGTA	AACGTACCCCAAAATTTCCCAACGGTA

B

CLV3 -1080M	GGCTCATATGATCCATTCAATTTATG
CLV3 1060M	GTCGGTTGGCCTTATCCTTCCCA
CLV3 1007M	ACATACAAGGGGAAAAATGATGATG
CLV3 997M	TTATTGTATGTTCCATTGTGACTAT
CLV3 970M	CACATCCATGGGGTATTTGCATTGACAATTG
CLV3 950M	AACGTACCCCAAAATTTCCCAACGGTA
CLV3 1007M 2bp	ACATACAATAGGAAAAATGATGATGATG

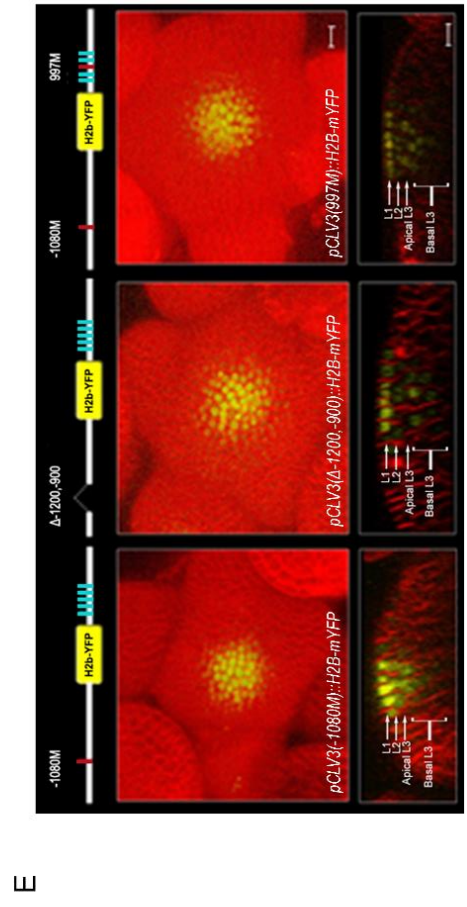
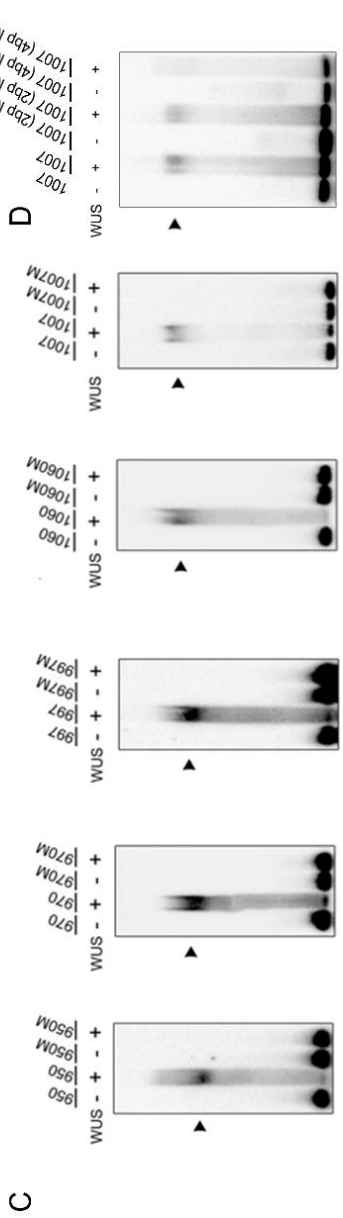


Fig. 2.2. Characterization of the WUS-binding cis elements in CLV3. (A) Sequence comparison of the WUS-binding cis elements of *pCLV3* (-1080, 1060, 1007, 997, 970, and 950); TAAT cores are underlined. (B) Sequences of mutated TAAT cores in WUS-binding cis elements of *pCLV3* are underlined and highlighted in gray. (C) EMSA showing WUS binding to the wild-type and mutated cis elements 950, 970, 997, 1060, and 1007. (D) A comparison of WUS binding to the oligos containing a 2-bp mutation or a 4-bp mutation in the TAAT core of the 1007 cis element. Black arrowheads indicate the monomer WUS-DNA complex. (E) 3D top views of SAMs showing the *pCLV3*(-1080M)::H2B-mYFP, the 300-bp deletion *pCLV3*(Δ-1200 to -900)::H2B-mYFP, and the double mutant (-1080 and 997) *pCLV3*(997M)::H2B-mYFP. Neither the single (-1080) nor the double (-1080 and 997) mutant altered CLV3 expression. H2B-mYFP (yellow) is overlaid on FM4-64 (red). (Scale bar: 10 μm.)

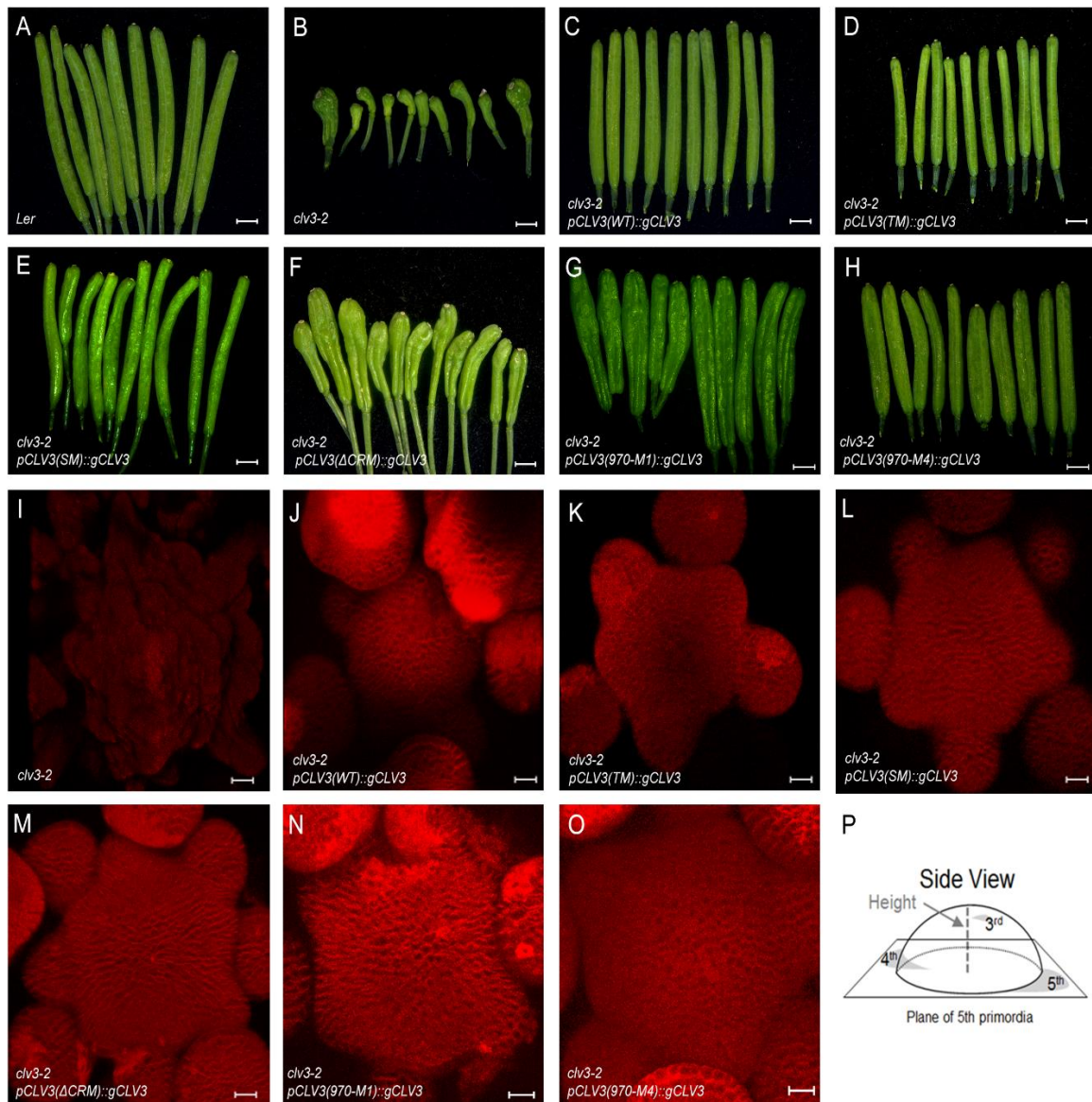


Fig. 2.3. Complementation analysis with *pCLV3* mutant promoters. (A–H) Images of siliques of wild-type (A), *clv3-2* (B), and *clv3-2* plants transformed with the CLV3 genomic rescue construct expressed from the mutant *pCLV3(WT)::gCLV3* mutant (C), mutant *pCLV3(TM)::gCLV3* mutant (D), mutant *pCLV3(SM)::gCLV3* (E), mutant *pCLV3(ΔCRM)::gCLV3* (F), mutant *pCLV3(970-M1)::gCLV3* (G), and mutant *pCLV3(970-M4)::gCLV3* (H). (Scale bars: 2 mm.) (I–O) Top views of 3D-reconstructed meristems of *clv3-2* (I) and *clv3-2* mutants carrying CLV3 genomic constructs expressed from *pCLV3(WT)::gCLV3* 9J0 (J), mutant *pCLV3(TM)::gCLV3* (K), mutant *pCLV3(SM)::gCLV3* (L), mutant *pCLV3(ΔCRM)::gCLV3* (M), mutant *pCLV3(970-M1)::gCLV3* (N), and mutant *pCLV3(970-M4)::gCLV3* (O). (Scale bars: 80 μm in I; 20 μm in J–O.) (P) Graphical sketch showing the spatial landmarks (flower primordia) used for measuring the inflorescence meristem height.

Fig. 2.4. The same cis elements mediate activation and repression of CLV3 expression. (A) Schematic of the CLV3 gene showing the location of the 3' CRM. The DNA sequence from +933 to +1080 is shown in black, and the TAAAT core containing WUS-binding elements on the CRM are labeled in red. (B–F) EMSAs (Left) and WUS–DNA saturation curves (Right) were performed using different concentrations of the WUS (amino acids 1–134) DNA-binding domain bound to radiolabeled oligonucleotides of 950 (B), 970 (C), 997 (D), 1007 (E), and 1060 (F) cis elements. Black arrowheads show the WUS–DNA complex. (G–P) All reporters carry mutations in –1080, the 5' cis element. Schematic representations of the reporter constructs are annotated with wild-type (cyan) and mutant (red) cis elements on their respective inflorescence (G, I, K, M, and O) and vegetative (H, J, L, N, and P) meristems. Side views show inflorescence and vegetative SAMs of wild-type pCLV3 (G and H); the 970 cis-element double mutant (pCLV3-DM) (I and J); the 970 plus 997 cis-element triple mutant (pCLV3-TM) (K and L); the 950, 970, 997, and 1060 cis-element quintuple mutant (pCLV3-QM) (M and N); and the 950, 970, 997, 1007, and 1060 cis-element sextuple mutant (pCLV3-SM) (O and P). In G, I, K, M, and O H2B-mYFP expression is shown in yellow and FM4-64 labeling is shown in red. In H, J, L, N, and P the H2B-mYFP expression (yellow) is overlaid onto the bright-field images. In G–P the white arrows show different cell layers. (Scale bars: 10 μ m.)

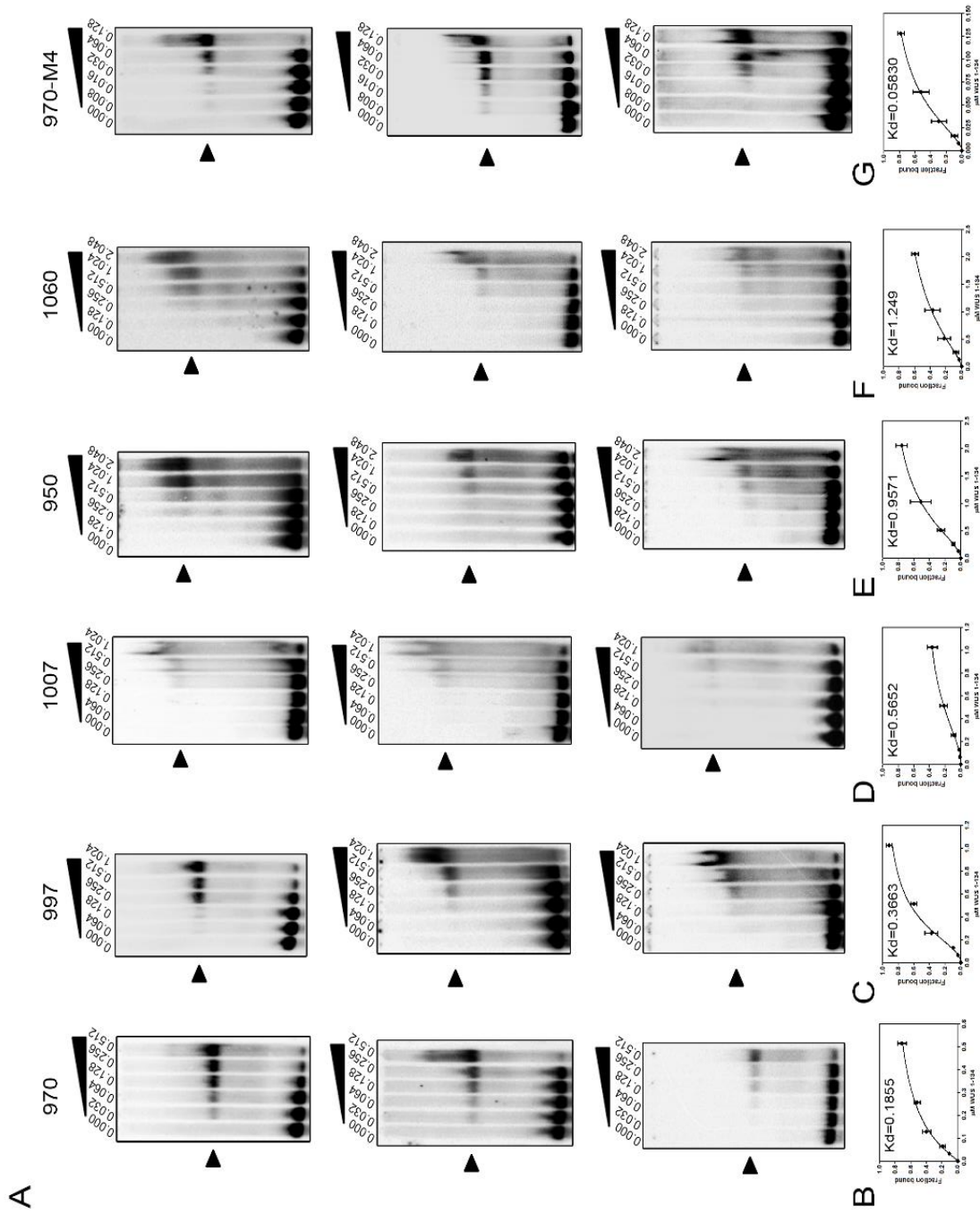


Fig. 2.5 Estimation of the binding affinities of WUS to the five *cis* elements in the CRM and to the higher-affinity (970-M4) mutant *cis* element. (A) EMSA using different concentrations of WUS (amino acids 1–134) bound to radiolabeled oligonucleotides of five *cis* elements in the CRM and the 970-M4. The three replicates for each *cis* element were used for estimating K_d values. Concentration range of WUS (amino acids 1–134) is stated in micromolars above each gel. Black arrowheads indicate the WUS–DNA complex. (B–G) WUS–DNA saturation curves for *cis* elements 970 (B), 997 (C), 1007 (D), 950 (E), 1060 (F), and 970-M4 (G). Quantification details are provided in methods in the main text.

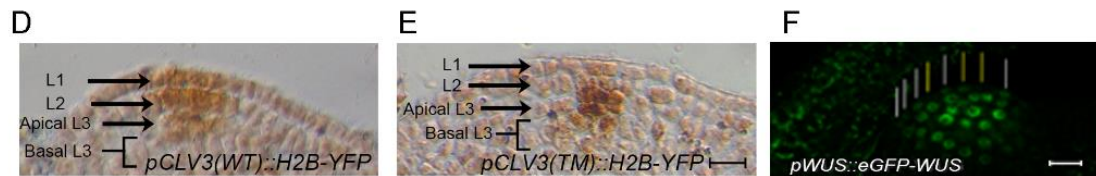
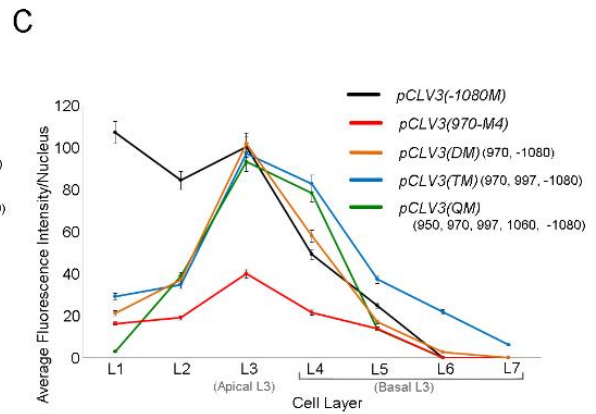
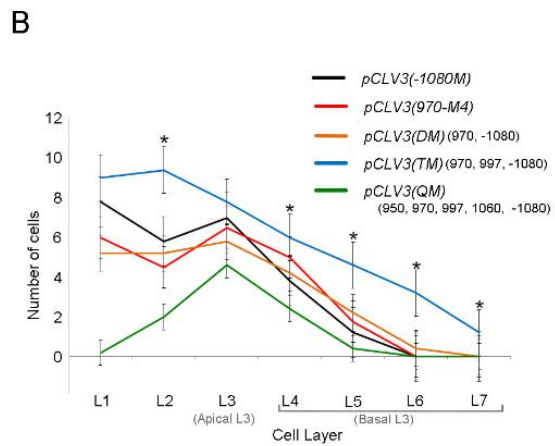
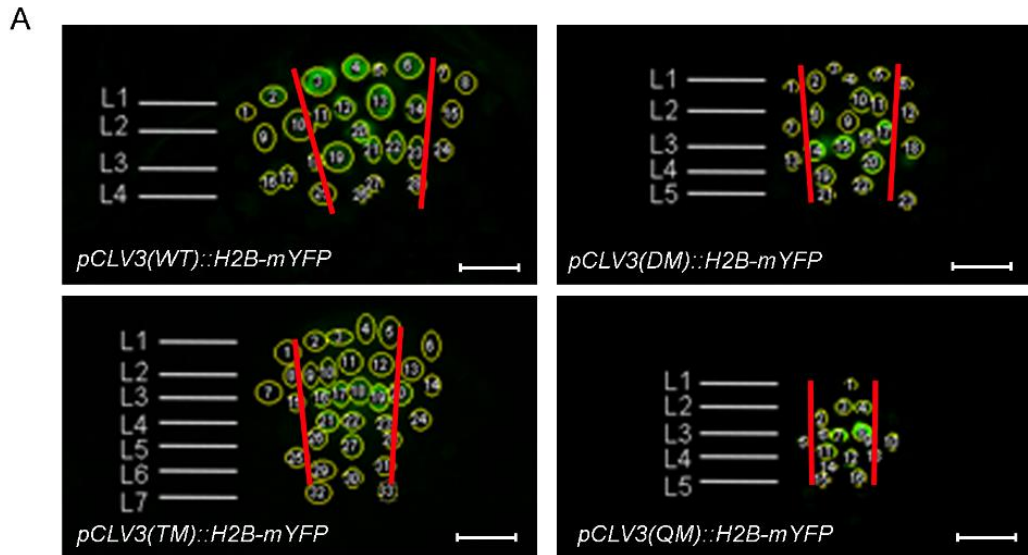


Fig. 2.6. The effect of *cis*-element deletions on *CLV3* expression. (A) Sample images of different *cis*-element mutants of *pCLV3::H2B-mYFP* used for quantification of fluorescence from nuclear-bound regions. Four centrally located cells (within the red lines) were considered. (B) Quantification of the number of cells with detectable expression found in different cell layers of *cis*-element mutations. (C) The average fluorescence was quantified from centrally located cells of five independent SAMs. Expression from *pCLV3(-1080M)::H2B-mYFP* was used as the wild-type reference for the *pCLV3(DM)::H2B-mYFP* mutant (970 and -1080), the *pCLV3(TM)::H2B-mYFP* mutant (970, 997, and -1080), the *pCLV3(QM)::H2B-mYFP* mutant (950, 970, 997, 1060, and -1080), and *pCLV3(970-M4)::H2B-mYFP*. The error bars represent the SE of each sample set. A single asterisk denotes statistical significance ($P < 0.05$) as determined by two-tailed Student's *t* test between *pCLV3(-1080M)::H2B-mYFP* and *pCLV3(TM)::H2B-mYFP*. (D and E) RNA in situ hybridization patterns of *pCLV3(WT)::H2B-mYFP* (D) and *pCLV3(TM)::H2B-mYFP* (E) using *mGFP5* as the anti-sense probe. (F) Side view of seedling SAMs with *eGFP-WUS* expressed from the *pWUS* showing cells in L1 with low (yellow lines) and high (white lines) fluorescence. (Scale bars: 10 μ m.)

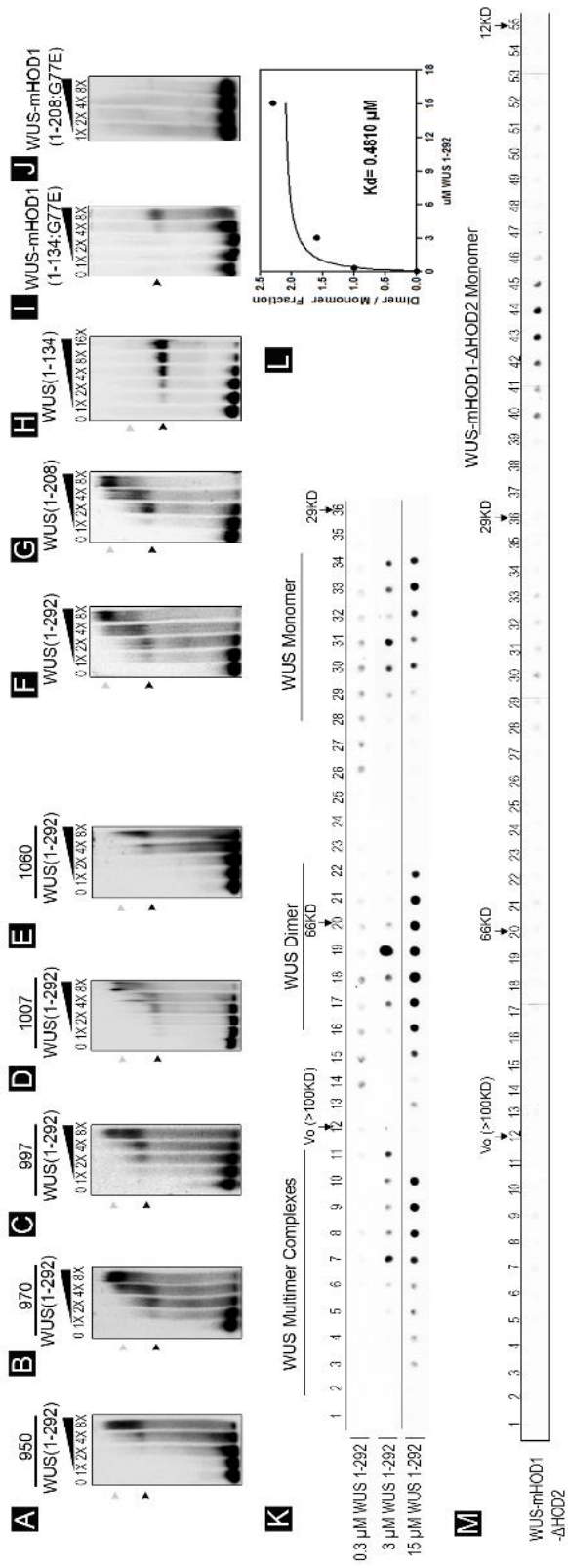


Fig. 2.7. DNA promotes homodimerization of WUS. (A–E) EMSAs showing the binding of five *cis* elements of the CLV3 CRM, 950 (A), 970 (B), 997 (C), 1007 (D), and 1060 (E), to increasing concentrations of full-length WUS (amino acids 1–292) which contains both HOD1 and HOD2. (F–J) EMSA showing the binding of the 970 *cis* element to increasing concentrations [0, 1× (0.5 ng/μL), 2×, 4×, and 8×] of full-length WUS (amino acids 1–292) (F), truncated WUS (amino acids 1–208) (G), truncated WUS (amino acids 1–134) lacking the HOD2 (H), truncated WUS (amino acids 1–134) containing the HOD1 (G77E) mutation (I), and truncated WUS (amino acids 1–208) containing the HOD1 (G77E) mutation (J). SEC experiments were performed using 0.3 μM, 3 μM, and 15 μM of full-length purified recombinant WUS protein. (K) Dot blot analyses of SEC-collected fractions containing WUS protein complexes were visualized by anti-WUS antibodies. (L) The WUS dimer/monomer ratio of WUS (amino acids 1–292) protein concentration and *K_d* was estimated from the saturation-fitting hyperbolic curve using GraphPad Prism 5 software. (M) Immuno dot blot analyses of SEC-collected fractions of the HOD1 (G77E) and HOD2 (Δ amino acids 134–208) double mutant using anti-WUS antibody. Positions of WUS monomer, dimer, and multimer complexes are shown. Elution positions of molecular mass standards (BSA: 66 kDa; carbonic anhydrase: 29 kDa; and cytochrome C: 12 kDa) are marked. The position of the void volume (V_o) (~100 kDa) is marked.

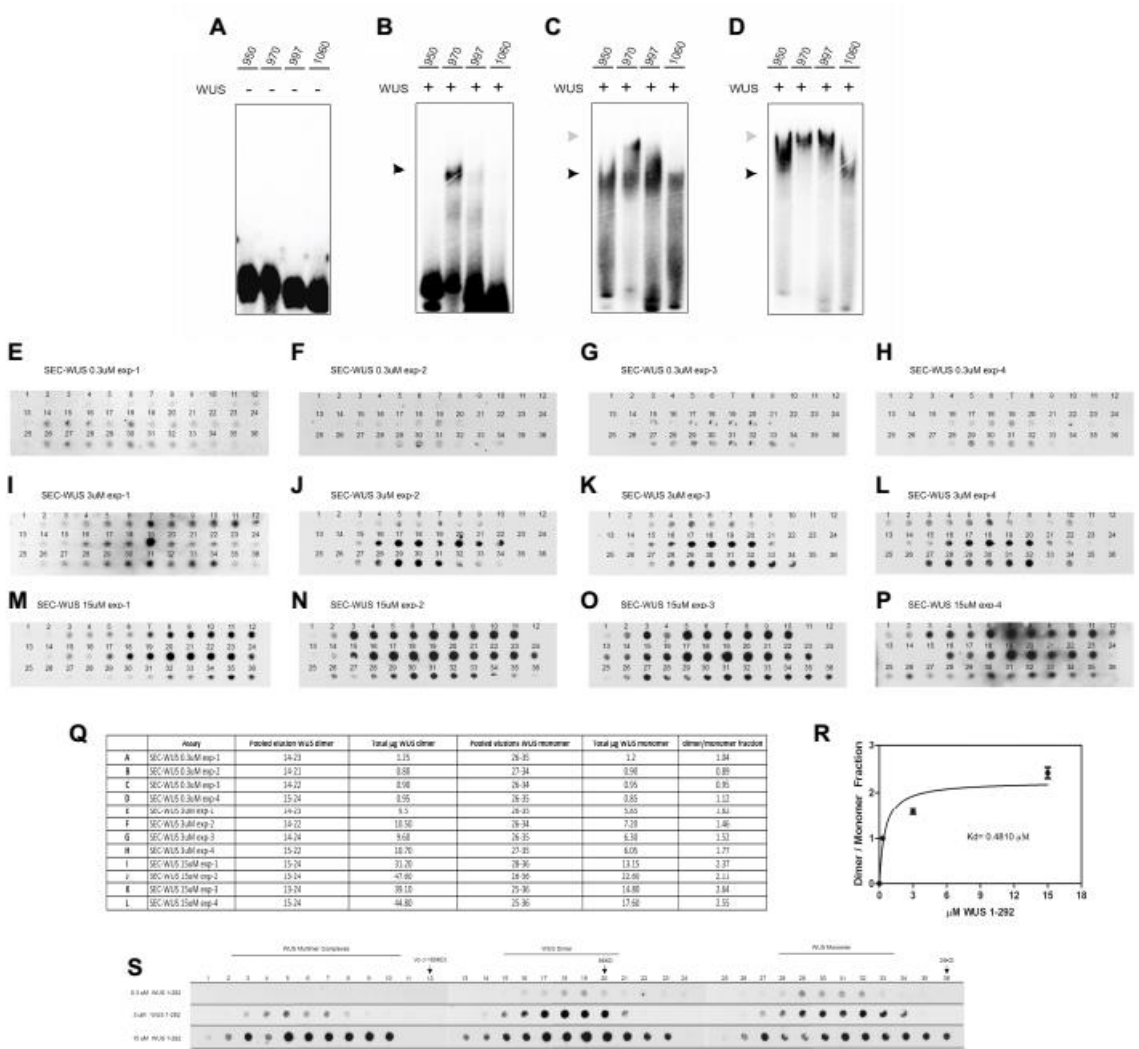


Fig. 2.8. The DNA promotes homodimerization of WUS. (A–D) EMSAs showing recombinant full-length WUS bound to radiolabeled oligonucleotides that contained individual *cis* elements (950, 970, 997, and 1060) found in *CLV3*. The binding behavior at increasing WUS concentrations is shown: (A) 0; (B) 1× (0.5 ng/μL); (C) 4× (2 ng/μL); (D) 16× (8 ng/μL). Black and gray arrowheads indicate positions in the gel that show lower and higher molecular weight complexes, respectively. (E–P) Dot blot analyses of SEC-collected fractions containing WUS protein complexes visualized by anti-WUS antibodies. SEC experiments were performed using 0.3 μM (E–H), 3 μM (I–L), and 15 μM (M–P) of full-length purified recombinant WUS (amino acids 1–292) protein. (Q) The fractions corresponding to the WUS dimer and monomer were pooled to measure the protein concentration. The table summarizes the number of fractions pooled, protein concentrations of dimers and monomers, and the dimer/monomer ratios. Procedural details can be found in **Materials and methods**. (R) The WUS dimer/monomer ratio was presented as a function of total WUS (amino acids 1–292) protein concentration using GraphPad Prism 5 software, and the *K_d* was estimated from the saturation-fitting hyperbolic curve. (S) Comparison of SEC experiments using 0.3 μM, 3 μM, and 15 μM of bacterially expressed purified full-length WUS (amino acids 1–292). Shown are immuno dot blot analyses of SEC-collected fractions using anti-WUS antibody. The positions of WUS monomer, dimer, and multimer complexes are shown. Elution positions of the molecular-mass standards are marked: BSA, 66 kDa; carbonic anhydrase, 29 kDa. The position of the void volume (*V_o*) ~100 kDa, is marked.

A

CACATCCATTAATTATTTGCATTGACAATTG	970-WT
CACATCCA G TAATTATTTGCATTGACAATTG	970-M1
CACATCCAT G AATTATTTGCATTGACAATTG	970-M2
CACATCCATT G ATTATTTGCATTGACAATTG	970-M3
CACATCCATTA G TTATTTGCATTGACAATTG	970-M4
CACATCCATTA A GTATTTGCATTGACAATTG	970-M5
CACATCCATTA A T G ATTTGCATTGACAATTG	970-M6
CACATCCATTA A TT G TTTGCATTGACAATTG	970-M7
CACATCCATTA A TT A G TTGCATTGACAATTG	970-M8
CACATCCATTA A TT A T G TCATTGACAATTG	970-M9

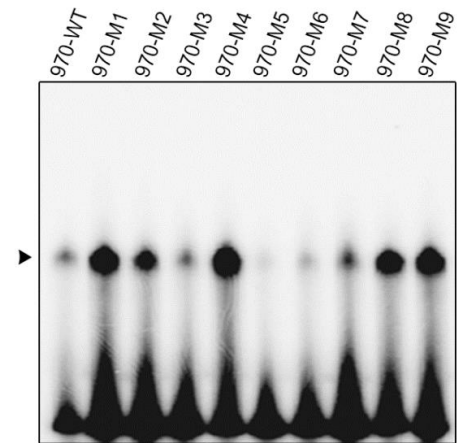
B

Fig. 2.9. Nucleotides within and outside the TAAT core modulate WUS binding. (A) Sequences showing single base substitutions of the 970 *cis* element. (B) EMSA comparing WUS (amino acids 1–134) binding to wild-type and mutated 970 *cis* elements shown in A. Note the higher-affinity *cis* elements including 970-M1 and 970-M4, which were used for further *in vivo* analysis. The black arrowhead indicates the WUS monomer.

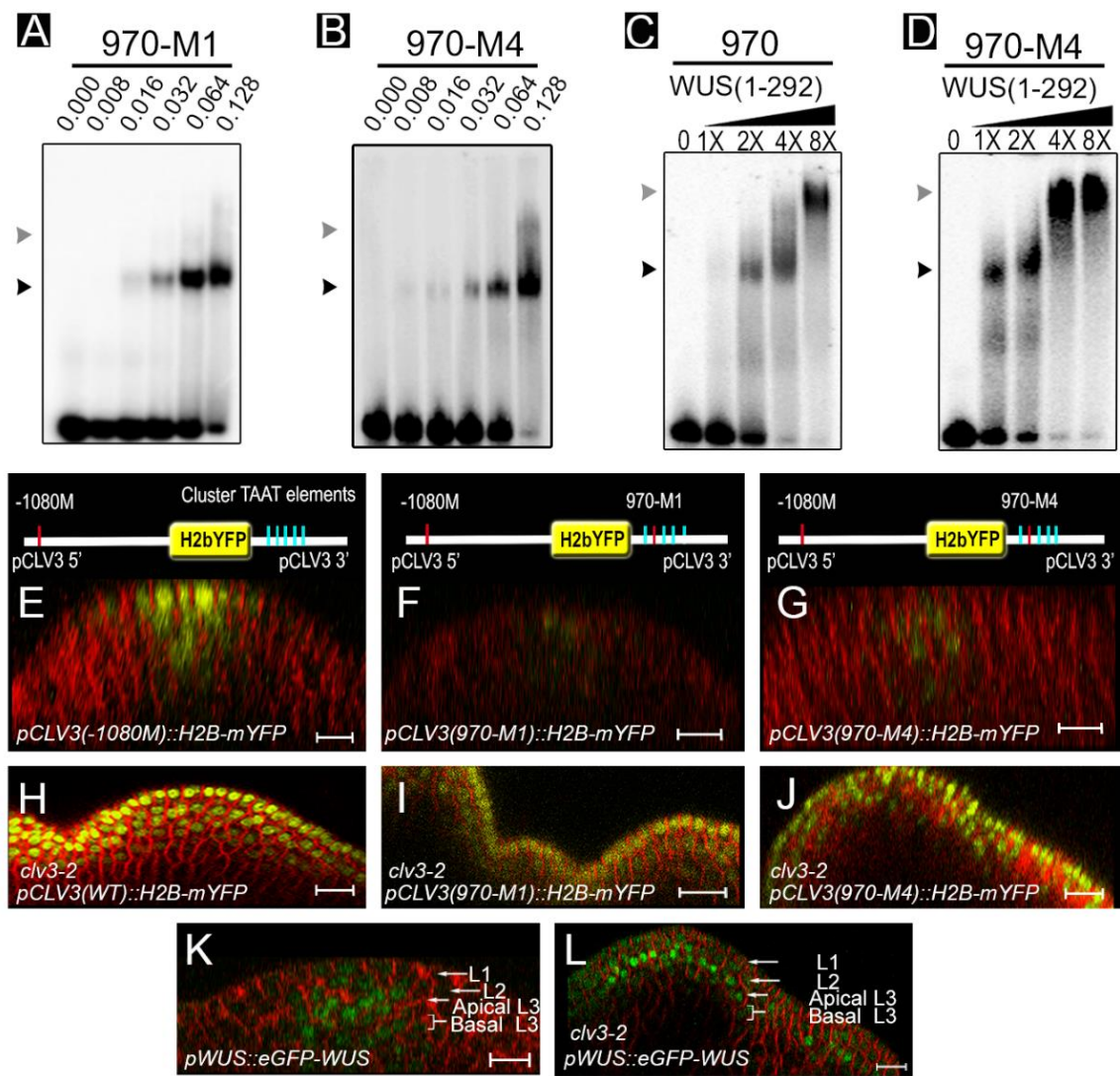


Fig. 2.10. Increasing the *cis*-element affinity lowers the dimerization threshold, leading to *CLV3* repression. (A and B) EMSAs showing binding of truncated WUS (amino acids 1–134) lacking the HOD2 at increasing concentrations to mutant versions of the 970 *cis* elements 970-M1 (A) and 970-M4 (B). The sequence is described in Fig. 2.9. The numbers above the autoradiograms indicate the WUS concentration in nanograms per microliter. Compare with the wild-type 970 *cis* element in Fig. 2.4C. Note dimerization at WUS levels in 970-M4 and 970-M1. (C and D) EMSAs showing the binding of wild-type 970 (C) and mutated 970 *cis* element (970-M4) (D) to increasing concentrations [0, 1× (0.5 ng/μL), 2×, 4×, 8×, and 16×] of the full-length WUS (amino acids 1–292). Black arrowheads indicate monomers, and gray arrowheads indicate dimers. (E–J) Side views of wild-type (E–G) and *clv3-2* (H–J) inflorescence meristems showing H2B-mYFP expression in mutated *pCLV3*(–1080M) (E and H), mutated *pCLV3*-970-M1 (F and I), and mutated *pCLV3*-970-M4 (G and J). (K and L) Side views of inflorescence meristems showing *pWUS:eGFP-WUS* expression in wild-type (K) and *clv3-2* (L) plants. H2B-mYFP (yellow in E–J) and eGFP-WUS (green in K and L) are superimposed on FM4-64–stained (red) inflorescence meristems. In K and L the white arrows show different cell layers. (Scale bars: 10 μm in E–G and K; 15 μm in H–J and L.)

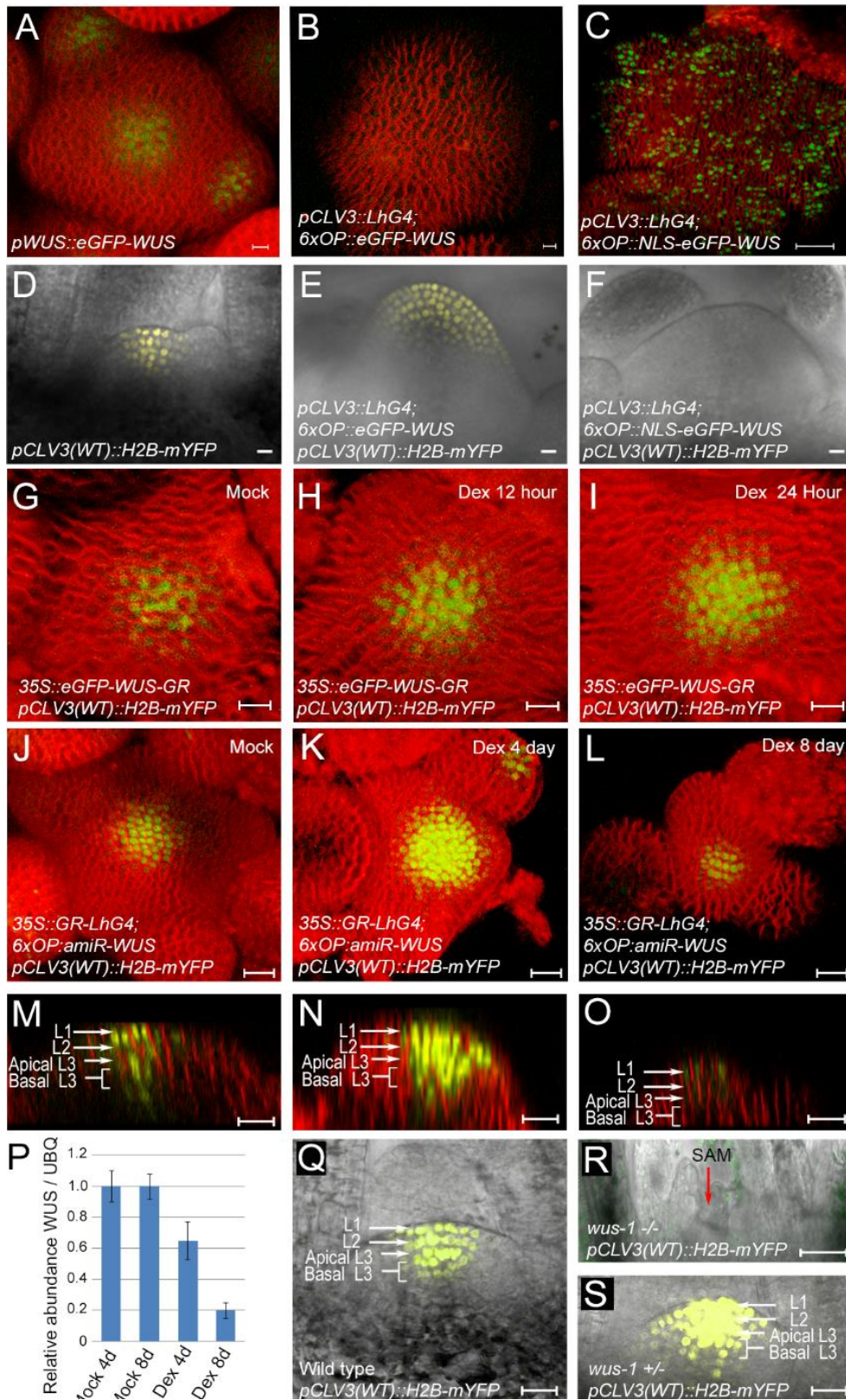


Fig. 2.11. The *CLV3* promoter is sensitive to *WUS* dosage. (A–C) 3D top views of inflorescence meristems expressing *pWUS::eGFP-WUS* (A), *pCLV3::LhG4;6XOP::eGFP-WUS* (B), and *pCLV3::LhG4;6XOP::NLS-eGFP-WUS* (C). eGFP-WUS is shown in green, and FM4-64 is shown in red. (D–F) Side views of vegetative SAMs expressing wild-type-*pCLV3* (H2B-mYFP) overlaid on bright-field images in wild-type (D), *pCLV3::LhG4;6XOP::eGFP-WUS* (E), and *pCLV3::LhG4;6XOP::NLS-eGFP-WUS* (F). H2B-mYFP is shown in yellow. (G–I) 3D top views of *35S::WUS-GR* inflorescence meristems showing *pCLV3::H2B-mYFP* mock treated (G) or treated with 10 μ M Dex for 12 h (H) or 24 h (I). (A–I) (Scale bars: 10 μ m in A, B, and D–I; 30 μ m C.) (J–L) 3D top views of *35S::GR-LhG4; 6XOP::amiR-WUS* inflorescence meristems mock treated (J) or treated with Dex for 4 d (K) or 8 d (L). M, N, and O are side views of J, K, and L, respectively. (P) Quantification of the *WUS* transcript levels in Dex- and mock-treated seedlings expressing *amiR-WUS*. Error bars represent SD. (Q–S) Side views of 7-d-old wild-type (Q), *wus-1-/-* (R), and *wus-1+/-* (S) vegetative SAMs showing the wild-type-*pCLV3* (H2B-mYFP). In M–O and Q–S the white arrows show different cell layers. (Scale bars: 20 μ m J–Q and S; 50 μ m in R.)

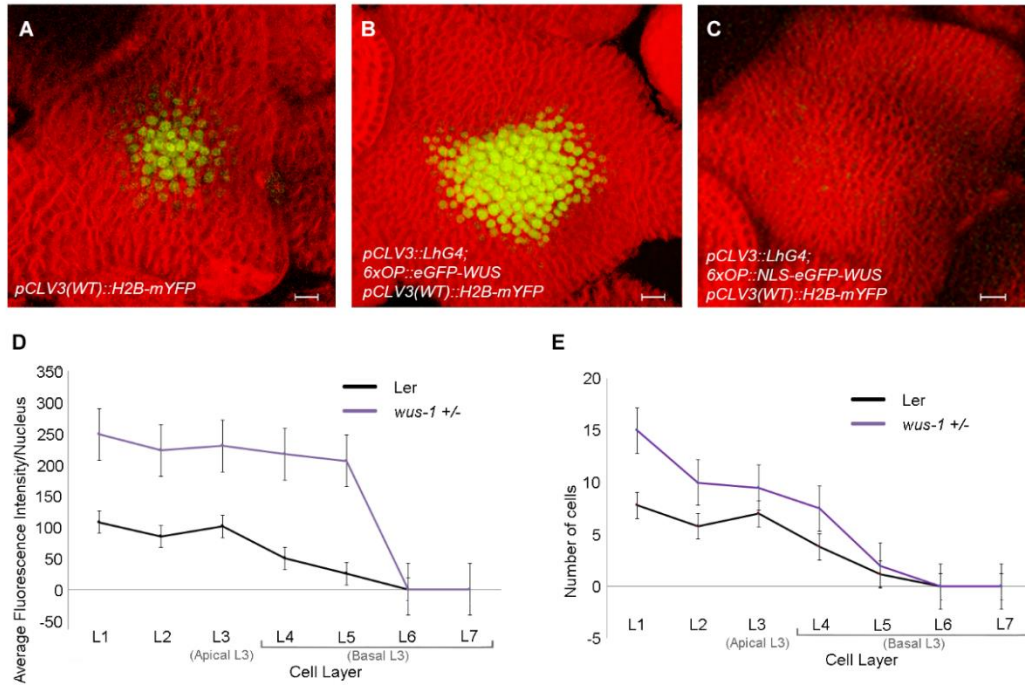


Fig. 2.12. *pCLV3* is sensitive to *WUS* dosage. (A–C) 3D reconstructions of inflorescence SAMs showing *pCLV3::H2B-mYFP* in wild type (A), *pCLV3::LhG4;6XOP::eGFP-WUS* (B), and *pCLV3::LhG4;6XOP::NLS-eGFP-WUS* (C). H2B-mYFP is shown as yellow. (Scale bars: 10 μ m in A and B; 15 μ m in C.) (D and E) Average fluorescence intensity from centrally located cells (D) and number of cells with detectable expression (E) found in different cell layers of *pCLV3(-1080M)::H2b-mYFP* (mutant -1080 was used as wild type) and *wus-1* heterozygous background. The error bars represent the SE of each sample set.

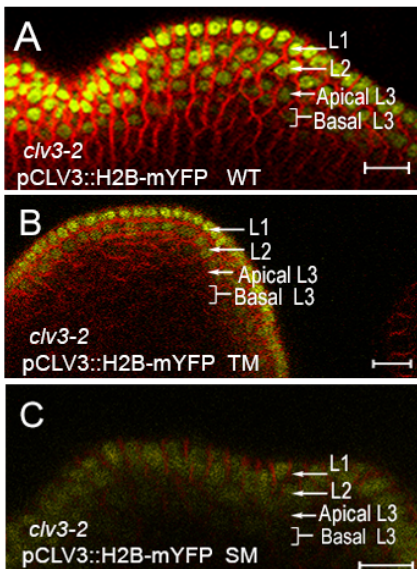


Fig. 2.13. The mutant *CLV3* promoters are repressed in the inner layers and are activated in the outer layers of *clv3-2* mutants. (A–C) Side views of *clv3-2* inflorescence meristems expressing wild-type *pCLV3* (H2B-mYFP) (A), *cis*-element mutant *pCLV3-TM* (H2B-mYFP) (B), and *cis*-element mutant *pCLV3-SM* (H2B-mYFP) (C). H2B-mYFP (yellow) is superimposed on FM4-64-stained (red) SAMs. The white arrows indicate different cell layers. (Scale bars: 15 μ m.)

CHAPTER 3:

Reciprocal interactions among cis elements within a WUSCHEL-binding homotypic cis-regulatory module regulate CLAVATA3 levels and spatial pattern

Abstract:

Most of the homotypic cis-regulatory modules (CRM) characterized so far across systems have been shown to activate transcription of target genes in response to transcription factor (TF) levels. In contrast, our earlier work has shown that the *CLAVATA3* (*CLV3*) enhancer region contains a WUSCHEL (WUS)-binding homotypic CRM that activates *CLV3* at lower WUS levels and repress at higher WUS levels. To understand how cis elements collectively mediate a concentration-dependent transcriptional switch, here we compared the intrinsic and collective roles of each cis element. Analysis of reporter expression shows that intrinsically each cis element can only activate *CLV3* in the RM but not in the CZ. However, the collective binding to the same cis elements leads to repression in the RM and activation in the CZ. To test the model further, we analyzed the spatio-temporal response of the mutant promoters to ubiquitous activation of WUS. Previous work shows that the ubiquitous overexpression of WUS destabilizes it, leading to very low accumulation in the CZ. The mutant promoters lacking two or more of the cis elements failed to fully express in the outer layers when compared to the wild-type promoter, showing that the collective binding to all cis elements is required to activate *CLV3* at lower WUS levels. We find that the intrinsic binding to each cis element was sufficient to repress *CLV3* in the inner layers and activate in the outer layers of *clv3* null mutants, suggesting that at higher WUS levels a single cis element is sufficient to repress *CLV3*. Activation of *CLV3* promoters with one functional cis element in the outer layers of *clv3* mutants can not be explained by limitation of WUS, suggesting that these cells may contain high levels of the activatable form of WUS. Consistent with this notion, the higher affinity cis-element mutants that downregulate *CLV3* in the CZ of wild-type SAMs were also reactivated in the outer cell layers of *clv3* null mutants. Taken together, these results

show that the affinity and the collective property of cis elements interpret differences in WUS levels to regulate *CLV3* transcription. In addition, *CLV3* signaling could modify the activation and repression function of the WUS protein to refine further the transcriptional regulation of *CLV3*, which is critical for stem cell homeostasis.

Introduction:

A spatio-temporal regulation of gene expression is critical for specification of different cell types during development (Ong et al., 2011; Levine, 2010; Spitz and Furlong, 2012). Eukaryotic gene regulation involves interactions among DNA sequences and proteins, many of which are transcription factors. Enhancers, the DNA sequences that bind a given transcription factor (TF) or multiple TFs, can regulate transcription irrespective of their location in the gene (Banerji et al., 1981; Levine, 2010; Spitz and Furlong, 2012). How TF levels influence spatial expression of target genes has been studied in animal systems, especially in *Drosophila* development (Driever and Nüsslein-Volhard 1988; Struhl et al., 1989; Ip et al., 1992a; Ip et al., 1992b; Reeves et al., 2009; Bothma et al., 2014). In *Arabidopsis*, this question becomes more complex since WUS functions as a bifunctional TF that can both activate and repress target genes (Ikeda et al., 2009; Yadav et al., 2013). Moreover, WUS binds the same cis-elements to activate and repress transcription at lower and higher levels respectively (Perales et al., 2016).

The CRMs, a subset of enhancers that contain binding sites for one or more TFs, have been shown to determine the expression of neighboring genes in a variety of organisms (Banerji et al., 1981; Struhl et al., 1989). In general, CRMs can be classified into homotypic where they bind a given TF or heterotypic where they bind different TFs

(Lifanov et al., 2003; Berman et al., 2002). The heterotypic CRMs largely have been thought to mediate spatio-temporal regulation of gene expression through their ability to recruit different collections of TFs in space and time (Small et al., 1992; Ip et al., 1992; Berman et al., 2002). Both the homotypic and heterotypic CRMs have been shown to regulate spatio-temporal patterns of gene expression in response to TF gradients. The earliest examples of homotypic CRMs have been described in the promoters of genes that are activated by the TFs that accumulate in a graded manner during early embryonic development in *Drosophila* (Driver et al., 1989; Gaudet and Mango, 2002; Jiang and Levine, 1993; Rowan et al., 2010). The TF gradients arise as a result of localized production and subsequent spread in space (Gregor et al., 2007; Liberman et al., 2009, example Dorsal, BCD) or spatial activation of TFs which function downstream of a diffusible extracellular ligand that signal through a membrane receptor (Aza-Blanc et al., 1997, example Ci). Classically, the French flag model proposed by Wolpert has been applied to explain the regulation of genes by TF gradients. According to the French flag model, the expression of the target gene is highest in places of highest concentration of the TF (Wolpert et al., 1969). Analysis of multiple CRMs have identified three recurring properties, number of cis elements, affinity, and cooperativity, which function to determine gene expression (Jiang and Levine, 1993). Essentially, decreasing any of the three CRM properties reduces the mean expression, whereas optimizing any of the properties leads to overexpression and misexpression (Jiang and Levine, 1993; Jiang et al., 1991, Gaudet and Mango, 2002; Parker et al., 2011).

It has also been shown that graded TFs can utilize both concentration and the heterotypic CRM to activate genes in regions of intermediate and low levels, thus deviating from the french flag model. This system utilizes localized co-regulators that bind along with the transcription factor to a heterotypic CRM (Ip et al., 1992; Jiang and Levine, 1993). For example, the function of Dorsal, a member of the Rel TF family proteins, is required for specification of the ventral region of the *Drosophila* embryo (Jia et al; 2002). It contains a 300 amino acid Rel homology domain (RHD) that can bind DNA, dimerize and is required for its nuclear import. Dorsal can function as a homodimeric TF (Govind et al., 1992). Dorsal forms a nuclear gradient with highest accumulation in ventral nuclei. Dorsal activates *Twist*, *Snail* and *Rhomboid* (Jiang et al., 1991). *Twist* expression in the regions of high and intermediate Dorsal levels is dependent on the number and affinity of Dorsal-binding sites. The *Snail* promoter contains weak Dorsal-binding sites, which limits its expression to the regions of the highest Dorsal concentration and also requires the aid of coactivator Twist. *Rhomboid* expression is limited to the regions of low Dorsal accumulation through the inhibition from Snail cooperatively working with Dorsal (Ip et al., 1992; Jiang and Levine, 1993). In regions of low Dorsal, where Snail is not found, the high affinity sites for Dorsal have been shown to cooperatively bind the coactivator Twist to drive the expression of *Rhomboid*. Thus a heterotypic CRM with the use of localized co-regulators determine expression of genes within the Dorsal gradient (Ip et al., 1992; Jiang and Levine, 1993). In addition, the homotypic CRMs, containing multiple low affinity cis elements, have been shown to activate genes in regions of low TF accumulation as seen in the case Hedgehog (Hh) target genes Decapentaplegic (DPP), which is another example that is inconsistent with the French flag model of concentration-dependent transcriptional activation (Ramos and Barolo, 2013; Parker et al., 2011). The Hh signaling

generates the opposing gradients of the TF-Cubitus Interreptus (activatable form-Ci^{ACT}) closer to the source and the repressive form (Ci^{REP}) away from the source (Aza-Blanc et al., 1997; Méthot and Basler, 1999). How these two forms function in tandem to determine spatial activation of DPP is discussed further in later sections.

In *Arabidopsis* SAMs, WUS is a stem-cell inducing TF expressed in the rib meristem (RM) [Mayer et al., 1998; Schoof et al., 2000]. WUS protein migrates into the overlying central zone (CZ) where it has been shown to activate its own negative regulator- *CLV3* (Yadav et al., 2011; Perales et al., 2016). *CLV3* encodes a secreted peptide that activates a receptor kinase pathway to restrict *WUS* expression (Clark et al., 1997; Brand et al., 2000). WUS has also been shown to bind to the promoters of key differentiation promoting TFs to repress transcription (Yadav et al., 2013). How the same TF activates some genes such as *CLV3* and also repress other genes in same cells is largely not known. However, a recent study has provided some clues to this regulation (Perales et al., 2016). This study shows that WUS binds a homotypic CRM, a collection of five closely spaced cis elements, in the *CLV3* enhancer region. Mutations in multiple cis-elements led to a gradual downregulation of *CLV3* in the CZ and upregulation in the RM, ultimately leading to a severe downregulation when all five cis elements were mutated. This suggested that the same cis elements are required for both activating *CLV3* in the CZ where WUS accumulates at lower levels and repressing in the RM where WUS accumulates at a higher level. Biochemical analysis revealed that WUS binds cis-elements as monomers at lower level and bind as dimers/multimers with increasing WUS concentrations, suggesting that dimerization/multimerization of WUS at higher levels may repress *CLV3*. The biochemical analysis also revealed that DNA promotes

homodimerization, and affinity and dimerization thresholds of cis-elements are inversely correlated. Increasing the affinity of one of the cis-elements decreased the dimerization threshold and led to the repression of *CLV3* in the CZ, supporting the affinity-based concentration dependent repression. Furthermore, the transient and partial depletion of WUS led to upregulation of *CLV3*, showing that WUS activates *CLV3* at lower levels. The severe depletion of WUS led to downregulation of *CLV3* and *wus* null mutants failed to express *CLV3*. Moreover, increased nuclear accumulation of WUS led to *CLV3* downregulation. Taken together, these results showed that *CLV3* expression is maintained over a window of WUS levels that is bound by the activation and repression thresholds. Concentration-dependent binding of WUS to the CRM, restricting the expression of *CLV3* in the CZ away from the maximal WUS accumulation in the RM, is an exception to the French flag model.

The WUS-binding *CLV3* CRM contains a higher affinity cis-element (970) that is flanked by relatively lower-affinity cis elements (950, 997, 1007 and 1060) [Perales et al., 2016]. Deletion of the highest-affinity element (970) led to downregulation of *CLV3* in outer layers and misexpression in inner layers, suggesting cis-element interactions. However, the role of lower-affinity cis elements in *CLV3* regulation is not clear. Moreover, the nature of interactions among cis elements and the role of cis-element affinities in this process have also remained elusive.

Results:

Mutations in individual cis elements have minimal effect on *CLV3* expression. To understand the contribution of each element to the regulation of *CLV3*, we analyzed mutations in individual WUS-binding cis elements (Fig. 3.1 A and B) (n = 12). All *CLV3* promoter contain an upstream cis-element mutations at -1080 which was previously shown not to change *CLV3* expression (Perales et al., 2016). Mutations were introduced into each of the five cis-elements in the *pCLV3::H2b-mYFP* reporter construct. Mutations in high-affinity cis element (970), as reported earlier, led to a noticeable downregulation in outer cell layers with subtle increase in inner layers (Fig. 3.1D) (n = 16). Mutations in 1007M (Fig. 3.1F) (n = 22) and 1060M (Fig. 3.1G) (n = 19) resulted in a subtle increase of reporter expression in deeper layers (L3 and L4). Mutations in elements 950M (Fig. 3.1C) (n = 10) and 997M (Fig. 3.1E) (n = 19) resulted in a very subtle reduction of the reporter expression in the L1 layer. Taken together, independent mutations in any of the cis-elements revealed minor changes in *CLV3* expression, among these only the higher affinity cis-element (970) revealed a relatively noticeable change. These results show that all elements can contribute to *CLV3* expression and compensate for the loss of a single element in the CRM.

Intrinsic activity of individual elements is sufficient to activate *CLV3* in the RM but insufficient to activate in the CZ. The subtle changes in expression observed with the single cis-element mutants suggested that they could play a role in regulating *CLV3* expression even in the presence of the higher-affinity cis element (970). To test this theory, we introduced mutations in four cis-elements (950M, 997M, 1007M and 1060M), leaving the high affinity-970 cis-element (referred to as 970 I, "I" stands for intrinsic activity

of an isolated cis-element). The 970I construct revealed a dramatic downregulation of *CLV3* in the outer cell layers and upregulation in inner cell layers (Fig. 3.1I) (n = 15). The change in *CLV3* expression in 970I was far more drastic than the individual mutations in any of the five cis-elements, showing that all elements contribute to the *CLV3* expression even in the presence of 970. This also shows that the high affinity 970 element, when isolated from the other elements, is not sufficient to maintain the wild type expression domain of *CLV3*. This suggests that collective binding to all cis-elements is required for repression in inner layers and activation in outer layers. To test this further, we introduce mutations in four cis-elements, leaving only one cis element. We generated and analyzed the effect of intrinsic activity of the remaining four lower-affinity cis elements in isolation (950I, 997I, 1007I, and 1060I). In all these cases, we largely observed a similar downregulation of *CLV3* in outer layers and misexpression in inner layers (Fig. 3.1 H-L). These results show that the intrinsic activity of a single cis element is only sufficient to activate *CLV3* in inner layers and the collective activity is required for repression of *CLV3* in inner layers and activation in outer layers. This also suggests that the intrinsic activity of cis-elements, regardless of affinity differences, is limited to sensing the highest WUS concentration in deeper cell layers. These results led us to new questions as to how does the intact CRM, which has a collection of cis-elements that intrinsically activate *CLV3* at high WUS levels, leads to repression when working together? Also, how does the CRM, which has intrinsic activity that was insufficient to activate *CLV3* at lower WUS levels, leads to activation of *CLV3* in the context of the intact CRM (Fig. 3.2)? It is possible that the number of cis-elements and relative affinities may contribute to the collective binding of WUS, which is also a function of WUS concentration in space.

Affinity and collective activity of multiple cis-elements determine *CLV3* expression and stem cell homeostasis. Our previous study showed that decreasing the number of cis elements led to activation of *CLV3* in inner layers. It also showed that increasing the affinity of a cis element led to downregulation of *CLV3*. For example, 970-M4 is a point mutation in the native 970 cis-element which bound WUS with approximately three times higher affinity and also dimerized WUS at much lower levels than the native 970 cis-element. The 970-M4 mutation resulted in the overall downregulation of *CLV3* (n = 12) and was unable to fully complement the *clv3* null mutant (Perales et al., 2016) (Fig. 3.3B, 3.4 and 3.5) (n = 18). This shows that affinity of the 970 cis-element (below the highest possible affinity) is critical for *CLV3* expression and stem cell homeostasis. Taken together, these results suggest that both a precise number of cis-elements and relative affinities could be important in regulating *CLV3*. To test further the relationship between cis-element affinity and the number of cis-elements, we analyzed the intrinsic activity of the synthetic higher affinity mutant, 970-M4. To analyze the effect of intrinsic activity of 970-M4, we mutated the remaining four cis-elements in the CRM which will be referred to as 970-M4I. The expression of the 970M4I reporter was largely found in the inner layers at much higher levels (n = 16) and complemented the *clv3* null mutants significantly better than the 970-M4 (Fig. 3.3C, 3.4 and 3.5) (n = 26). This analysis shows that the higher affinity-induced repression of 970M4 requires additional cis-elements in the CRM. Taken together, our analysis thus far shows that the intrinsic WUS binding affinity of cis-elements is not sufficient to define the spatial regulation of *CLV3*, however cis-element affinity becomes important in the context of other functioning cis elements in the CRM. This would explain why the mutation that abolished WUS binding to the higher affinity cis-element

(970M) altered *CLV3* expression more drastically than the individual mutations in relatively lower-affinity cis elements.

Collective activity of the CRM is required for both sensitivity and spatial regulation of *CLV3*. The number of cis elements may also determine the sensitivity of the promoter to WUS levels in addition to regulating spatial expression, which could be important in regulating *CLV3* expression under fluctuating WUS levels. Our previous work shows that it is not possible to increase or decrease overall levels of the WUS protein evenly across SAMs due to the intricate spatial regulation of the protein (Rodriguez et al., 2016). This is further complicated as a sustained increase or decrease of the WUS protein levels also lead to effects on the CZ identity. (Yadav et al., 2013). Therefore, we measured the temporal response of the mutant promoters lacking several WUS-binding cis elements as a function of time by using the ubiquitously expressed dexamethasone (Dex)-inducible form of WUS (35S::WUS-GR). Our previous work using the 35S::eGFP-WUS-GR shows that Dex application led to nuclear accumulation and immediate destabilization of the protein in the CZ within 6hrs (Rodriguez et al., 2016). By 24hrs of Dex application, the protein was only detected in the nuclei of cells in the edge of the PZ and in deeper cell layers of the RM. This dynamically destabilizing system creates distinct domains of WUS protein levels in space and time without compromising the CZ identity, thus forming a better system to carry out the temporal analysis of the dosage sensitivity of the mutant promoters. As shown earlier, upon Dex application, the wild type *pCLV3* expression increased in the CZ and expanded radially across cell layers L1 to L3, reaching the lateral edge of the PZ by 48hrs (Fig. 3.6 A-F and Perales et al., 2016). The mutant promoter lacking the two functional WUS-binding cis elements (970 and 997)-*pCLV3(TM)::H2b-*

mYFP was initially expressed in the deeper cell layers at expression levels below that of the wild-type promoter (Fig. 3.6 G and H). After 24hrs Dex application *pCLV3(TM)* was weakly activated in the CZ but failed to expand into the PZ (Fig. 3.6 I and J) (n = 8). By 48hrs after Dex application, *pCLV3(TM)* expression slightly expanded into the PZ and the expression also expanded into the deeper basal L3 layers. In addition, expression levels were found to fluctuate in adjacent cells (Fig. 3.6 K and L). The mutant promoter lacking four cis-elements (950M, 970M, 997M, and 1060M)-*pCLV3(1007I)::H2b-mYFP* was expressed only in the deeper layers (Fig. 3.6 M and N). After 24hrs of Dex application, the mutant promoter was mildly upregulated in deeper layers, however it failed to expand radially (Fig. 3.6 O and P) (n = 8). By 48hrs after Dex application, the expression expanded only into the basal L3 layers and expression levels were found to fluctuate in adjacent cells leading to “spotty” appearance (Fig. 3.6 Q and R). Considering that the WUS protein levels deplete in outer cell layers more rapidly than in inner layers upon Dex application, the behavior of the mutant promoters suggests that all five cis-elements are required to achieve rapid activation in outer cell layers and consistent repression in inner layers. The misexpression of the *pCLV3-TM* and *pCLV3-1007I* in the basal L3 layers compared to the wild type promoter shows that the CRM translates WUS levels into transcriptional activation or repression.

The intrinsic behavior of cis-elements is altered in *clv3* null mutants. Our previous work has shown that a range of mutant promoters starting with the high affinity promoters (970-M1 and 970-M4), which repress *CLV3* and the weak promoters (the *pCLV3-TM* and *pCLV3-SM*) that fail to express *CLV3* in outer layers are reactivated in the L1 layer of *clv3-2* mutants (Perales et al., 2016). A similar reactivation of the *pCLV3-1007I*

was also observed in *clv3-2* mutants (Fig. 3.7) (n =8). The same pCLV3-1007I failed to express in the L1 layer of dex-treated *35S::WUS-GR*, suggesting that it falls below the detection threshold due to a higher destabilization of WUS-GR in the outer cell layers. The difference in the response patterns of the same pCLV3-1007I in these two conditions suggests that the L1 layer of *clv3-2* mutants may only contain the activatable form of WUS. This notion is supported by the reactivation of the higher affinity mutant promoters (970-M1 and 970-M4) that readily dimerize (Perales et al., 2016) and the expression of mutant promoter with just the intrinsic activity of cis-elements (*pCLV3-1007I*) only in outer layers of *clv3-2* mutants (Fig. 3.7). WUS protein accumulates at extremely low levels in the L1 layer and at extremely high levels in the inner layers of *clv3-2*, which alone can not explain the differences in expression patterns of the mutant promoters in *clv3* null mutants (Perales et al., 2016). In addition to the differences in WUS protein levels, it is possible that the WUS protein gradient may be extensively reorganized to produce only the activatable form of WUS in the L1 layer while the inner layers either lack the activatable form of WUS. Alternatively it is possible that extremely high levels of WUS due to higher synthesis may repress the mutant promoters.

Discussion:

A homotypic cluster of 5 cis-elements with varying affinities is critical to sense WUS levels and determine *CLV3* levels and spatial expression, that is *CLV3* activation in regions of low WUS accumulation and *CLV3* repression in regions of high WUS accumulation. All five elements collectively play a role in interpreting WUS levels in regulating *CLV3* expression. The relative affinities of each element and the number of cis-elements contributes to the collective effect. Within a CRM, cis-element affinities can

influence the activation and repression of *CLV3* in response to the WUS gradient. The number of elements also contributes to the collective effect observed in a CRM, which in turn determines the spatial-temporal expression and robustness of the response to the WUS concentration gradient. The overall sensitivity is sufficient to transform the shallow and noisy WUS protein gradient into relatively sharp windows of activation and repression. It is possible that the collective activity of the CRM could arise because of cooperative binding of WUS binding to neighboring cis-elements. WUS was previously shown to form a mixture of monomers, dimers, and oligomers in solution over a wide concentration range (Perales et al., 2016). Moreover, DNA/cis-elements have been shown to promote dimerization or multimerization of WUS over a small 2-4 fold increase in WUS level. This concentration-dependent dimerization/multimerization on each cis-element could allow the formation of higher order complexes with neighboring elements. Such a cooperative behavior was observed for the LEAFY transcription factor (Sayou et al., 2015). Similar to WUS, LEAFY has two dimerization domains, one of which is near the DNA binding domain and the other outside the DNA binding domain. The second dimerization domain allows for protein-protein interaction across neighboring cis-elements, which then allows for cooperative binding across the cis-elements. Cooperativity across cis elements could explain how the increase in affinity of 970 was able to change the CRM function from activation to repression at lower WUS concentrations, only in the context of the whole CRM. The tighter binding of WUS to 970-M4 could induce a better cooperative binding to the neighboring cis-elements leading to a repressed state. Further biochemical tests of the DNA-protein interactions across multiple cis elements is required to determine the binding behavior of WUS to neighboring cis elements.

Homotypic CRMs are widespread, however among the few that have been characterized *CLV3* CRM is unique. CRMs have been shown to control spatial activation of genes in response to graded transcription factor levels (Driever et al., 1989; Gaudet and Mango, 2002; Jiang and Levine, 1993; Rowan et al., 2010; Struhl et al., 1989). Co-operative interactions among cis-elements within the BICOID (BCD)-binding CRM in the *HUNCHBACK (HB)* enhancer region have been shown to improve overall binding affinity (Ma et al., 1996). This may be important in inducing a threshold response to activate *HB* expression in regions of lower BCD levels in *Drosophila* embryos. On the other hand, TF binding sites in the CRM have been shown to act non-cooperatively to mediate a linear response to graded TF levels (Driever and Nüsslein-Volhard, 1989; Gaudet and Mango, 2002; Rowan et al., 2010; Giorgetti et al., 2010). In both these cases, increasing the binding affinities of cis-elements led to stronger activation or increased the domain of expression of target genes. A recent study of the *Drosophila SHAVENBABY* homotypic CRM shows that increasing the binding affinity of one of the cis-elements resulted in a strong ectopic activation suggesting that low-affinity homotypic CRMs may lead to higher specificity (Crocker et al., 2015).

The *CLV3* CRM, in mediating the activation-repression switch, is unique when compared to previously studied enhancers and CRMs that work to express genes in a pattern that does not follow the French flag model (Wolpert et al., 1969). The first case discussed above places *Rho* expression away from the highest Dorsal accumulation through the use of additional co-regulators that also bind DNA to form a heterotypic cluster (Ip et al., 1992a; Jiang and Levine, 1993). In regions of high nuclear accumulation, Dorsal activates a co-repressor by binding the low-affinity cis elements in the CRM. The

coactivator utilizes multiple cis elements with specific affinities to expand its expression domain past the repressor (Jiang et al., 1991). This ultimately leads to repression of *Rho* in regions of high Dorsal accumulation and activation in regions of low Dorsal accumulation (Ip et al., 1992a; Jiang and Levine, 1993). The second case discussed uses a homotypic cluster of three low-affinity cis elements in the (DPP) enhancer, which are recognized by a single transcription factor, to express DPP in regions of low concentration of the transcriptional activator (Parker et al., 2011). Limiting the expression of DPP in the region of high Ci concentration is achieved through the use of an additional co-regulator. The activation of DPP is regulated by a homotypic cluster recognized by the Ci transcription factor. Hedgehog signaling in a concentration dependent manner modifies Ci to produce of an activated form (Ci^{ACT}), closer to the source of signaling and a repressive form (Ci^{REP}), away from the source of signaling (Méthot and Basler, 1999; Aza-Blanc et al., 1997). Thus the two forms of Ci make opposing gradients that compete for the same binding sites. The cooperative binding of Ci^{REP} to the CRM produces high affinity binding in the region of intermediate concentration leading to the repression of DPP (Parker et al., 2011). Converting them into low affinity elements or reducing the number of elements decreases cooperativity, leading to the expression of DPP in the region of intermediate concentration (Parker et al., 2011). The co-operative binding of WUS to the *CLV3* CRM is required for both activation at lower WUS and repression at higher WUS concentration. No additional regulator has been shown to bind the *CLV3* CRM. The intrinsic activity, which can be interpreted as loss of co-operativity, shifts the expression maxima of *CLV3* towards the RM in the wild-type background, which suggests that the concentration of both activating and repressing forms of WUS are highest in the RM. Although there may be similarity between WUS and Ci in using the activating and repressing forms, in the case

of WUS both these forms must produce overlapping gradients that originate from the RM and extend into the L1. Although there is no biochemical evidence to support the theory of activating and repressing forms of WUS, the curious case of the expression behavior of cis-element mutants in *clv3* null mutants discussed below hints at this possibility.

CLV3 signaling could be involved in a feedback that modifies the WUS protein state in addition to traditional transcription repression of the WUS promoter.

Traditionally, the CLV3-mediated receptor kinase signaling has been shown to repress *WUS* transcription in the RM (Clark et al., 1997; Brand et al., 2000). Therefore, *clv3* null mutants express *WUS* at higher level and the expression moves up into the L2 layer (Fiers et al., 2006). Despite higher accumulation of the WUS protein in the RM of *clv3* null mutants, it fails to accumulate at a higher level in the L1 layer, thus forming a much steeper difference in WUS levels between cell layers than what was observed in the case of wild type condition (Perales et al., 2016). Our results show that cis-element mutants that either increase or decrease WUS binding express mostly in the L1 layer of *clv3-2* mutants. This suggest that the L1 layer of *clv3-2* mutants must contain only the activating form of WUS. This could arise as a result of higher levels of instability of WUS protein, which can explain the levels observed in *clv3-2* mutants (Rodriguez et al., 2016, Perales et al., 2016). This suggests that wild-type levels of CLV3 signaling may be required for stabilizing the WUS protein, thus balancing the stable (repressing) and unstable (activating) forms. In such a scenario, the repressing form may compete with activating form for the same cis-elements in all cell layers while the relative ratios favor activation in outer layers and repression in inner layers. Alternately, lower WUS accumulation in the L1 layer of *clv3-2* could be explained by reduced rate of diffusion from the inner layers due to higher protein levels

that can form larger aggregates. However, limitation of WUS protein in the L1 layer fails to explain the activation of *CLV3* mutant promoters that bind WUS poorly. Therefore, we favor an activating/repressing WUS forms as a model which can be achieved through either protein instability to generate a non-dimerizable form of WUS or a WUS form that fails to engage repression machinery. It is also possible that higher protein instability is coupled to transcriptional activation. This phenomenon is referred to as “unstable when active” (Muratani and Tansey, 2003) has been shown to operate in the case of Aryl hydrocarbon receptor (Ma and Baldwin, 2000), Transforming Growth Factor- β activated SMAD2 (Lo and Massagué, 1999) and Interferon-gamma activate STAT1 (Kim and Maniatis, 1996). This mechanism has been postulated to provide tighter control of transcription by regulating the local concentration of TFs. It is also interesting to note that almost all of the unstable TFs in eukaryotes and eubacteria (reviewed in Muratani and Tansey, 2003) use their transcriptional activation domains (TADs) as degradation signals (degrons). Our previous analysis shows that the Dex-induced nuclear translocation of eGFP-WUS-GR immediately destabilized the protein, which in turn resulted in *CLV3* activation showing a link between protein instability and transcriptional activation (Perales et al., 2016; Rodriguez et al., 2016). The same study also revealed that the C-terminal 63 amino acid stretch of WUS, which is required for protein instability also contains transcriptional regulatory domains: an acidic region, the WUS-box and the EAR-like motif. This suggests that the transcriptional activity and destruction of WUS may be coupled. Therefore, high concentration of WUS in the deeper layers may reduce protein turnover, which in tandem with the CRM co-operativity, may produce higher levels of repression. On the other hand, in outer cell layers, a relatively higher turnover of WUS may lead to *CLV3* transcription. This further shows the protein degradation, the activation of *CLV3* and

hence the CLV3 signaling are linked. Thus, higher WUS levels repress *CLV3* expression, which will lead to higher WUS transcription, however, it also leads to instability of WUS, which in turn activates *CLV3* transcription to stabilize the WUS protein (Fig. 3.8).

The affinity and number of cis-elements acting in concert to interpret different TF levels to achieve spatial spatio-temporal regulation of gene expression is novel. The lessons learned from the *CLV3* CRM regulation will be useful to predict expression patterns of the other genes in the WUS-regulated network in future work (Yadav et al., 2013). For example, do WUS-regulated genes expressed in the RM utilize weaker CRMs? Are those that are repressed, whose expression is limited to the PZ, utilize much stronger CRMs to sense lower WUS levels? The next big goal is to understand how WUS regulates some of these genes. Analyzing the regulatory sequences should provide some clues to the cis-element code utilized to translate the WUS protein levels into transcriptional output. In *Solanum lycopersicum* (Xu et al., 2015), *Glycine max* (Wong et al., 2013) and *Lotus japonicus* (Okamoto et al., 2011), *CLV3* expression overlaps with that of WUS in deeper cell layers. Whether this difference with *Arabidopsis* is due to the cis-element regulation and its significance to WUS regulation and stem cell homeostasis must be probed in future studies.

Acknowledgments

We thank Vanessa Ceja, Dariush Neja, Isabel Gutierrez, Valery Franco, Paul Rubiro and Kyle Hill for supporting experimental work, Alex Plong for model in Fig. 3.8, and members of the Reddy lab for comments on the manuscript. This work was supported by the National Science Foundation Grant IOS-1456725 to G.V.R.. The authors declare no competing financial interest.

Authors contribution

KR, MP and GVR conceived research, analyzed the data and performed experiments. KR and GVR wrote the paper. All the authors edited and approved the final version of the manuscript.

M.P. Present address: Centro de Biotecnología y Genómica de Plantas, Universidad Politécnica de Madrid (UPM)–Instituto Nacional de Investigación y Tecnología Agraria y Alimentaria (INIA) Campus Montegancedo UPM, Pozuelo de Alarcón, Madrid, 28223, Spain.

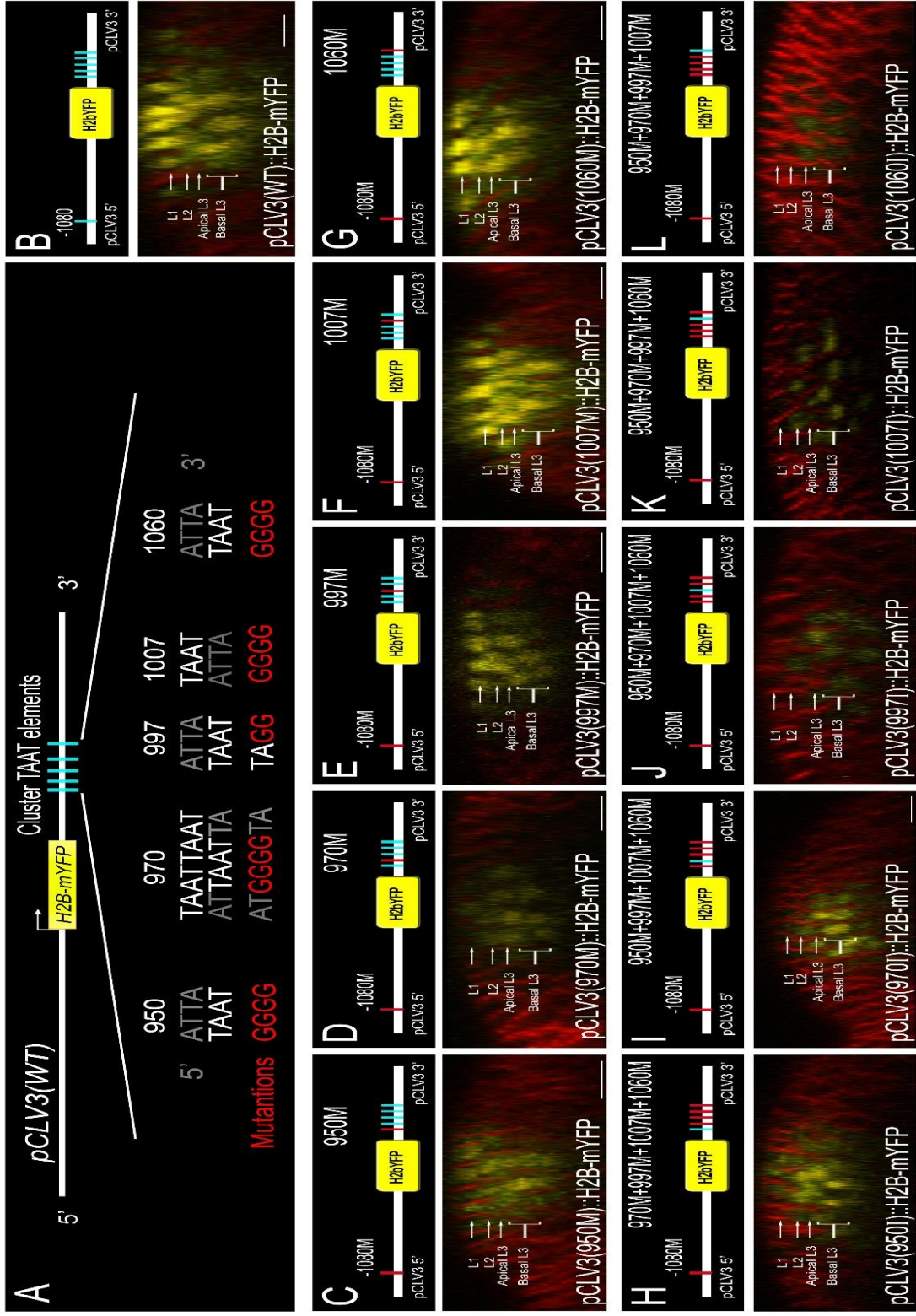


Fig. 3.1. The CRM context determines the cis element's ability to interpret the WUS dependent transcriptional discrimination. (A) Schematic of the CLV3 promoter expressing the Histone 2B modifiedYFP(H2B-mYFP) reporter construct with cis elements of the CRM annotated by cyan bars. Sequences of the wild type (White) and loss of binding cis-element mutation (Red) which, were used in the following panels. Schematic representations of the reporter constructs are annotated with wild-type (cyan) and mutant (red) cis elements above their respective inflorescence meristems. Side view of inflorescence SAM of wild-type pCLV3 (B). Side views of inflorescence SAM of independent loss of binding mutations on 950 cis element [pCLV3(950M)::H2B-mYFP] (C), 970 cis element [pCLV3(970M)::H2B-mYFP] (D), 997 cis element [pCLV3(997M)::H2B-mYFP] (E), 1007 cis element [pCLV3(1007M)::H2B-mYFP] (F), and 1060 cis element [pCLV3(1060M)::H2B-mYFP](G). Side views of inflorescence SAM of promoters with 4 of 5 elements with loss of binding mutations: mutations on 970, 997, 1007 and 1060 [pCLV3(950I)::H2B-mYFP] n =12 (H), mutations on 950, 997, 1007, and 1060 [pCLV3(970I)::H2B-mYFP] n =15 (I), mutations on 950, 970, 1007, and 1060 [pCLV3(997I)::H2B-mYFP] n =13 (J), mutations on 950, 970, 997, and 1060 [pCLV3(1007I)::H2B-mYFP] n =14 (K), mutations on 950, 970, 997, and 1007 [pCLV3(1060I)::H2B-mYFP] n = 13 (L). Independent mutations show mild misexpression for each cis element. However, the intrinsic expression of each element is limited to the RM where WUS concentration is the highest. Results are representative of the number of independent lines analyzed (n) for each reporter version. Reporter H2B-mYFP expression is shown in yellow and cell walls are stained with FM4-64 (Red). The three clonal layers in SAMs are marked as L1, L2, Apical L3 and Basal L3. Scale bar = 10 μ m.

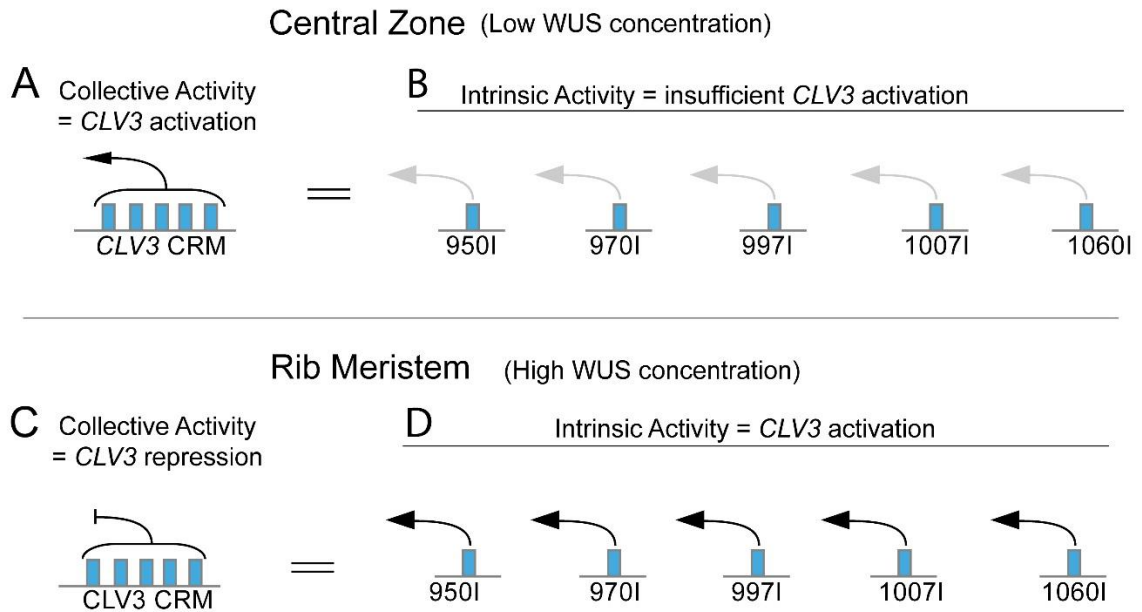


Fig. 3.2. Model of interaction among elements in *CLV3* CRM. Low WUS protein concentration in the central zone leads to activation of *CLV3* from a CRM with 5 elements (A) while the CRM mutants that only contain 1 element are unable to achieve a robust expression of *CLV3* (B). High WUS levels in the rib meristem lead to repression of *CLV3* from the CRM with 5 elements (C) while the CRM mutants that only contain 1 element activate *CLV3* expression (D).

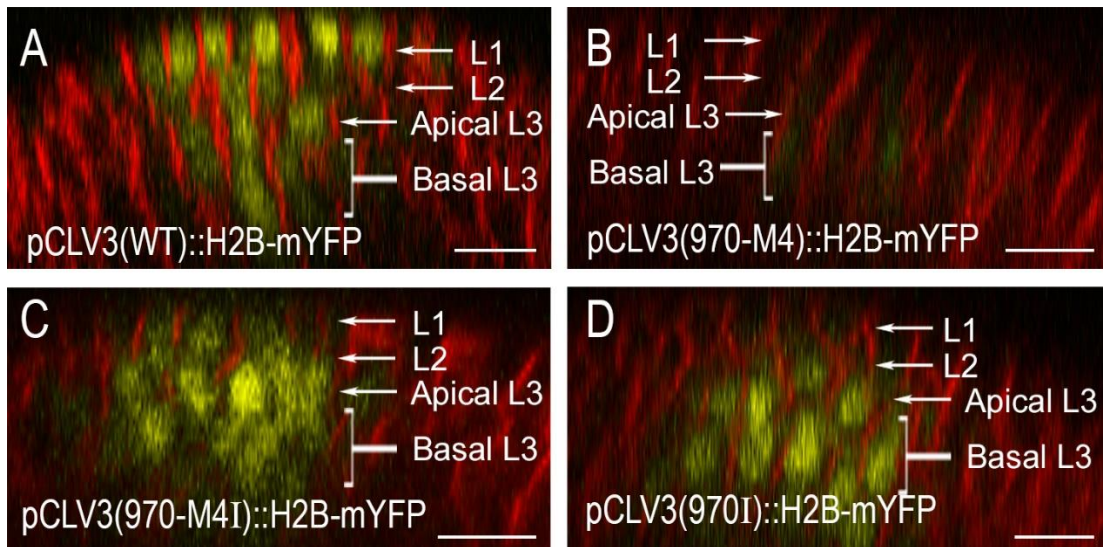


Fig. 3.3. Affinity and integrated signaling from all elements determine expression level and domain. Side views of inflorescence SAM of wild type [*pCLV3(WT)::H2B-mYFP*] (A), high-affinity mutant [*pCLV3(970-M4)::H2B-mYFP*] (B), high-affinity mutant and loss of binding mutations on 950, 997, 1007, and 1060 [*pCLV3(970-M4I)::H2B-mYFP*] (C), and loss of binding mutations on 950, 997, 1007, and 1060 [*pCLV3(970I)::H2B-mYFP*] (D). Results are representative of the number of independent lines analyzed (n) for each reporter version. Reporter H2B-mYFP expression is shown in yellow and cell walls are stained with FM4-64 (Red). The three clonal layers in SAMs are marked as L1, L2, Apical L3 and Basal L3. Scale bar = 10 μ m.

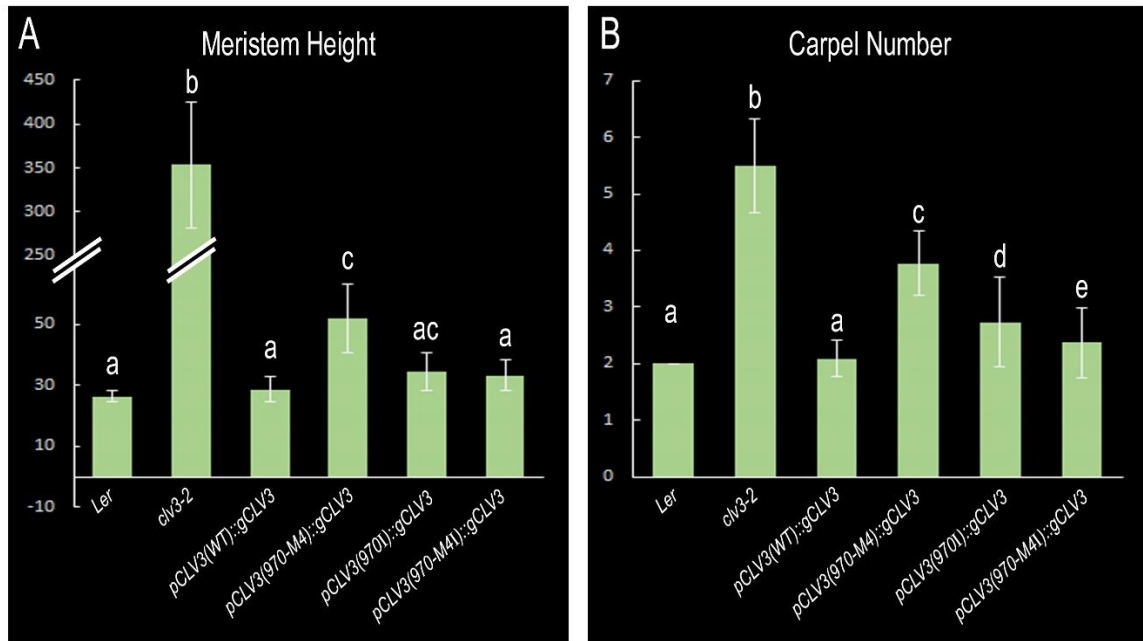


Fig. 3.4. Complementation analysis of *clv3-2* with mutant constructs. The phenotypic complementation analysis with the genomic *CLV3* (*gCLV3*) region expressed from mutant promoters. The inflorescence meristem height (A) and the number of carpels (B) in *clv3-2* plants transformed with wild type *CLV3* promoter [*pCLV3(WT)::gCLV3*] and various *CLV3* mutant promoters: high-affinity mutation 970-M4 [*pCLV3(970-M4)::gCLV3*], loss of binding mutations on 950, 997, 1007, and 1060 [*pCLV3(970I)::gCLV3*], high-affinity mutation 970-M4 and loss of binding mutations on 950, 997, 1007, and 1060 [*pCLV3(970-M4I)::gCLV3*]. The error bars represent SE. Different letters indicate statistical differences between cis lines ($P < 0.001$) as determined by the Tukey's Honest Significant Difference (HSD) tests.

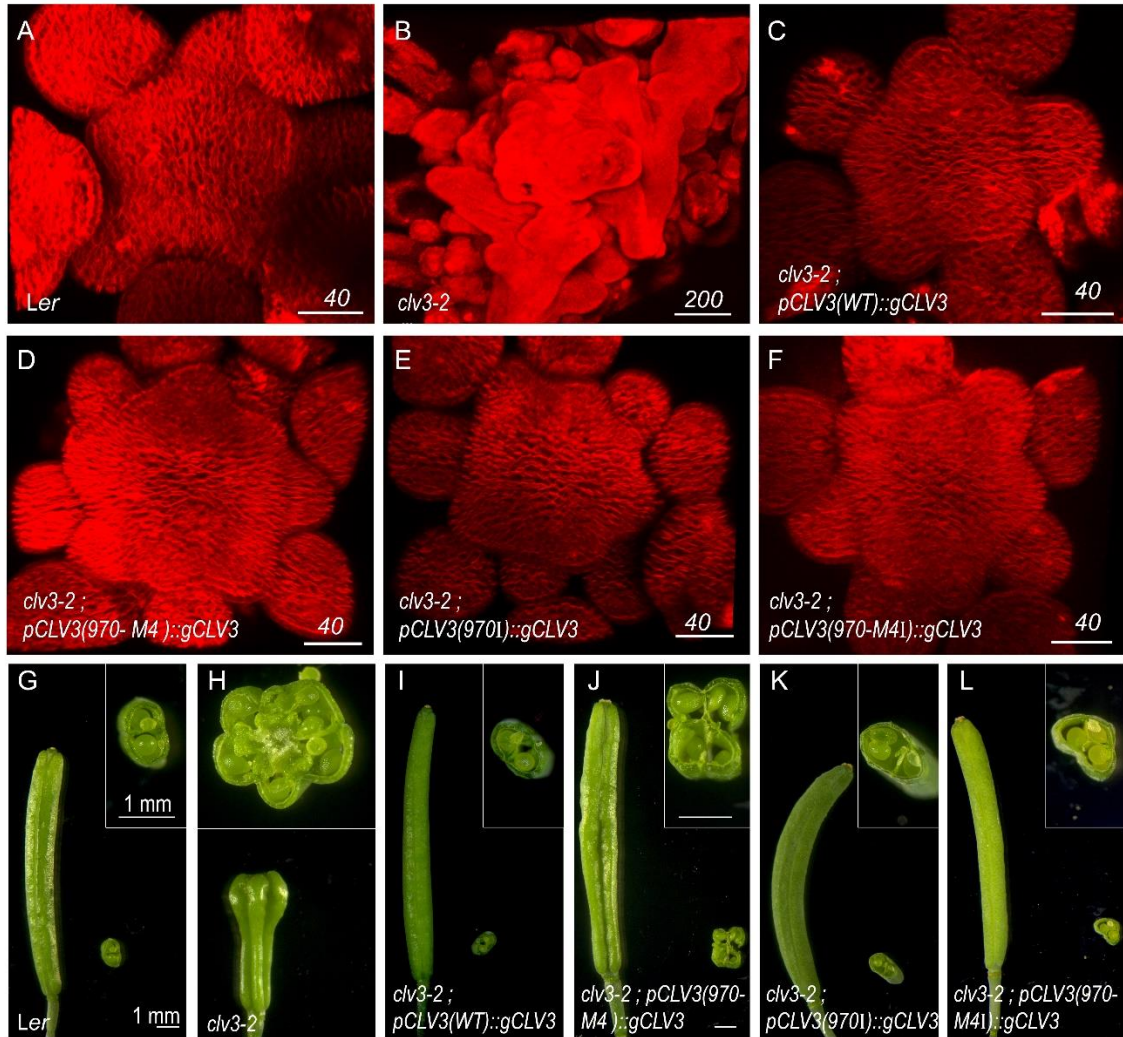


Fig. 3.5 Complementation of *clv3-2* with mutant *pCLV3* construct. (A-F) Top views of 3D-reconstructed meristems stained with cell wall dye FM4-64 (Red). Wild type (A), *clv3-2* (B) and *clv3-2* complemented with wild type genomic *CLV3* (*gCLV3*) driven from the *CLV3* promoter with CRM variants, wild type [*pCLV3(WT)::gCLV3*] (C), high affinity mutant [*pCLV3(970-M4)::gCLV3*] (D), loss of binding mutation on 950, 997, 1007, and 1060 [*pCLV3(970I)::gCLV3*] (E), and high-affinity mutation 970-M4 and loss of binding mutations on 950, 997, 1007, and 1060 [*pCLV3(970-M4I)::gCLV3*] (F). (G-L) Side view of intact siliques and cross section of sliced siliques. Insets show a higher magnification view of the cross section of the sliced siliques. Wild type (G), *clv3-2* (H) and *clv3-2* complemented with wild type genomic *CLV3* driven from the *CLV3* promoter with CRM variants, wild type [*pCLV3(WT)::gCLV3*] (I), high affinity mutant [*pCLV3(970-M4)::gCLV3*] (J), loss of binding mutation on 950, 997, 1007, and 1060 [*pCLV3(970I)::gCLV3*] (K), and high-affinity mutation 970-M4 and loss of binding mutations on 950, 997, 1007, and 1060 [*pCLV3(970-M4I)::gCLV3*] (L). Scale bars (A-F) are given in μm and (G-L) are given in mm in each image.

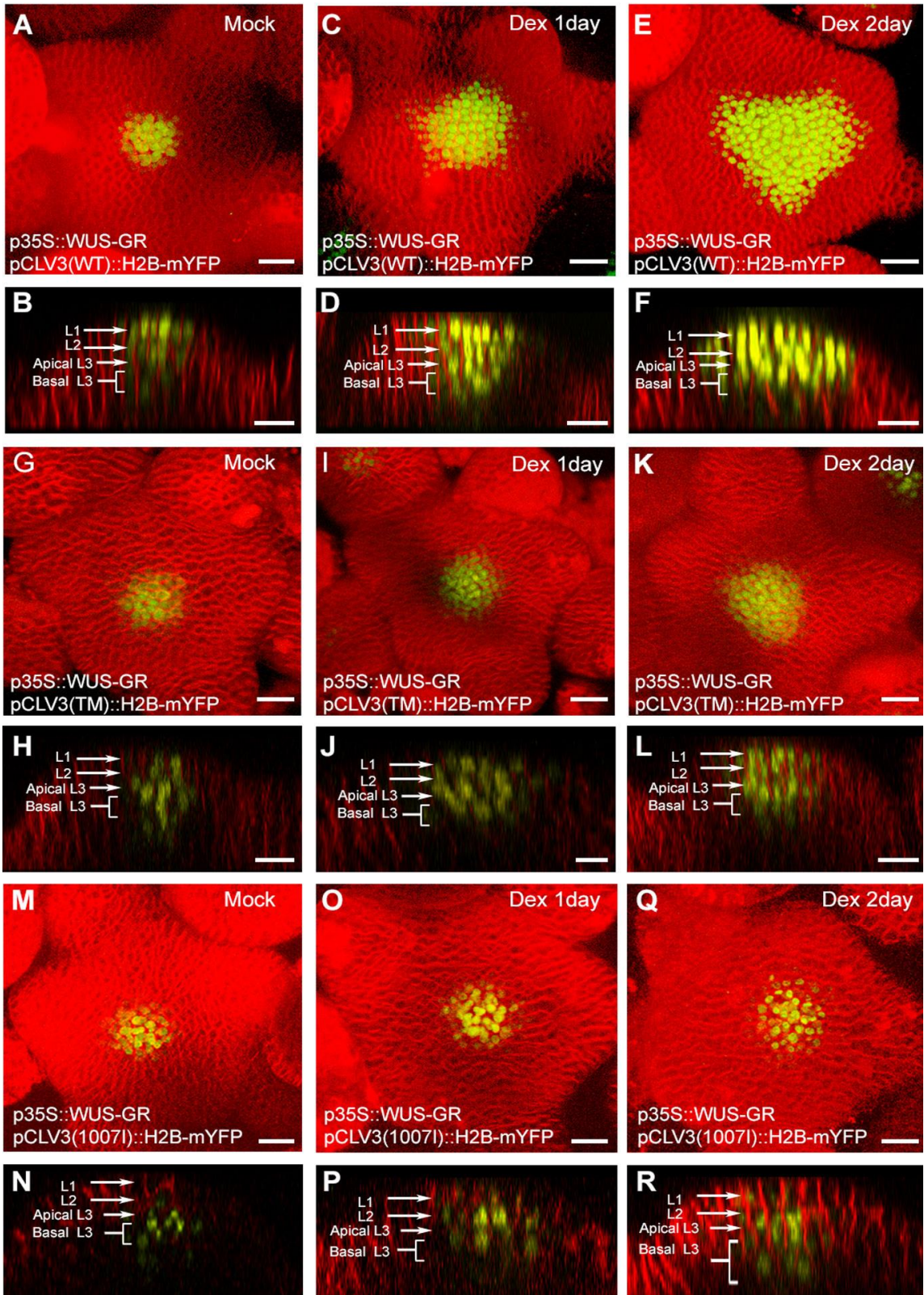


Fig. 3.6. Expression of reporters upon ubiquitous overexpression of WUS protein. Response of wild type [*pCLV3(WT)::H2B-mYFP*] (A-F), loss of binding mutations on 970 and 997 [*pCLV3(Triple Mutant)::H2B-mYFP*] (G-L) and loss of binding mutations on 950, 970, 997, and 1060 [*pCLV3(1007I)::H2B-mYFP*] (M-R) to *p35S::WUS-GR* upon Mock treatment (column 1) and Dex application for 1 day (column 2) and 2 day (column 3). Dex treatment of *pCLV3(WT)* leads to expansion of robust expression into the L3 and PZ within 2 days. Dex treatment of *cis*-element mutant constructs leads to spotty expansion into L4 and L5. (A), (C), (E), (G), (I), (K), (M), (O) and (Q) are 3D top views and corresponding side views are shown in (B), (D), (F), (H), (J), (L), (N), (P) and (R). H2B-mYFP (Yellow). Cell walls are stained with FM-4-64 dye (Red); The three clonal layers in SAMs are marked as L1, L2, Apical L3 and Basal L3. Scale bar = 20 μ m.

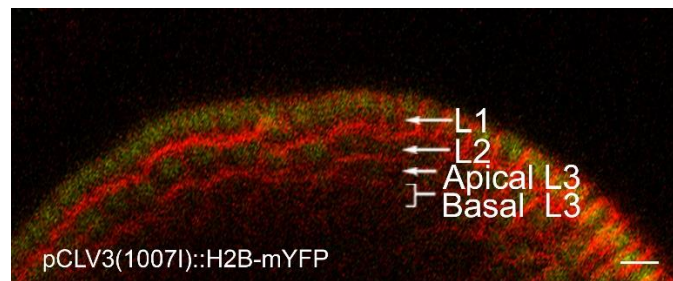


Fig. 3.7. Expression of reporters from 1007I mutant promoter in *cv3-2* background. Side view of *cv3-2* inflorescence meristem showing H2B-mYFP reporter expression (Yellow) driven *CLV3* promoter with loss of binding mutations on 950, 970, 997, and 1060 [*pCLV3(1007I)::H2B-mYFP*]. Meristem stained with cell wall dye FM4-64 (Red). The three clonal layers in SAMs are marked as L1, L2, Apical L3 and Basal L3. Scale bar = 20 μ m.

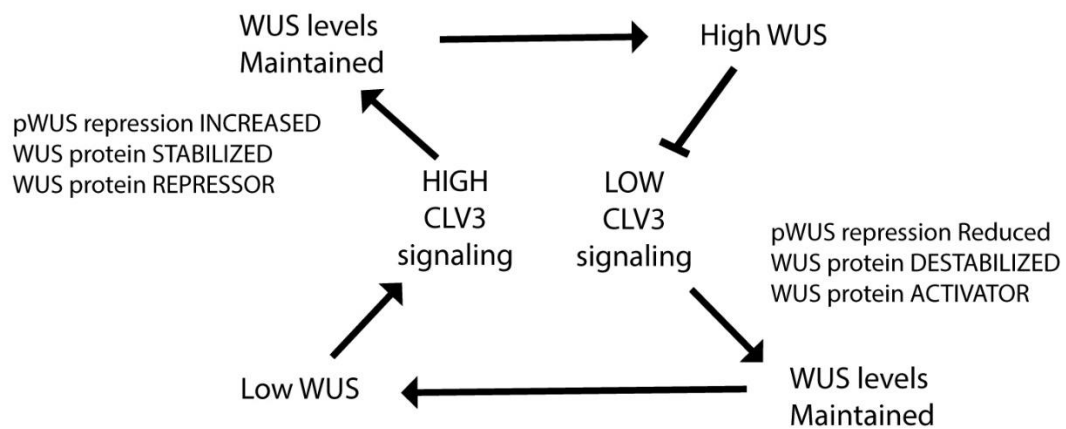


Fig. 3.8. WUS and CLV3 regulatory loops. CLV3 regulates transcriptional expression from the *WUS* promoter and post-translational regulation of WUS protein. WUS activates and represses *CLV3* promoter in a concentration dependent manner. A spike in the CLV3 levels leads to repression of *pWUS* which drops the WUS levels. The WUS protein is post-translationally regulated to function as a stronger repressor and is stabilized in the outer layers. The high levels of WUS (repressive forms) repress *CLV3* and so restores CLV3 levels back to normal. On the other hand, a depletion of CLV3 levels leads to loss of *pWUS* repression. Although there is more production of *WUS*, the WUS protein is post-translationally regulated to be unstable and is a strong activator. The high levels of WUS (activator form) activates *CLV3* promoter and so restores CLV3 levels back to normal.

CHAPTER 4:

DNA-dependent homodimerization, sub-cellular partitioning, and protein destabilization control WUSCHEL levels and spatial patterning

The text of chapter 4 in this dissertation, in whole, is a reprint of the material as it appears in: **Rodriguez K**, Perales M, Snipes S, Yadav R, Diaz-Mendoza M, and Reddy GV. (2016) DNA-dependent homodimerization, sub-cellular partitioning, and destabilization control WUSCHEL levels and spatial patterning. Proc Natl Acad Sci USA 113:E6307-E6315. The co-author Reddy GV. listed in that publication directed and supervised the research which forms the basis for this dissertation.

Abstract

The homeodomain transcription factor WUSCHEL (WUS) promotes stem cell maintenance in inflorescence meristems of *Arabidopsis thaliana*. WUS, which is synthesized in the rib meristem, migrates and accumulates at lower levels in adjacent cells. Maintenance of WUS protein levels and spatial patterning distribution is not well-understood. Here, we show that the last 63-aa stretch of WUS is necessary for maintaining different levels of WUS protein in the rib meristem and adjacent cells. The 63-aa region contains the following transcriptional regulatory domains: the acidic region, the WUS-box, which is conserved in WUS-related HOMEODOMAIN family members, and the ethylene-responsive element binding factor-associated amphiphilic repression (EAR-like) domain. Our analysis reveals that the opposing functions of WUS-box, which is required for nuclear retention, and EAR-like domain, which participates in nuclear export, are necessary to maintain higher nuclear levels of WUS in cells of the rib meristem and lower nuclear levels in adjacent cells. We also show that the N-terminal DNA binding domain, which is required for both DNA binding and homodimerization, along with the homodimerization sequence located in the central part of the protein, restricts WUS from spreading excessively and show that the homodimerization is critical for WUS function. Our analysis also reveals that a higher level of WUS outside the rib meristem leads to protein destabilization, suggesting a new tier of regulation in WUS protein regulation. Taken together our data show that processes that influence WUS protein levels and spatial distribution are highly coupled to its transcriptional activity.

Introduction

Inflorescence meristems (IMs) harbor a set of pluripotent stem cells in the central zone (CZ) (Steeves et al., 1989). A subset of stem cell progeny that are displaced into the adjacent peripheral zone (PZ) differentiate as lateral organs whereas those that are displaced into the rib meristem (RM), located beneath the CZ, differentiate and become part of the stem (Steeves et al., 1989). The inflorescence meristems are organized into three cell layers that are clonally distinct; the outermost-L1 and the subepidermal-L2 form monolayers, together referred to as the tunica (Steeves et al., 1989). The cells located beneath the L2 layer are collectively referred to as the L3 layers/corpus (Steeves et al., 1989).

In *Arabidopsis* inflorescence meristems, WUSCHEL (WUS), a homeodomain transcription factor (TF) synthesized in a few cells of the RM/L3/corpus (Laux et al., 1996; Mayer et al., 1998), migrates into adjacent cells (Yadav et al., 2011). WUS accumulates at a lower level in the nuclei of cells in the L1 and L2 cell layers compared with the inner layers (Fig. 4.1 A–D) (Yadav et al., 2011). WUS protein also diffuses radially and accumulates at a lower level in the peripheral zone (Yadav et al., 2011). WUS regulates its own transcript levels by activating CLAVATA3 (CLV3) in the central zone (Schoof et al., 2000). CLV3, a secreted peptide, activates a receptor kinase pathway to restrict WUS transcription (Clark et al., 1997; Fletcher et al., 1999; Brand et al., 2000; Kondo et al., 2006). Previous studies have shown that ectopic activation of WUS in the central zone leads to meristem overproliferation (Brand et al., 2002; Yadav et al., 2010). Conversely, the depletion of WUS leads to premature differentiation of stem cell progeny (Yadav et al., 2010; Müller et al., 2006; Yadav et al., 2013), showing the importance of the regulation of WUS protein levels.

The processes and mechanisms that control differences in WUS protein accumulation between cells of the rib meristem and adjacent cells are not well-understood. The predominant models for protein gradient formation in animal systems involve processes that control the amount of protein synthesis in the source, the rate of diffusion or movement of the protein, and degradation rates (Roger et al., 2011). The rate of protein diffusion or movement can be influenced by several factors, such as the constraints imposed by the subcellular compartments, the size of the protein, and the nature of its interactions with other molecules. Protein interactions can lead to the formation of homo-multimers or even hetero-multimers, which results in an increased size and decreased diffusion rates. In addition, the mobile proteins can form complexes with nonmobile molecules, such as the DNA or cytoskeleton elements, that can impede movement. Finally, the differential degradation rates of the protein in the source cells versus the surrounding cells can contribute to the differences in protein levels.

The factors and processes that can influence WUS movement are beginning to emerge. WUS is synthesized in the rib meristem, and its expression levels are limited by the receptor kinase signaling pathway mediated by the CLAVATA class of proteins (Mayer et al., 1998; Schoof et al., 2000; Clark et al., 1997; Fletcher et al., 1999; Brand et al., 2002). WUS diffuses into the adjacent CZ and the PZ where it accumulates at a lower level (Yadav et al., 2011). Transcription factors (TFs) in plants have been shown to migrate between cells through plasma membrane-lined pores in cell walls, plasmodesmata (PDs) (Crawford et al., 2000). Several aspects, such as the density and distribution of PDs, may influence the rate of protein movement; however, they are poorly studied in shoot meristems of *Arabidopsis*. The PDs have also been shown to have a size exclusion limit

(SEL), which allows movement of those TFs whose molecular size falls below the SEL (Crawford et al., 2000). Therefore, the size of WUS protein and the WUS containing protein complex may influence the rate of movement. An earlier study has shown that the movement of WUS from the rib meristem to adjacent cells could be inhibited by using a WUS protein of higher molecular weight (2XeGFP-WUS), suggesting that WUS likely moves between cells through plasmodesmata and that the SEL of PDs may influence mobility (Yadav et al., 2011). A later study used an alternate approach, involving overexpression of CALLOSE SYNTHASE 3 to reduce the pore size of PDs (Vatén et al., 2011), which also led to inhibition of WUS movement (Daum et al., 2014).

Earlier studies have shown that WUS can bind DNA, form homodimers, and interact with other proteins. WUS has been shown to homodimerize by using sequences between the N-terminal homeodomain and the C-terminal region (amino acids 100 to 249) (Daum et al., 2014). WUS lacking the homodimerization sequences not only complemented *wus-1* mutants but also caused meristem overproliferation, showing that homodimerization restricts meristem growth (Daum et al., 2014). An independent study has shown that WUS also interacts with HAIRYMERISTEM (HAM) proteins that are required for meristem maintenance (Schulze et al., 2010; Zhou et al., 2015). The HAM proteins have been shown to bind the WUS sequence located between amino acids 203 and 236 (referred to as the HAM binding domain) (Zhou et al., 2015). WUS lacking the HAM binding domain failed to complement the *wus-1* mutant defects, showing that this region of WUS is critical for its function in promoting stem cell specification and shoot apical meristem (SAM) growth (Zhou et al., 2015). Therefore, it is not clear whether homodimerization of WUS or HAM binding impedes WUS movement through the

formation of larger homo-complexes or hetero-complexes. It is also unclear how the overproliferation of meristems observed in an earlier study (Daum et al., 2014) was possible with a large deletion (amino acids 100 to 249) that removed a domain of WUS that is critical for HAM binding and WUS function.

The subcellular localization of WUS may also contribute to the observed differences in WUS protein accumulation between cells of the rib meristem and cells located in adjacent domains. An earlier study has shown that increased nuclear targeting of WUS impedes its mobility into the outer cell layers of inflorescence meristems, suggesting that nuclear-cytoplasmic partitioning plays a critical role in intercellular movement of WUS (Yadav et al., 2011). However, it is not known whether WUS protein contains intrinsic signals and/or whether any spatially localized factors exist that influence nuclear-cytoplasmic partitioning. Earlier studies have shown that ectopic overexpression of *WUS* in the central zone increases *CLV3* expression and promotes meristem overproliferation (Brand et al., 2002; Yadav et al., 2010). A straightforward logic from these experiments suggests that WUS protein instability in the central zone may not be a contributing factor to the observed differences in WUS protein levels.

To understand the processes and decipher the mechanisms that influence the observed differences in WUS protein accumulation, we have used structure-function analysis and transient studies involving a hormone-inducible form of WUS. Our analysis reveals that the homodimerization and DNA binding mediated by the N-terminal DNA binding domain, together with the central part of the protein, restrict WUS from spreading excessively in inflorescence meristems. We also find that homodimerization of WUS is

critical to promote meristem maintenance. The transcriptional regulatory domains located at the C terminus of WUS, the WUS-box and EAR-like domain, influence nuclear-cytoplasmic partitioning, thereby controlling the nuclear levels of WUS. Contrary to the perceived logic, we also find that ectopic overexpression of WUS destabilizes WUS protein, which adds another tier to the regulation of WUS protein levels. We discuss possible mechanisms and protein regulators that may influence multiple processes regulating WUS protein concentration, which is critical for transcriptional regulation and meristem maintenance [see Chapter 4].

Results:

A 63-aa Stretch at the C Terminus Is Sufficient for Spatial Patterning of WUS.

A simple diffusion of WUS protein from the site of synthesis, the rib meristem, into adjacent cells could theoretically account for the observed variation in nuclear levels (Fig. 4.1 A–D). However, we observed the uniform distribution of fluorescence signal when a free (untagged) eGFP (Fig. 4.1 E–H) ($n = 20$) or nuclear-localized eGFP (NLS-eGFP) (Fig. 4.1 I–L) ($n = 17$) was expressed from the WUS promoter described in an earlier study (Yadav et al., 2011). This result indicates that the cells of the inflorescence meristem are interconnected through their plasmodesmata. Thus, WUS may contain domains that limit its movement and are responsible for the observed variation in nuclear levels.

To identify the domains within WUS that are required to limit its movement and that determine its concentration in the nucleus, we expressed various truncations of WUS fused to eGFP from the WUS promoter. The deletion of the C-terminal half resulted in an intense and relatively uniform distribution of fluorescence in all cell layers, suggesting that the C terminus may contain information to control WUS spatial distribution (Fig. 4.1 M–P)

($n = 20$). A finer deletion within the C terminus showed that the last 63-aa stretch was sufficient to allow higher WUS accumulation in inner cell layers compared with the outer cell layers, showing that this part of the protein contains the necessary information to maintain spatial patterning of WUS protein in inflorescence meristems (Fig. 4.1 Q–T and Fig. 4.2 U–X) ($n = 12$).

Mutations in the WUS-Box and the EAR-Like Domains Disturb Subcellular Accumulation of WUS. Earlier work has shown that the C-terminal 63-aa stretch of WUS, which includes the acidic region, the WUS-box, and the EAR-like domains, is necessary for its biological function (Kieffer et al., 2006; Ikeda et al., 2009). Loss-of-function analyses in transient transcriptional assays carried out in leaf protoplasts have implicated the acidic region in transcriptional activation and the EAR-like domain and WUS-box in transcriptional repression (Ikeda et al., 2009). A recent study using the loss-of-function and domain complementation studies has demonstrated that WUS-box is a transcriptional repressor domain essential for stem cell maintenance (Dolzblasz et al., 2016). Nevertheless, their role in the regulation of spatial patterning of WUS protein is still unclear. Therefore, we investigated the role of these C-terminal domains in spatial patterning of WUS protein by generating individual deletions of each of the three domains, which resulted in destabilization (Fig. 4.2 A–L), except for a few cells of the RM that revealed a faint nuclear signal in the case of WUS-box domain deletion (Fig. 4.2H) and acidic region deletion (Fig. 4.2L). These results suggest that deletion of any one of the C-terminal domains exposes the signatures necessary for destabilization of WUS.

Because deletion of the three WUS domains destabilized the protein, we introduced point mutations in the WUS-box and the EAR-like domain (Fig. 4.3A). An earlier study has shown that the WUS-box contains two conserved amino acids at invariant positions (L255 and L257) in WOX family members (Ikeda et al., 2009). The L255A and L257A substitutions have been shown to abolish the biological functions of WUS, including the transcriptional regulation of the putative direct targets regulated by WUS: *CLV3*, *ARABIDOPSIS RESPONSE REGULATOR 5 (ARR5)*, *ARR6*, and *AGAMOUS* (Ikeda et al., 2009). The expression of eGFP-WUS carrying these same point mutations in the WUS-box (referred to as WBM) from the *pWUS* led to a dramatic non-nuclear accumulation of WUS (Fig. 4.4 M–O) ($n = 13$). These results suggested that WUS-box is required for either nuclear import or nuclear retention. The EAR-like domain, which has been shown to contribute to the transcriptional activity of WUS (Ikeda et al., 2009), also resembles nuclear export signals (NESs), which are characterized by the presence of a short patch of hydrophobic amino acids (Fig. 4.3B) (Haasen et al., 1999). Substituting hydrophobic leucine residues for alanine (L>A) has been shown to prevent nuclear exclusion (Haasen et al., 1999). The expression of eGFP-WUS protein with L>A substitutions (L287A, L289A, and L291A) from the WUS promoter [*pWUS::eGFP-WUS (EARLM)*] led to a relatively higher level of WUS protein in the L1 and the L2 layers, and the protein was detected in a wider region in all cell layers of the inflorescence meristems (Fig. 4.4 D–F and Fig. 4.3 M and N) ($n = 22$) compared with WT (Fig. 4.4 A–C and Fig. 4.3 E and I).

Of the 48 T1 plants that expressed *pWUS::eGFP-WUS* (*EARLM*), only 6 of them showed variable enlargement of inflorescence meristems (Fig. 4.3 F–H and J–L). The RNA in situ analysis, using a *WUS* antisense probe on enlarged inflorescence meristems, revealed the expansion of the *WUS* domain (Fig. 4.3 C and D) in inner cell layers, which ruled out misexpression of the *WUS* promoter in the outer cell layer. None of the *WBM* and *EARLM* double mutant plants developed larger inflorescence meristems, which is consistent with the requirement of the *WUS*-box in the regulation of transcriptional activity (Ikeda et al., 2009).

Because we observed nonnuclear accumulation of the *WBM*, we hypothesized that the opposing activities of the *WUS*-box and *EAR*-like domains might determine nuclear levels of *WUS*. To test this hypothesis, we expressed a double mutant of the *WBM* and *EARLM* from the *pWUS*, which resulted in nuclear accumulation and resembled the *WUS* distribution pattern observed in single *EARLM* (Fig. 4.4 S–U) ($n = 12$). Taken together, these results suggest that *WBM* can translocate into the nucleus but that it cannot be retained in the nucleus in the presence of a functional *EAR*-like domain, thus implicating the *WUS*-box in nuclear retention and the *EAR*-like domain in nuclear export.

Addition of an Exogenous Nuclear Localization Signal or Nuclear Exclusion Signals Supports the Roles of *WUS*-Box and *EAR*-Like Domains in Nuclear-Cytoplasmic Partitioning. The nonnuclear accumulation of the *WBM* may be either due to a lack of protein import into the nucleus or due to a lack of retention of the protein in the nucleus. To further investigate whether the *WUS*box functions in either nuclear retention or nuclear import, we expressed a *WBM* fused to a strong foreign nuclear localization

signal (NLS) from the WUS promoter. An earlier study has shown that addition of a strong NLS resulted in nuclear enrichment and limited protein mobility into the L1 layer (Yadav et al., 2011). The WBM that contained a strong NLS was not detected in the nucleus (Fig. 4.4 P–R) ($n = 6$), which supports that WBM is required for nuclear retention and not for nuclear import. The protein also failed to move into the L1 layer (Fig. 4.4P); this restricted distribution may be due to the efficient cycling of the protein into and out of the nucleus, which could limit the cytosolic pool.

To test further whether the EAR-like domain functions as a nuclear export signal (NES), we examined whether the EARLM can offset the nuclear export mediated by exogenous NES. The addition of an exogenous NES to WUS led to nonnuclear accumulation (Fig. 4.4 G–I) ($n = 24$). Conversely, the introduction of the EARLM into WUS carrying exogenous NES led to a nuclear accumulation of WUS in the L2 and L3 cell layers (Fig. 4.4 J–L) ($n = 12$), further supporting that the EAR-like domain may participate in mediating nuclear export. The EARLM carrying the NES was not detected in the nuclei of the L1 layer cells. Perhaps a relatively higher nuclear export activity in these cells might have prevented nuclear accumulation of the protein.

In summary, our results show that the WUS-box is necessary for nuclear retention and that the EAR-like domain is required for nuclear export. These results are not in agreement with an earlier study, which found that mutations in either the WUS-box or EAR-like domains did not significantly influence WUS protein distribution (Daum et al., 2014). Perhaps the C-terminal GFP fusion used in the earlier study might have masked the nuclear export activity of EAR-like domain, which is located at the very end of the C

terminus. Masking of the EAR-like domain function, in turn, might have prevented the nonnuclear accumulation of the WUSbox mutant protein, which is consistent with our results showing that double mutants of the WUS-box and EAR-like domains resemble single EAR-like mutants. Taken together, these results show that the transcriptional regulatory domains also participate in nuclear-cytoplasmic partitioning.

DNA Binding and Homodimerization Restrict WUS Protein from Excessive Spreading. The analysis presented in the previous section reveals that the C-terminal stretch of WUS contains necessary information for differential accumulation of WUS protein. Therefore, the C-terminal GFP fusion to WUS used in an earlier study might have produced a stable form (Daum et al., 2014). The use of the shorter form [WUS (amino acids 100 to 249)] of such a stable protein that can diffuse farther might have resulted in meristem overproliferation, despite lacking the HAM binding domain. To understand precisely the role of homodimerization in WUS function, protein mobility, and spatial patterning, and the role of the HAM binding domain in spatial patterning of WUS protein, we revisited the structure-function analysis of WUS.

Our yeast two-hybrid (Y2H) analysis revealed two homodimerization contact points in WUS: a DNA binding homeodomain located at the N terminus and a 74-aa stretch (amino acids 134 to 208) in the central part of the protein (referred to as HOD2) (Fig. 4.5A and Fig. 4.6A). An earlier study isolated a *wus-7* allele, which carries a missense mutation (G77E), in the loop that connects the second and third alpha helices of the homeodomain (Graf et al., 2010). The same point mutation (G77E) was introduced into the truncated WUS lacking the HOD2 (amino acids 1 to 134), which failed to homodimerize in Y2H

assays, revealing the homodimerization residue in the DNA binding domain, referred to as HOD1 (Fig. 4.5A). The bimolecular fluorescence complementation (BiFC) assay, in *Nicotiana benthamiana* leaves and in onion epidermal cells, with the WT WUS protein, revealed a higher signal in nuclei than in the cytoplasm (Fig. 4.5 B–D and Fig. 4.6 B–J). The deletion of HOD2 alone failed to produce a fluorescence signal in 59 of the 60 cells tested (Fig. 4.6 D and E). The HOD1 mutation in the context of HOD2 deletion failed to produce a fluorescence signal (Fig. 4.5D) ($n = 60$). Taken together, these results show that both HOD1 and HOD2 are required for homodimerization.

Because HOD1 resides within the homeodomain, we tested whether it is also necessary for DNA binding. The analysis presented in the accompanying manuscript (Perales et al., 2016) shows that HOD1 is also required for DNA binding. Consistent with the compromised DNA binding ability of HOD1, *wus-7* homozygous mutants failed to activate *pCLV3::H2B-mYFP* expression at levels comparable with the WT (Fig. 4.5 E–L) ($n = 21$). The expression of WUS forms carrying deletions in HOD2 from the WUS promoter in *wus-1*, a strong loss-of-function allele, resulted in plants with much smaller inflorescence meristems and incomplete flowers (Fig. 4.7 A–C) ($n = 18$). Remarkably, the expression of WUS carrying the mutated HOD1 residue that also lacked the HOD2 failed to rescue *wus-1* mutant phenotypes (Fig. 4.7A). In summary, these results show that both HOD1 and HOD2 mediate homodimerization and that HOD1 also participates in DNA binding. These results also show that homodimerization is critical for WUS function in promoting meristem maintenance.

In light of these results, it is conceivable that Daum et al., despite using WUS lacking the HOD2 and the HAM binding region, were able to observe stem cell overproliferation because of the combined effects of improved protein stability caused by the defective C-terminal fusion and the higher mobility associated with the shorter form of the protein (Daum et al., 2014). Our work also shows that, at higher WUS levels, HOD1 alone is sufficient to mediate homodimerization (Perales et al., 2016). The redundant function of HOD1 in promoting homodimerization may explain the inflorescence meristem overproliferation observed in the earlier study (Daum et al., 2014), despite the use of a WUS form that lacked HOD2. Thus, our work shows that homodimerization of WUS is necessary to promote meristem growth rather than to restrict it, as suggested by an earlier study (Daum et al., 2014). Because the deletion used in that previous study (Daum et al., 2014) also included the HAM binding region, our work also suggests that the requirement of HAM binding may become dispensable at higher WUS levels, which needs to be tested in future studies with the WT WUS protein.

The discovery of homodimerization domain HOD1 and a better demarcation of HOD2 led us to investigate the individual and combined roles of both HOD domains on the spatial distribution of the WUS protein. The eGFP-WUS-mHOD1 mutant protein expressed from the WUS promoter was detected in a broader domain in the L2 and L3 layers, and it was relatively delocalized from the nucleus (Fig. 4.5 P–R) compared with the WT protein (Fig. 4.5 M–O), showing that DNA binding or homodimerization restricts spatial distribution and is also required for proper nuclear accumulation in the L1 and L2 cell layers. The eGFP-WUS- Δ HOD2 mutant protein expressed from the WUS promoter was delocalized from the nucleus, although to a lesser extent than the mHOD1, whereas no

significant change in spatial distribution was observed (Fig. 4.5 S–U and Fig. 4.2 Q–T). The expression of eGFP fused to WUS carrying the HOD1 mutation that also lacked HOD2 was detected in a much broader domain and also accumulated at higher levels, and the protein was relatively delocalized from the nucleus compared with the WT protein, particularly in the L1 layer (Fig. 4.5 V–X). Interestingly, the expression of eGFP fused to a WUS deletion (amino acids 208 to 229), a region largely responsible for binding HAM proteins, did not significantly affect WUS protein localization (Fig. 4.2 M–P). Taken together, these results show that both DNA binding and homodimerization limit spatial distribution of WUS, presumably by restricting mobility and also by retaining the protein in the nucleus.

Ectopic Overexpression of WUS Leads to WUS Protein Destabilization. Our results, thus far, show that a combination of mechanisms involving DNA binding and homodimerization, along with the C-terminally encoded nuclear-cytoplasmic partitioning domains, determine the spatial limits and observed variations in nuclear levels of WUS protein. Nevertheless, the variations in WUS protein levels may also be due to a reduction of protein accumulation caused perhaps by the targeted destabilization in cells located outside the rib meristem. To test this hypothesis, we first expressed eGFP-WUS from a central zone-specific promoter, which led to lower levels of the protein than the eGFP-WUS expressed from the *WUS* promoter (Perales et al., 2016). This result shows that ectopic overexpression of WUS in the central zone does not result in higher protein levels, suggesting a destabilization of WUS.

The destabilization of WUS protein observed upon misexpression of eGFP-WUS in the central zone could also be due to an indirect consequence of meristem overproliferation (Brand et al., 2002; Yadav et al., 2010; Perales et al., 2016). To exclude such a possibility, we transiently overexpressed WUS, using a dexamethasone (Dex)-inducible form of WUS protein where eGFP-WUS was fused with the hormone binding domain of the rat glucocorticoid receptor (GR). The GR fusion allows visualization of the protein fate before and immediately after the Dex-induced release of WUS from the HSP-90-mediated cytoplasmic sequestration and subsequent translocation of the protein into the nucleus. The eGFP-WUS-GR expressed from the ubiquitous promoter (*35S::eGFP-WUS-GR*), before the Dex treatment, was detected mostly uniformly in the cytoplasm of all cells (Fig. 4.8 A–D) ($n = 4$). Upon 6 h of Dex treatment, the protein was detected in the nucleus in all cells, except for a few cells of the central zone, which accumulated relatively lower levels of the protein (Fig. 4.8 I–L). The region of lower protein accumulation expanded radially within 12 h of Dex treatment (Fig. 4.8 M–P). Within 24 h of Dex treatment, the protein was undetectable in cells located in the central part of the inflorescence meristem, except for a few cells that were located in the lateral edge of the peripheral zone and in the rib meristem (Fig. 4.8 Q–T). Conversely, mock treatment did not alter subcellular localization or levels of eGFP-WUS-GR (Fig. 4.8 E–H). A similar time course experiment with the *35S::eGFP-GR* (Fig. 4.9 B–E) ($n = 4$), lacking the coding sequences of the WUS protein, revealed the stable nuclear accumulation of the protein upon Dex treatment, showing that the protein destabilization is specific to WUS. As seen with the *35S::WUS-GR*-expressing seedlings, the *35S::eGFP-WUS-GR* seedlings also failed to develop on Dex-containing plates and activated CLV3 (Perales et al., 2016), upon

Dex application, confirming its functionality (Fig. 4.9A). Taken together, these results show that ectopic induction of WUS activity leads to instantaneous destabilization of WUS protein.

Discussion

The regulation of WUS protein levels is critical for maintaining the central zone identity and for the regulation of meristem proliferation (Mayer et al., 1998; Schoof et al., 2000; Brand et al., 2002; Yadav et al., 2010). Our work shows that multiple processes control nuclear levels and the spatial pattern of WUS protein accumulation in inflorescence meristems (Fig. 4.10 A and B). Both binding of WUS to DNA and homodimerization may sequester WUS. Our analysis reveals that DNA promotes homodimerization of WUS (Perales et al., 2016). Therefore, DNA-mediated sequestration may reduce the free pool of WUS that is available for nuclear export into the cytosol and subsequent migration into adjacent cells, thus influencing the spatial distribution of WUS protein (Fig. 4.10).

Our results assign functions for the EAR-like domain in mediating nuclear export and for the WUS-box in mediating nuclear retention. Earlier studies have shown that the WUS-box is both necessary and sufficient to mediate transcriptional repression activity of WUS (Ikeda et al., 2009). The WUS-box has been shown to be critical for the interaction of WUS with TOPLESS (TPL) and TOPLESSRELATED (TPR) proteins (Kieffer et al., 2006). The TPL and TPR proteins have been shown to interact with HISTONE DEACETYLASE19 to form a transcriptional repression complex (Szemenyei et al., 2008). Our work showing the requirement of the WUS-box for nuclear retention suggests that it could tether WUS to chromatin by assembling a repressor complex (Fig. 4.10C). Perhaps

the WUS pool that is not part of the repressor complex may be exported out of the nucleus by the hypothetical regulators that use the EAR-like domain. Our results also show that the EARLM was able to migrate into adjacent cells, which suggests that the nuclear export within the rib meristem was not affected to an extent that it could trap the mutant protein. Therefore, the nuclear export machinery may be highly active in cells that are located outside the rib meristem. In addition, the nuclear retention may be relatively weaker in cells located outside the rib meristem because our work shows that the WUS that fails to bind DNA and homodimerize was more highly nonnuclear in the L1 layer than in inner layers (Fig. 4.5 P–R and V–X). Therefore, a combination of potent nuclear export and a weaker nuclear retention may decrease WUS levels in the nuclei of cells located outside the rib meristem (Fig. 4.10C).

The destabilization of WUS, observed upon ectopic overexpression, suggests an additional layer of control in maintaining different WUS protein levels between the rib meristem and the adjacent regions. Moreover, the destabilization of WUS observed upon its nuclear translocation suggests a possibility of self-destabilization. The variability observed in the accumulation of EARLM of WUS in different transgenic lines (Fig. 4.3 E–N) could be due to self-destabilization, which might depend on WUS levels. However, a transient analysis involving the transcriptionally inactive versions and mutant versions that alter subcellular distribution of WUS is required to test whether WUS destabilizes itself and the importance of WUS concentration in self-destabilization. The instability that has been observed upon deletion of each of the acidic domain, the EAR-like domain, and the WUS-box suggests that this region may fold as a single module that can either engage or disengage with destabilization machinery. Taken together, our work shows that the

transcriptional regulatory domains also influence the processes that regulate nuclear levels as well as the spatial patterning of WUS protein (Fig. 4.10 B and C). We find that WUS activates the transcription of CLV3 at a lower level and represses at a higher level by binding the same cis-elements as monomers and as dimers, respectively (Perales et al., 2016). The utilization of transcriptional regulatory domains in fine tuning the nuclear levels and the spatial pattern of WUS accumulation allows a cross-talk between regulation of protein concentration and transcriptional regulation, which could lead to the spatiotemporal control of gene expression.

Acknowledgements

We thank Thomas Laux, University of Freiburg, for sharing driver lines and *wus* mutants; Jacqueline Le for supporting experimental work; and members of the G.V.R. laboratory for comments on the manuscript. This work was supported by NSF Grant IOS-1456725 (to G.V.R.).

Footnotes

- K.R. and M.P. contributed equally to this work.
- M.P. and M.D.-M. Present address: Centro de Biotecnología y Genómica de Plantas, Universidad Politécnica de Madrid (UPM)–Instituto Nacional de Investigación y Tecnología Agraria y Alimentaria (INIA) Campus Montegancedo UPM, Pozuelo de Alarcón, Madrid, 28223, Spain.
- R.K.Y. Present address: Department of Biological Sciences, Indian Institute of Science Education and Research, Mohali, 140306, India
- Author contributions: M.P. and G.V.R. designed research; K.R., M.P., S.S., R.K.Y., M.D.-M., and G.V.R. performed research; K.R., M.P., R.K.Y., and M.D.-M. contributed new reagents/analytic tools; K.R., M.P., S.S., and G.V.R. analyzed data; and K.R., M.P., and G.V.R. wrote the paper.

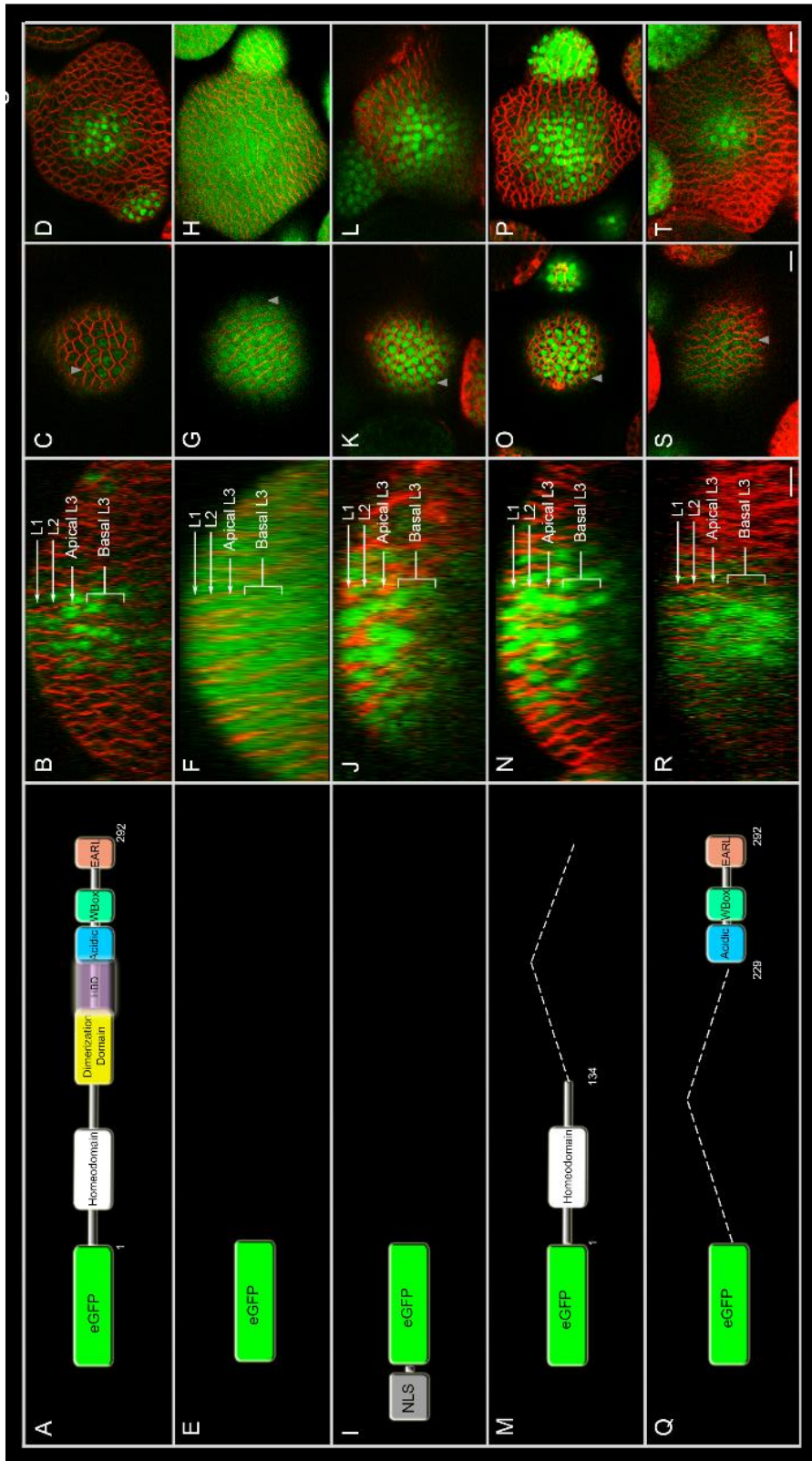


Fig. 4.1. The C terminus of WUS is sufficient for the spatial patterning of WUS protein. The first column shows diagrams of various constructs expressed from the WUS promoter: (A) eGFP-WUS, (E) free (untagged) eGFP, and (I) nuclear localization tagged NLS-eGFP. (M) [eGFP-WUS (amino acids 1 to 134)] and (Q) [eGFP-WUS (amino acids 229 to 292)] show schematics of several deletions of WUS fused to eGFP and expressed from the WUS promoter. The break points of deletions are marked as amino acid positions. The second column (B, F, J, N, and R) shows side views of IMs showing eGFP protein distribution for the constructs shown in the corresponding panels in column 1. The third column (C, G, K, O, and S) shows the top views of the L1 layer of IMs for the constructs shown in the corresponding panels in column 1. The fourth column (D, H, L, P, and T) shows the top views of the apical L3 layers of IMs for the constructs shown in the corresponding panels in column 1. Gray arrowheads mark the spread of protein. All constructs were expressed from *pWUS*. eGFP (green) and FM4-64 (red). (Scale bars: 10 μ m.)

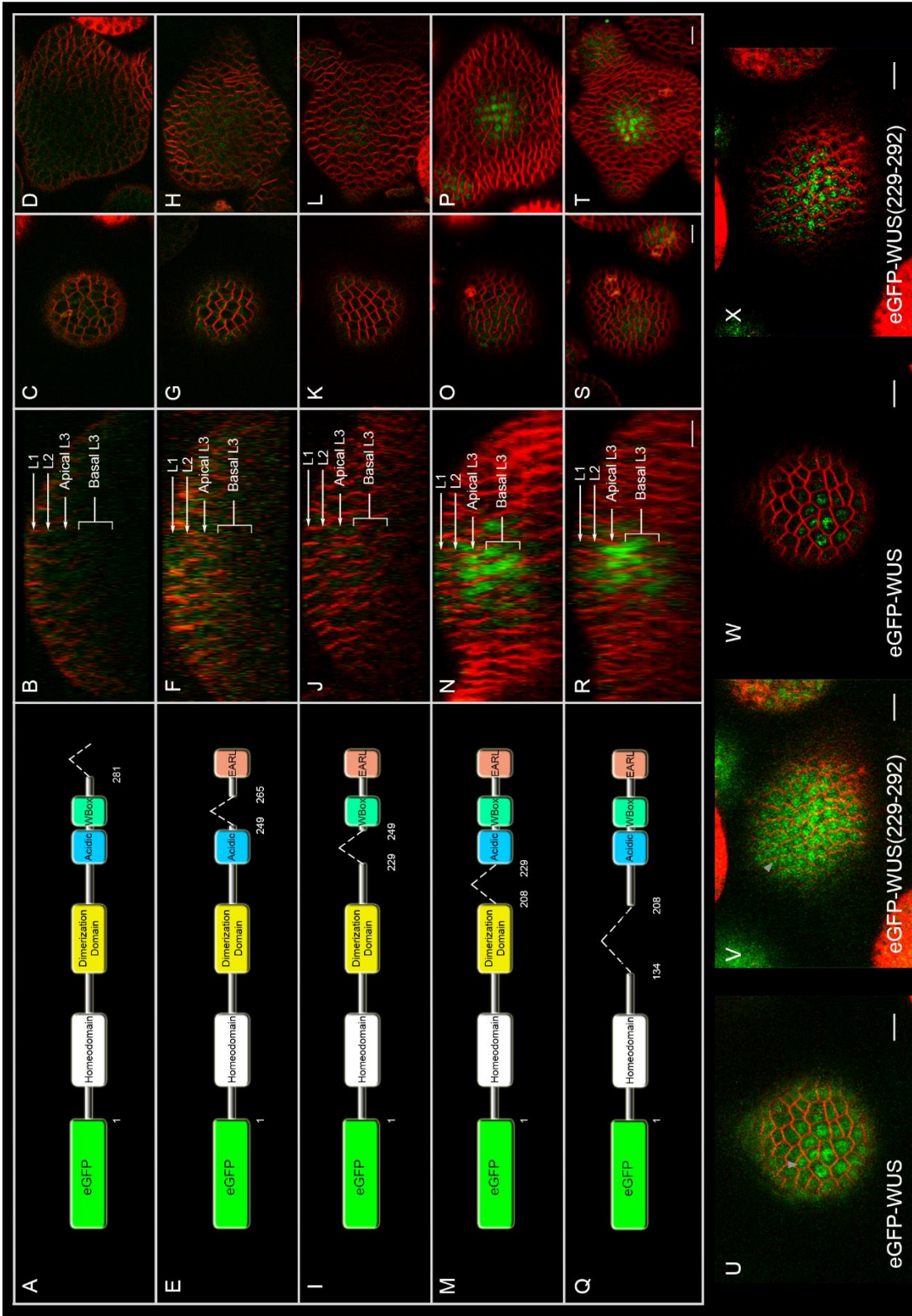
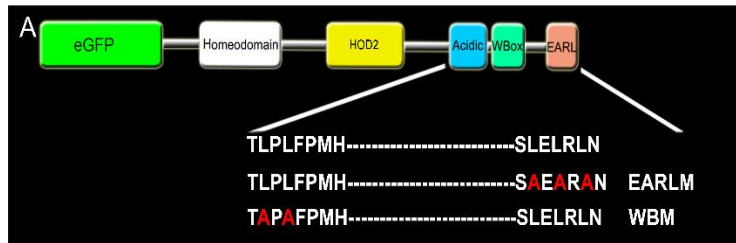


Fig. 4.2. The stability of WUS is determined by a 63-aa region in the C terminus. Column 1 shows various WUS truncations expressed from the *WUS* promoter: (A) eGFP-*WUS* (Δ amino acid 281 to amino acid 292), (E) eGFP-*WUS* (Δ amino acid 249 to amino acid 265), (I) eGFP-*WUS* (Δ amino acid 229 to amino acid 249), (M) eGFP-*WUS* (Δ amino acid 208 to amino acid 229), and (Q) eGFP-*WUS* (Δ amino acid 134 to amino acid 208). The break points of deletions are marked as amino acid positions. Column 2 is the side views of inflorescence meristems (IMs) showing eGFP-*WUS* protein distribution for the various constructs shown in the corresponding panels in column 1: (B) eGFP-*WUS* (Δ amino acid 281 to amino acid 292), (F) eGFP-*WUS* (Δ amino acid 249 to amino acid 265), (J) eGFP-*WUS* (Δ amino acid 229 to amino acid 249), (N) eGFP-*WUS* (Δ amino acid 208 to amino acid 229), and (R) eGFP-*WUS* (Δ amino acid 134 to amino acid 208). The cell layers in IMs are indicated by white arrows and brackets. Column 3 shows the top views of the L1 layer of IMs for the constructs shown in the corresponding panels in column 1: (C) eGFP-*WUS* (Δ amino acid 281 to amino acid 292), (G) eGFP-*WUS* (Δ amino acid 249 to amino acid 265), (K) eGFP-*WUS* (Δ amino acid 229 to amino acid 249), (O) eGFP-*WUS* (Δ amino acid 208 to amino acid 229), and (S) eGFP-*WUS* (Δ amino acid 134 to amino acid 208). Column 4 shows the top views of the apical L3 layers of IMs showing eGFP-*WUS* protein distribution for the constructs shown in the corresponding panels in column 1: (D) eGFP-*WUS* (Δ amino acid 281 to amino acid 292), (H) eGFP-*WUS* (Δ amino acid 249 to amino acid 265), (L) eGFP-*WUS* (Δ amino acid 229 to amino acid 249), (P) eGFP-*WUS* (Δ amino acid 208 to amino acid 229), and (T) eGFP-*WUS* (Δ amino acid 134 to amino acid 208). All constructs were expressed from *pWUS*. eGFP-*WUS* (green) and FM4-64 (red). (Scale bars: 10 μ m.) (U–X) Enhanced versions of main (Fig. 4.1 C and S) images with increase in intensity (U and V) and thresholding (W and X). Note expansion of domain with higher nuclear levels. (Scale bars: 10 μ m.)



B

ArRanBP1a	171:	D T A G L L E K L T V E E T K T E E K T	:190
AtRanBP1b	173:	D T A G L L E K L T V E E K E S E K K P	:192
AtRanBP1c	170:	E A A G L I E N L S V E E N I S E E K A	:189
mRanBP1	178:	K V A E K L E A L S V R E A R E E A E E	:197
hRanBP1	179:	K V A E K L E A L S V K E E T K E D A E	:198
Rev	73:	L Q L P P L E R L T L D	:84
mPK1α	37:	L A L - K L A G L D I N	:46
WUS	282:	R P C A S L E - L R L N	:292

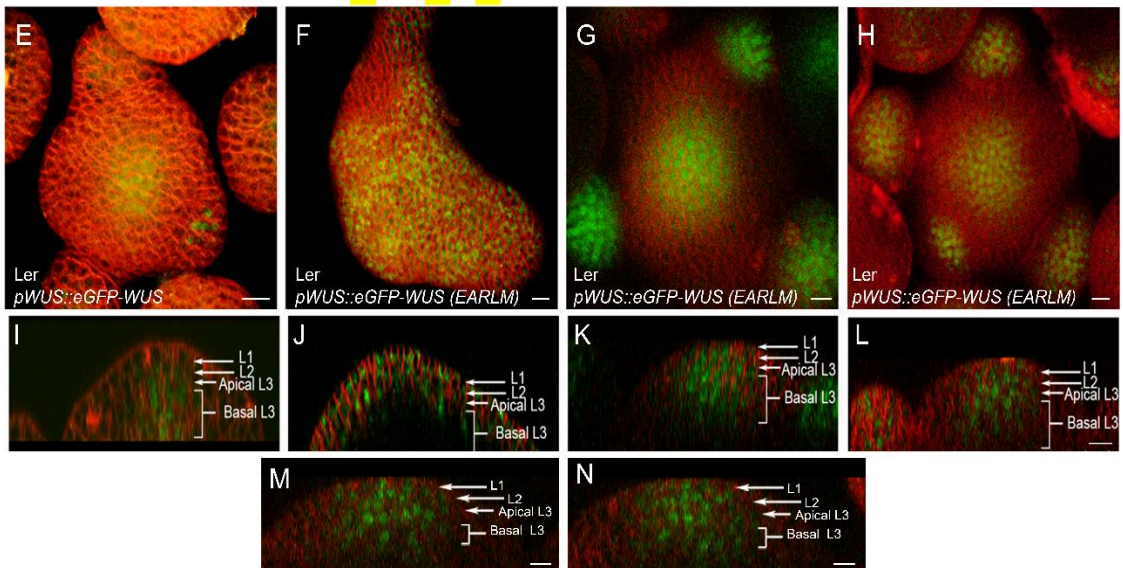
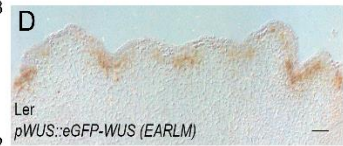
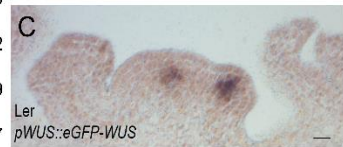


Fig. 4.3. The EAR-like domain influences nuclear accumulation of WUS. (A) A schematic of WUS protein domains showing amino acid sequences of the WT, the mutant WUS-box domain, and the mutant EAR-like domain (EARLM). Amino acid substitutions are shown in red. (B) Sequence alignment of nuclear export signals (NESs) of RAN binding proteins (RanBPs) from *Arabidopsis*, mouse, human, HIV1 protein Rev, and heat stable inhibitor of cAPK (mPKI α) along with the EAR-like domain of WUS. The leucine residues are highlighted in yellow. RNA in situ with WUS anti-sense probe in (C) *pWUS::eGFP-WUS* and (D) one of the enlarged IMs of *pWUS::eGFP-WUS (EARLM)*. *E* and *I* are the 3D top and side views of IM expressing *pWUS::eGFP-WUS*. (*F–H*) and (*J–L*) are the 3D top and side views of three independent IMs expressing *pWUS::eGFP-WUS (EARLM)*. *M* and *N* are side views of different sections of an IM expressing *pWUS::eGFP-WUS (EARLM)*. The cell layers in SAMs are indicated by white arrows and brackets. eGFP-WUS (green) and FM4-64 (red). (Scale bars: 10 μ m, except *F*, 15 μ m and *D*, 30 μ m.)

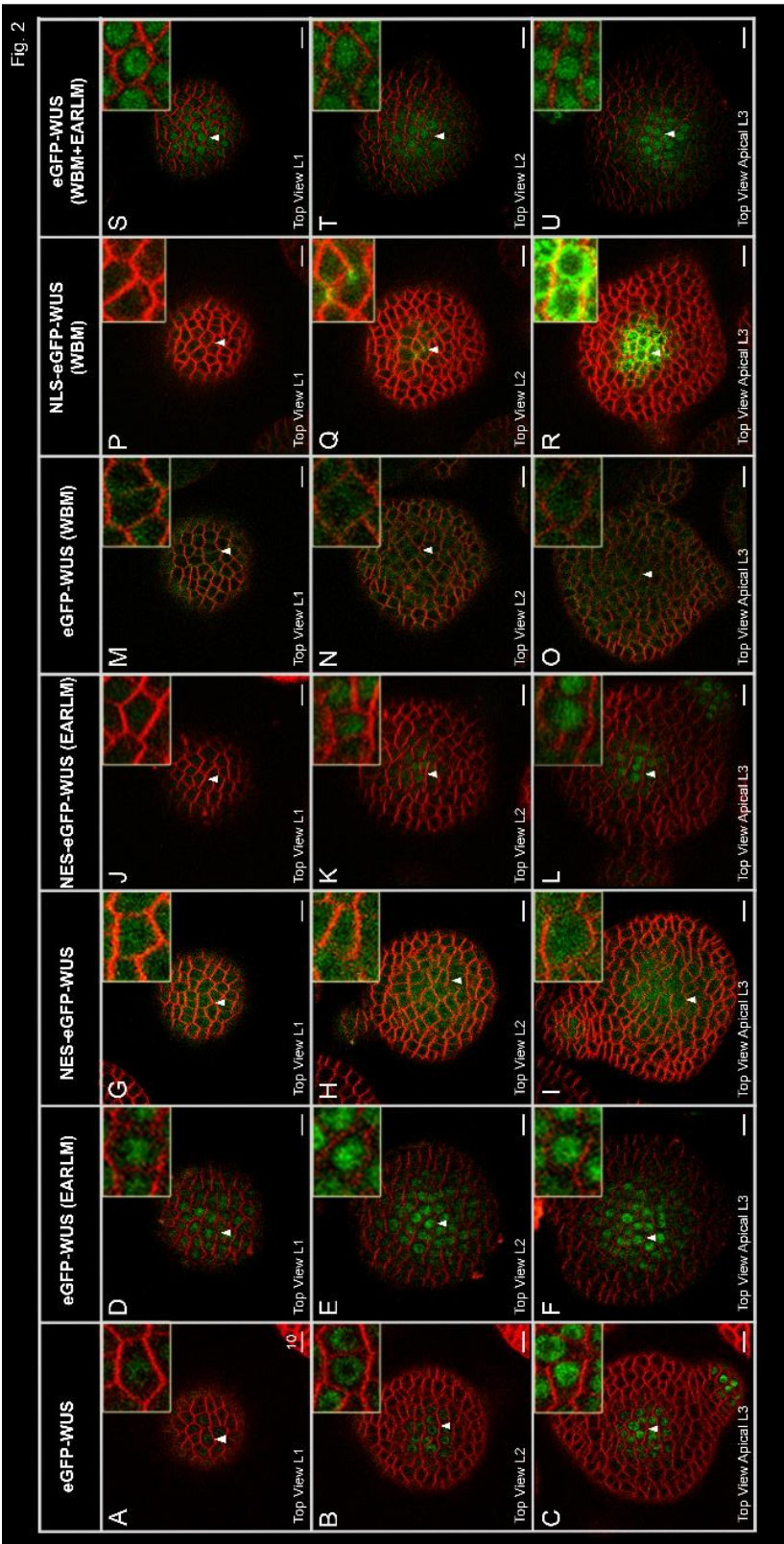


Fig. 4.4. The transcriptional regulatory domains influence the subcellular localization of WUS. Horizontal rows represent (A, D, G, J, M, P, and S) L1 layers, (B, E, H, K, N, Q, and T) L2 layers, and (C, F, I, L, O, R, and U) apical L3 layers of IMs expressing various constructs: (A–C) eGFP-WUS (EARLM), (G–I) NES-eGFP-WUS, (J–L) NES-eGFP-WUS (EARLM), (M–O) eGFP-WUS (WBM), (P–R) NLS-eGFP-WUS (WBM), and (S–U) eGFP-WUS (WBM+EARLM). All constructs are expressed from the *pWUS*. Insets on each panel show a higher magnification (3x) view of the region identified by the white arrowheads. (Scale bars: 10 μ m.)

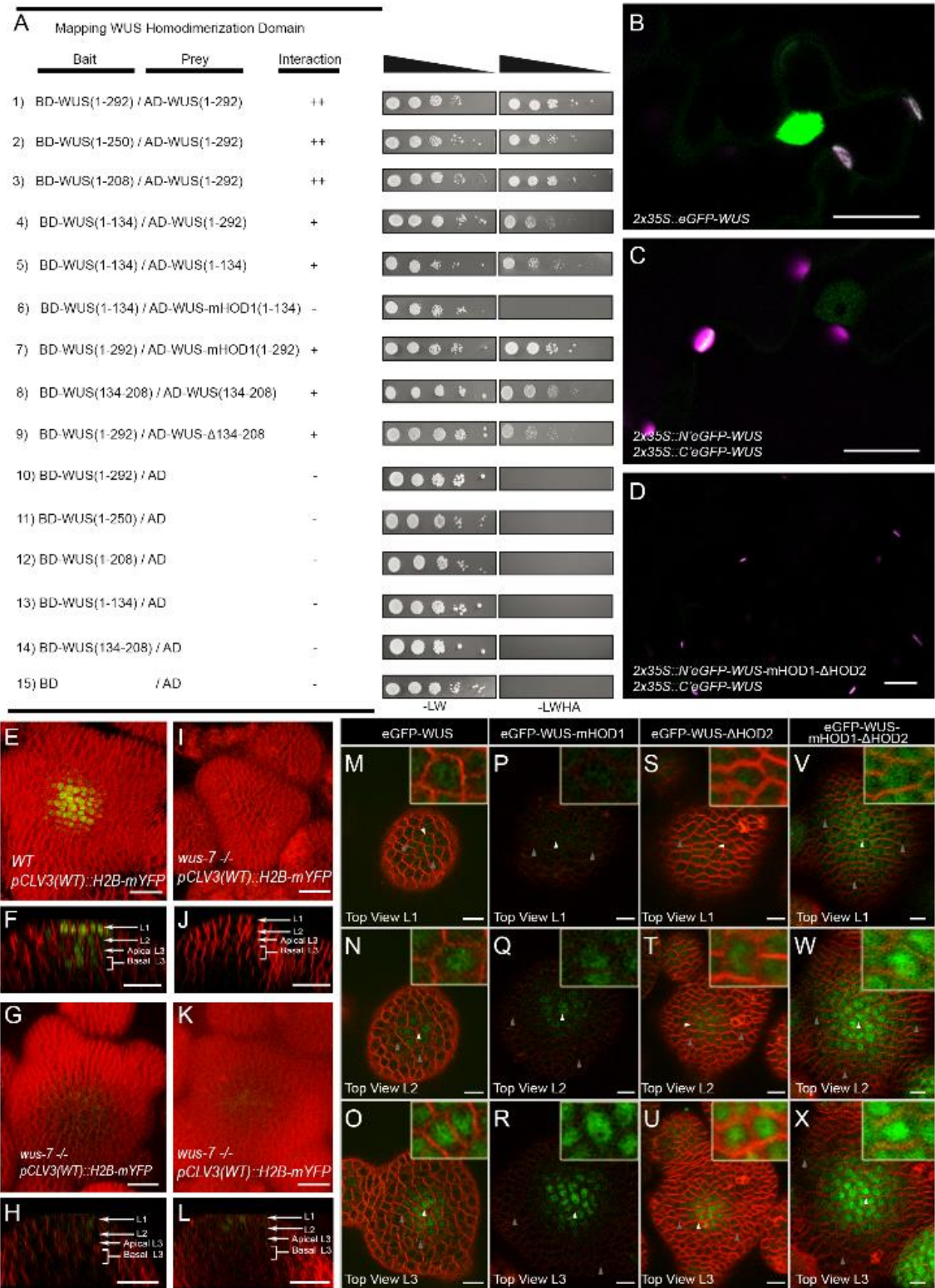


Fig. 4.5. The DNA binding and dimerization of WUS restrict its spatial localization. Mapping the homodimerization domains of WUS using a yeast two-hybrid analysis (A). The break points of WUS deletions are indicated by the amino acid positions. +, stronger interaction; -, no interaction. Expression of (B) 35S::eGFP-WUS and (C) BiFC signal of WT and (D) the double homodimerization mutant in *N. benthamiana* leaves. Shown are 3D top views of IMs expressing WT *pCLV3* (H2B-mYFP) in (E) WT and (I, G, and K) *wus-7* mutant plants. A side view of E is shown in F. Side views of I, G, and K are shown in J, H, and L, respectively. H2B-mYFP images in (G, H, K, and L) were taken at three times laser intensity used in E, F, I, and J. Horizontal rows represent (M, P, S, and V) the L1 layers, (N, Q, T, and W) the L2 layers, and (O, R, U, and X) the apical L3 layers of IMs expressing (M-O) eGFP-WUS, (P-R) eGFP-WUS-mHOD1 (G77E), (S-U) eGFP-WUS- Δ HOD2 (Δ amino acid 134 to amino acid 208), and (V-X) eGFP-WUS-mHOD1(G77E)- Δ HOD2 (Δ amino acid 134 to amino acid 208) from *pWUS*. Insets on each panel show a higher magnification (3 \times) view of region identified by the white arrowheads. WUS protein detected in a broader domain is indicated by gray arrows. H2B-mYFP (yellow), eGFP (green), and FM4-64 (red). (Scale bars: B-L, 20 μ m; M-X, 10 μ m.)

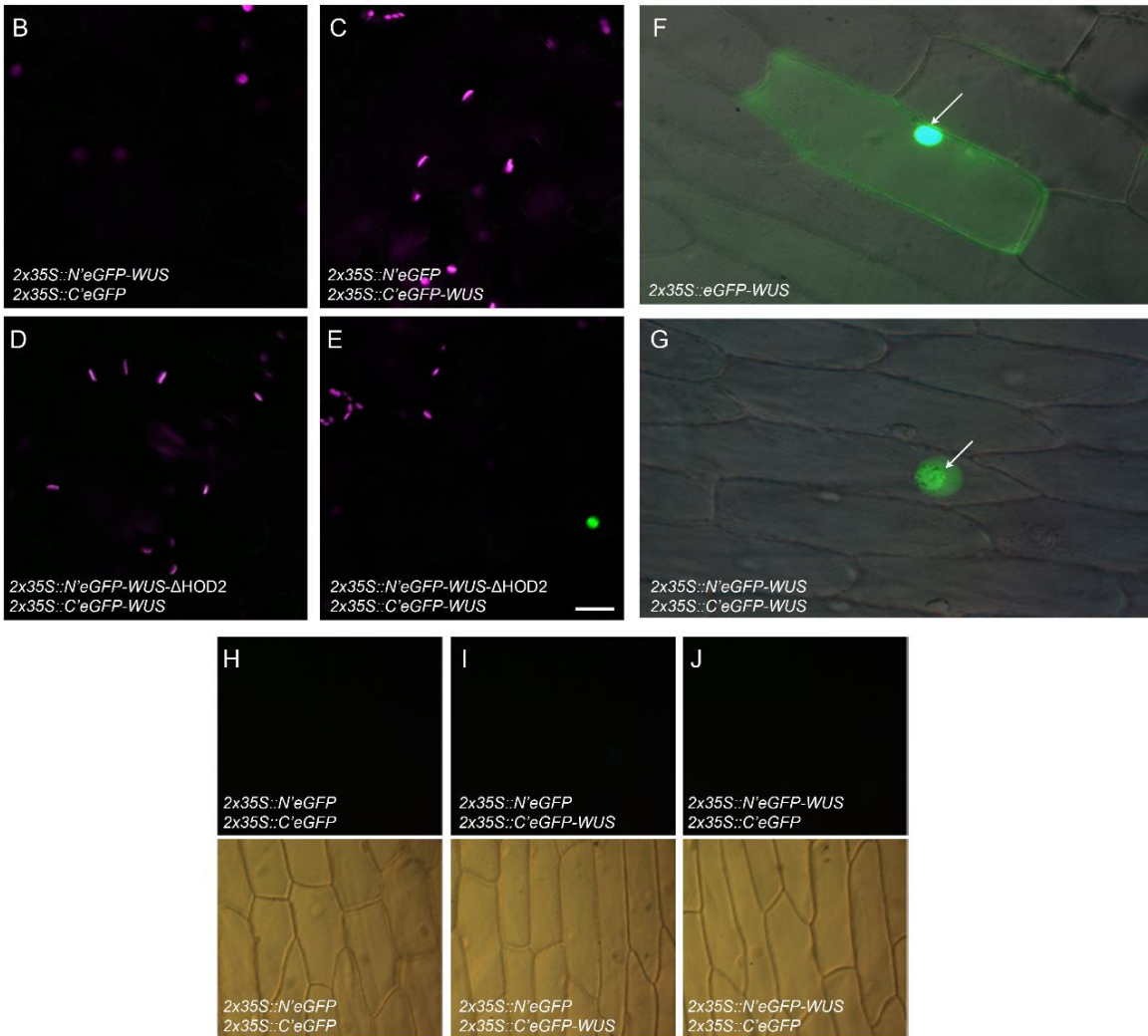
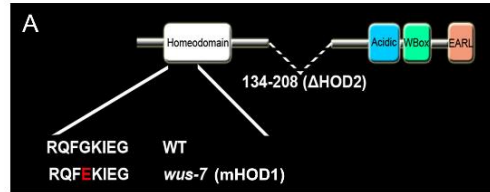


Fig. 4.6. WUS contains two homodimerization domains. (A) A schematic of WUS protein domains showing amino acid sequences of the WT, the mutant HOD1 (G77E), a single amino acid mutated in *wus-7* allele, and the deletion of HOD2 (Δ amino acid 134 to amino acid 208). Amino acid sequence is shown, and substitutions are shown in red. (B and C) Negative controls of BiFC in transfected *Nicotiana benthamiana* leaves. (D and E) Independent transfections carrying BiFC constructs *N'eGFP-WUS- Δ HOD2* (Δ amino acid 134 to amino acid 208), which produce nuclear signal only once (E) in 60-cell analysis. Green signal is from GFP fluorescence whereas magenta is chlorophyll autofluorescence. Expression of (F) *35S::eGFP-WUS* and (G) BiFC signal in onion epidermal cell. The white arrows point to the nuclei. (H–J) The negative controls for BiFC experiments. (H) (*N'eGFP* and *C'eGFP*), (I) (*N'eGFP* and *C'eGFP-WUS*), (J) (*N'eGFP-WUS* and *C'eGFP*). (Upper) Fluorescence images. (Lower) Differential interference contrast (DIC) images. All constructs were expressed from the 2X35S promoter. (Scale bar: 20 μ m.)

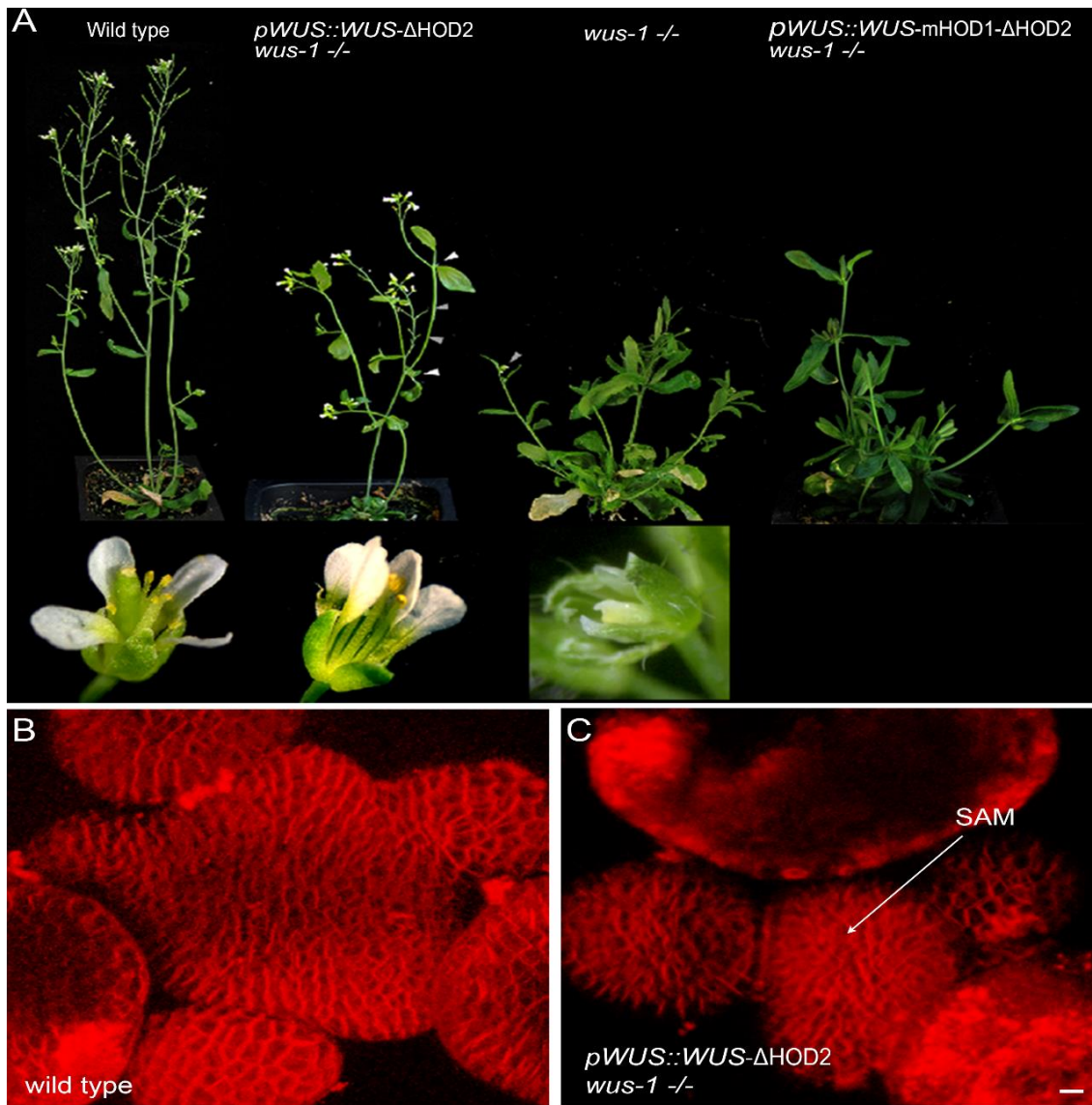


Fig. 4.7. The two homodimerization domains are required for WUS function. (A) *pWUS::WUS-ΔHOD2* (Δ amino acid 134 to amino acid 208) in *wus-1* homozygous mutants showing partially rescued and partial flowers devoid of carpels. $n = 18$ (*wus-1* homozygous plants derived from four independent lines). *pWUS::WUS-mHOD1* (G77E)- Δ HOD2 (Δ amino acid 134 to amino acid 208) in *wus-1* homozygous mutants showing lack of rescue (14 *wus-1* homozygous plants were identified from six independent transgenic lines). White arrowheads indicate lack of auxiliary SAM development, and gray arrowheads indicates empty peduncles of partially rescued flowers. (Lower) Higher magnification images of flowers of each genotype indicated above. (B) A 3D reconstructed top view of a WT IM. (C) A 3D reconstructed top view of an IM of *wus-1* carrying *pWUS::WUS-ΔHOD2* (Δ amino acid 134 to amino acid 208), showing extremely small meristem. FM4-64 (red). (Scale bar: 10 μ m.)

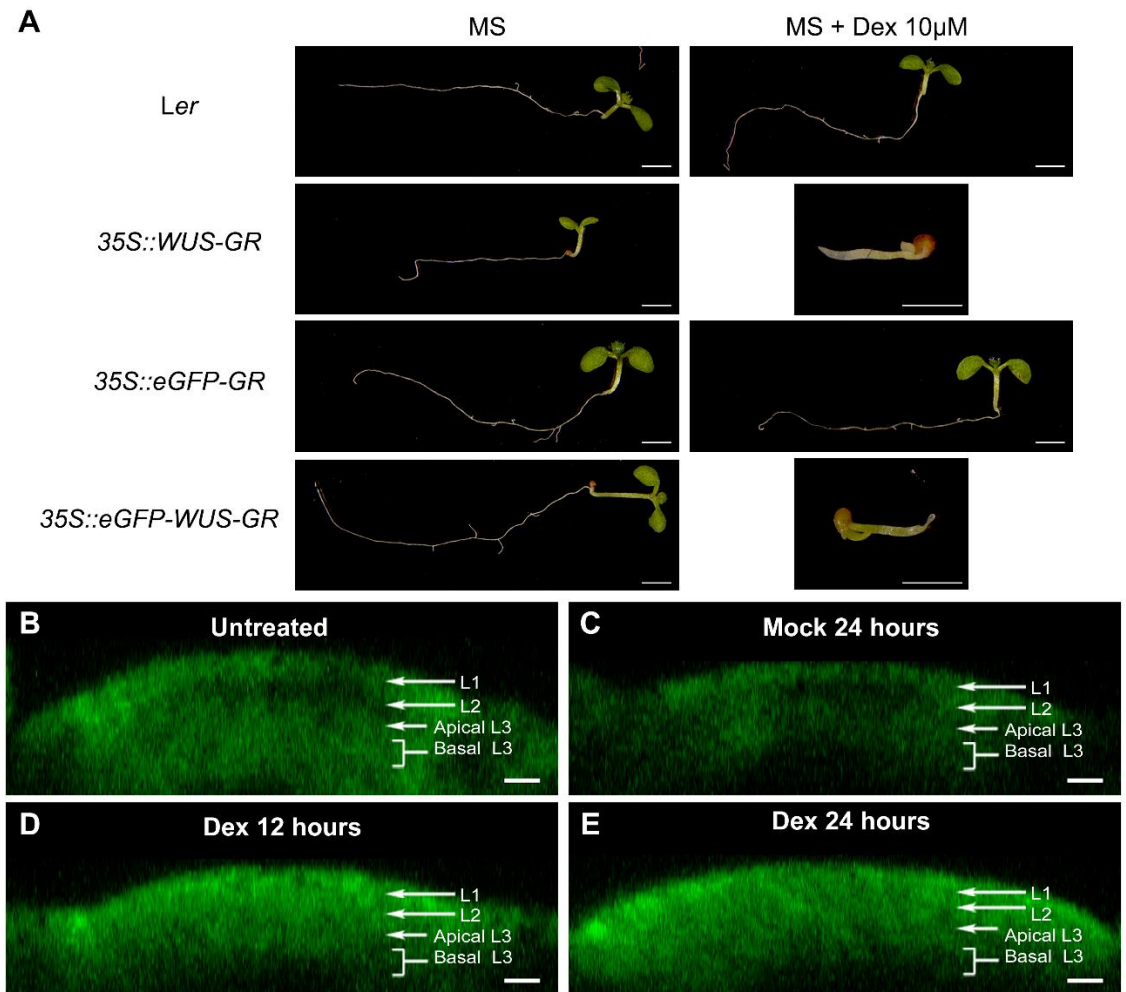


Fig. 4.8. Ectopic overexpression of *WUS* destabilizes *WUS* protein. Vertical columns represent (A, E, I, M, and Q) the L1 layers, (B, F, J, N, and R) the L2 layers, (C, G, K, O, and S) the apical L3 layers, and (D, H, L, P, and T) the side views of inflorescence meristems expressing *35S::eGFP-WUS-GR*. Shown are (A–D) untreated and (E–H) 24 h mock treatment. Dex treatment for (I–L) 6 h, (M–P) 12 h, and (Q–T) 24 h. White arrowheads indicate high nuclear levels, and gray arrows indicate cells with low nuclear accumulation. The domains of low nuclear accumulation, shown in side views, are noted with black brackets. Green channel is enhanced in all images to increase visibility of the protein. eGFP-WUS-GR (green) and FM4-64 (red). (Scale bars 15 μ m.)

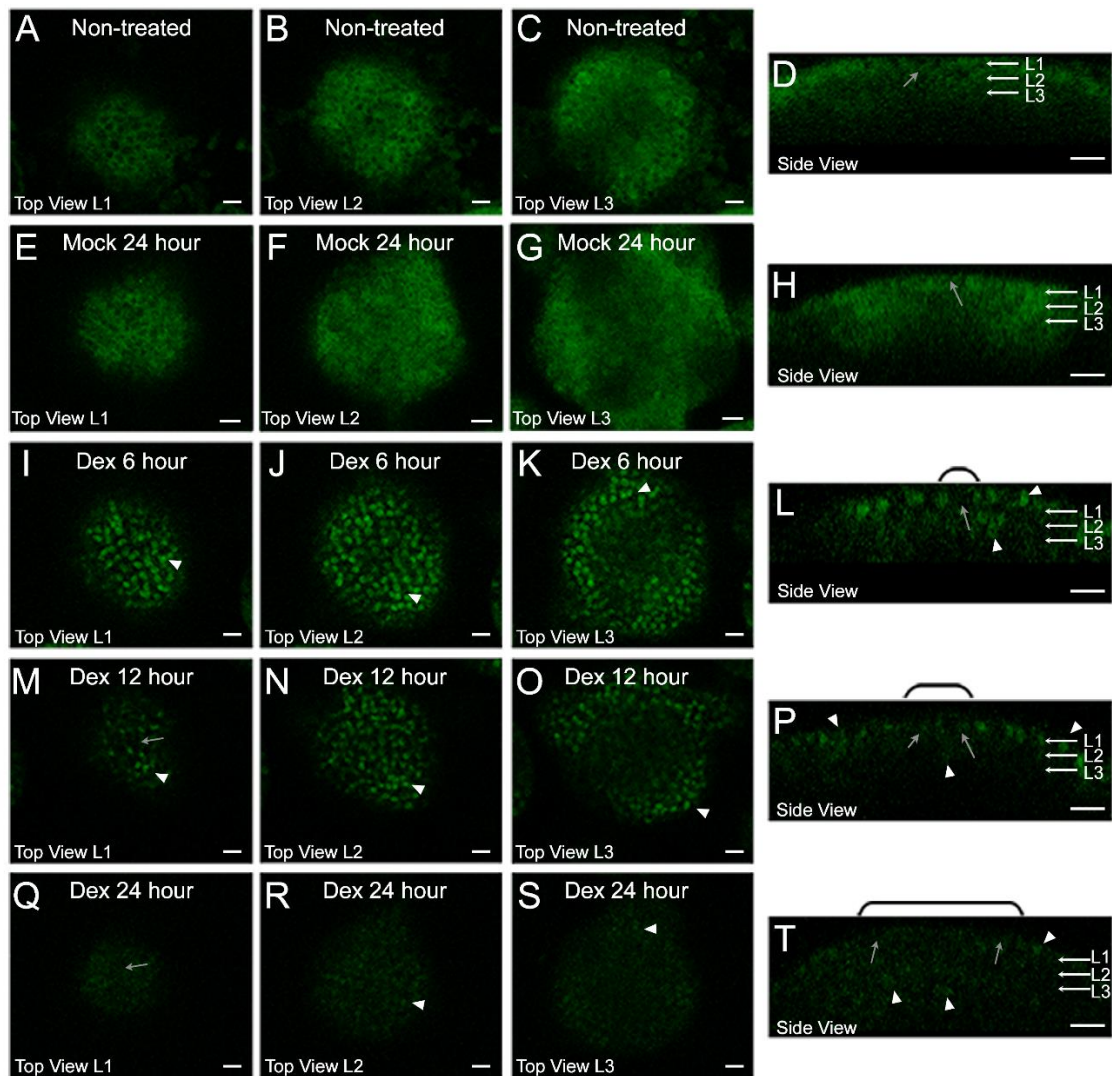


Fig. 4.9. Characterization of a Dex-inducible eGFP-WUS system. (A, Left) Genotypes of seedlings shown in A: *Ler*, *35S::WUS-GR*, *35S::eGFP-GR*, and *35S::eGFP-WUS-GR*. (A, Middle and Right) Representative seedling images that were grown on MS media without and with Dex, respectively. (Scale bars: 1 mm.) (B–E) Side views of IMs showing expression of untreated *35S::eGFP-GR* (B), mock-treated (C), treated with Dex for 12 h (D), and treated with Dex for 24 h (E). eGFP-GR (green). The cell layers in SAMs are indicated by white arrows and brackets. (Scale bar: 10 μ m.)

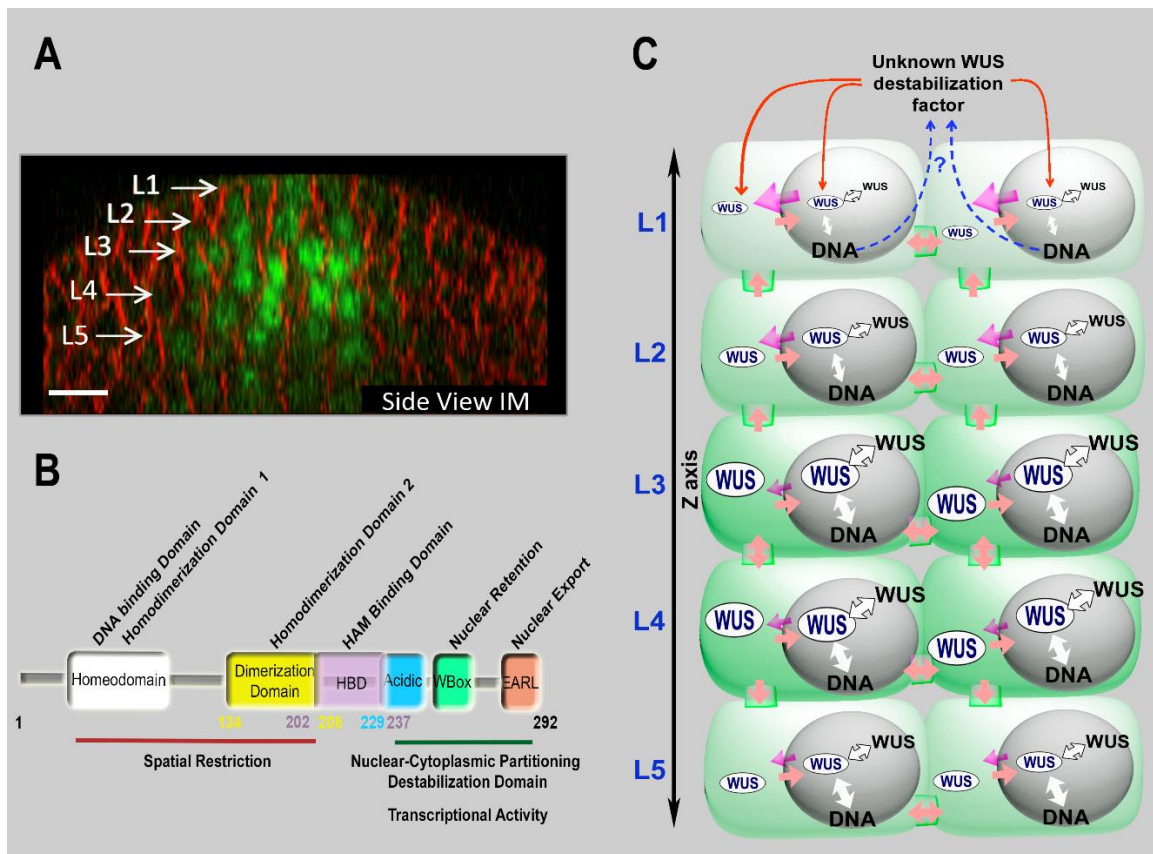


Fig. 4.10. A sketch illustrating the control of WUSCHEL levels and spatial patterning in IMs. (A) A side view of the IM showing the spatial pattern of eGFP-WUS expressed from the WUS promoter. White arrows show different cell layers. eGFP (green) and FM4-64 (red). (Scale bar: 10 μ m.) (B) The function of individual domains of WUS protein as inferred from the structure-function analysis and the ectopic overexpression of WUS. The functions of individual domains are depicted on WUS protein. The numbers indicate position of amino acids, starting with the N terminus. (C) A sketch illustrating the maintenance of WUS levels and spatial patterning, through DNA-dependent homodimerization, nuclear-cytoplasmic partitioning, and WUS protein destabilization represented on the inflorescence meristem cell layers. WUS is synthesized in a few cells of the rib meristem and migrates into adjacent cells, where it accumulates at a lower level in the nuclei of cells in the L1 and the L2 layers compared with the inner layers. Our analysis suggests a relatively higher nuclear export (indicated by the strength of magenta colored arrows) and a lower nuclear retention of WUS, which could be due to the lower affinity to the DNA (indicated by the strength of the white arrows) and a lower dimerization propensity (indicated by the strength of the white arrows with black outline) in the top layers than in the inner layers. WUS could be destabilized in outer layers (indicated by red arrows). We hypothesize that this destabilizing factor may be WUS-dependent (represented by the blue dashed arrows), which needs to be tested in future studies.

CHAPTER 5:

Concluding discussion and future research

We have uncovered several regulatory processes linked to specific domains/motifs of WUSCHEL protein, which determine its spatial accumulation and nuclear levels (Fig. 4.10). Many of these processes described below are inter-dependent and function simultaneously to influence the WUS protein gradient (Fig. 5.1). The first level of regulation is the amount of WUS protein synthesis in the RM, which in turn is maintained through the CLV3 signaling, which limits *WUS* transcript levels. The second level of regulation is the movement of the protein from the RM into adjacent cells, which depends on the balance between multiple processes. The higher WUS levels increase both the DNA binding and dimeric/multimeric complexes of WUS bound to the DNA. The ability of DNA to induce dimerization of WUS will in turn limit the mobility of the protein. The balance between nuclear accumulation (determined by the WUS-box and DNA binding) and cytoplasmic accumulation (determined by the nuclear export by the EAR-like domain) is critical to movement, as the nuclear-cytoplasmic ratios have been shown to influence the extent of WUS mobility into neighboring cells (Fig. 5.1 and 4.10). In the target cells (that is outside the RM), the regulation of the amount of WUS in the nucleus, mediated by the balance between nuclear retention and export, is critical as WUS concentration has been shown to influence gene expression (Yadav et al., 2011; Perales et al., 2016). Protein degradation is another mechanism that regulates WUS protein levels. Our analysis showing the immediate protein destabilization of dexamethasone-induced nuclear translocation of ubiquitously expressed WUS (35S::eGFP-WUS-GR) suggests a higher WUS protein turnover (Fig. 4.9). A recent study showing a complete lack of WUS protein accumulation within 8hrs of blocking the movement (Daum et al., 2014) through misexpression of CALLOSE SYNTHASE 3, which blocks plasmodesmata, also supports the theory of higher WUS turnover in the target cells. The WUS protein turnover could be

a buffering response to increased accumulation of WUS. The nuclear enrichment of WUS has been shown to improve protein stability suggesting that the protein degradation may occur over a window of WUS levels. Therefore, the concentration-dependent protein turnover may allow higher and lower WUS accumulation in the RM and the CZ. Whether the destabilization mechanism is enriched only in outer cell layers or it is present ubiquitously, which can be offset by higher synthesis and/or a mechanism that stabilizes the protein in the RM needs to be explored in future studies. The protein degradation may depend on transcriptional status of the WUS protein as we have observed highest transcriptional activity of WUS (as suggested by the *CLV3* levels) in cells where WUS protein is highly unstable (Perales et al., 2016; Rodriguez et al., 2016). For example, in the outer cell layers of the central zone upon Dex-mediated nuclear translocation of WUS and in the outer cell layers of *clv3-2* mutants. In this respect, WUS may function similar to other transcriptional activators where transcriptional activation has been shown to depend on protein turnover (Muratani and Tansey, 2003; Ma and Baldwin, 2000). In summary, all these processes may work harmoniously to increase WUS protein levels in deeper cell layers, which is critical for WUS to function as a transcriptional repressor. In outer layers, the appropriate level of transcriptional activation is maintained by lower WUS which is a combined effect of higher levels of nuclear export and higher protein turnover.

A labyrinth of properties is critical to balance the WUS-*CLV3* feedback loop, which functions to maintain stem cell homeostasis. The same intrinsic signals within the WUS protein that determine its levels and spatial accumulation are also required for its transcriptional activity (Chapter 4). The elaborate organization of cis-elements within the target gene *CLV3* interprets WUS concentration to translate into proper *CLV3* levels and

the spatial pattern (Chapter 2 and 3). The CLV3 signaling-mediated feedback influences WUS protein levels and spatial accumulation. Transcriptional and possibly post-translational mechanisms exist to determine the WUS concentration, spatial accumulation and its transcriptional activity (Fig. 2.10 H-L). This suggest that the CLV3 signaling could serve a 2-fold function in regards to determining the WUS protein. 1) through regulation of the *WUS* promoter, it limits the overall levels and domain of expression of the WUS protein. 2) through post translational regulation of WUS, it determines the spatial accumulation and possibly the function of the WUS protein. Thus the feedback loop between WUS and CLV3 ensures the proper amount of WUS protein and the correct ratio of activating/repressing activities of WUS.

The next big question is to understand how the precise concentration and function of the WUS protein can maintain the correct transcriptional programs such as repression of differentiation program in SAMs (Yadav et al., 2013). This can be accomplished by deciphering the genome wide transcriptional regulation of the WUS protein. That entails determining the direct targets of the WUS protein, WUS DNA binding elements in those targets, and the mechanism for determining activation and repression on a target.

Understanding the biochemical basis of WUS-mediated cis-element interactions. To understand the biochemical basis of cis-element interactions (collective properties), it requires testing how WUS binds to the two adjacent cis-elements in EMSA experiments. EMSAs can be used to separate complexes based on molecular weight (Perales et al., 2016). The radiolabeled oligos containing two adjacent cis-elements [(950+970), (970+997), (997+1007) and (1007+1060)] can be used to analyze complex

formation with increasing concentrations of WUS. The binding kinetics compared with oligos containing single cis-elements will reveal the nature of the interaction. A cooperative interaction is expected to produce sigmoidal kinetics in transitioning from monomeric to higher molecular weight complexes (beyond the dimeric form observed with single cis-element oligos) [Perales et al., 2016]. Non-competitive interaction is expected to produce a step-wise switch from monomeric to higher molecular weight complexes at WUS concentrations where individual cis-elements switch from monomeric to higher molecular weight complexes. Competitive interaction is expected to limit complex formation to dimeric complexes. It is possible that binding of WUS to one cis-element may inhibit WUS binding to the adjacent cis-element. However, interference is unlikely because the intrinsic binding of any cis-element can lead to *CLV3* activation in the RM and collective binding leads to repression. If WUS bound to one cis-element is dominantly suppressing WUS binding to others, both the collective and intrinsic binding should produce the same output (*CLV3* activation in the RM), which is not the case. The results from biochemical experiments that reveal collective binding patterns of two neighboring cis-elements would be sufficient to understand the nature of local co-operativity. However, we have also observed a partial downregulation of *CLV3* in the CZ and upregulation in the RM upon mutation of a pair of lower-affinity cis elements (950+1060) that are separated by 110bps (Data not shown). This suggest that long range interactions among cis-elements influence WUS binding to the centrally located cis-elements. It may be difficult to test long range interactions in EMSA as it may not be possible to resolve multiple binding events and oligomerization to the CRM of 110bps in length. Therefore, as an alternate approach, DNaseI footprinting (Ma et al, 1996) can be used to quantitatively analyze WUS binding behavior of each cis-element in the context of an intact *CLV3* CRM (collective binding). In

brief, the radiolabeled 110 bps of the WUS binding CRM pool can be analyzed with different concentrations of purified WUS, subjected to DNaseI treatment, and DNA samples purified and separated on polyacrylamide sequencing gel. Quantitative analysis of DNA fragments would provide information on binding behavior of each cis-element within the intact CRM (collective binding).

EMSA analysis is certain to provide data to infer the nature of interactions among neighboring pairs of cis-elements in dimerization or oligomerization of WUS. The DNaseI footprinting would provide binding affinities (strength) and patterns of WUS binding (one or more WUS molecules bind for instance to the complex 970 cis-element with 3 “TAAT” cores, at single nucleotide resolution. This can be determined for the entire CRM, thus allowing us to generate better models of co-operativity that are inclusive of all cis-elements in the CRM.

Characterize the genome-wide WUS-binding to assess the cis-regulation associated with the activation-repression switch. The work presented in Chapter 2 and Chapter 3 revealed the features of the homotypic CRM in regulating *CLV3*. However, a genome-wide analysis of similar regions (which may function as bifunctional switches like the one produced by the *CLV3* CRM), may allow development of robust models of the cis-regulation underlying the concentration-dependent switch between activation and repression. The genome scale analysis provides an opportunity to understand and validate cis-regulatory models associated with rest of the WUS-regulated network. To focus on cis-element analysis on specific sets of genes, previous work has identified part of the transcriptome that switches between activation and repression from the rest of the

transcriptome that is insensitive to WUS levels (Yadav et al., 2013). Developing additional transcriptome data at different WUS-levels and in parallel developing high-resolution maps of genome-wide WUS binding patterns should provide insights into all the functional CRMs in modulating gene expression.

Our earlier study has employed Dex-inducible overexpression of WUS (*35S::WUS-GR*, a ubiquitous promoter driving the expression of WUS protein linked to the hormone binding domain of rat glucocorticoid receptor) to develop a picture of the WUS-regulated transcriptome in *apetala1;cauliflower1* (*ap1;cal1*) [a mutant combination that produces many SAMs] background (Yadav et al., 2013). *CLV3* was identified as an activated target gene while the key differentiation promoting TFs were identified as repressed targets (Yadav et al., 2013). (Fig. 4.9 and 2.11 G-I) show that the Dex-induced translocation of WUS into the nucleus leads to a rapid destabilization of the protein resulting in much lower accumulation in the CZ than in the PZ suggesting that the dilution of WUS leads to *CLV3* activation (Perales et al., 2016; Rodriguez et al., 2016). This was later confirmed upon transient downregulation of WUS by using a Dex-inducible artificial microRNA system (Fig. 2.11 J-L). Subsequent analysis revealed that a higher WUS level (achieved through nuclear enriched forms of WUS, nls-WUS) was able to repress *CLV3* (Fig. 2.11 C and F). In short, we have discovered that *CLV3* acts as a WUS driven concentration-dependent switch. Probing the breadth of the transcriptome by using a Dex-inducible nuclear-enriched form of WUS would make it possible to identify WUS-regulated genes that follow a similar expression behavior as that of *CLV3*. The *35S::NLS-WUS-GR* developed for this purpose was constitutively nuclear even before Dex application and therefore was not suitable for time resolved experiments (Data not shown). To circumvent

this, we have developed a Dex-inducible two component system that drives the expression of nuclear enriched forms of WUS (*35S::GR-LhG4;6xoP::NLS-WUS*). LhG4 is a bacterial TF that has been fused to GR, the LhG4-GR migrates into nucleus after Dex application and activates expression of *NLS-WUS* by binding the operator sequences. This construct will be introduced into *ap1;cal1* background. The comparison of the transcriptomes regulated by *35S::WUS-GR* (Yadav et al., 2013) with *35S::LhG4-GR;6xOP::NLS-WUS* will allow us to identify those genes that are activated by WUS at low level and repressed at higher level (*CLV3*-like genes). Many of the repressed targets of WUS may also switch to activation at extremely low WUS levels. Therefore, in parallel, developing plant lines that deplete WUS (an artificial microRNA against WUS in *ap1;cal1* background [Perales et al., 2016]) can be used to further investigate the transcriptome.

To decipher the cis-element organization associated with the promoters of WUS regulated genes, employing a chromatin immunoprecipitation-exonuclease (ChIP-exo) method is required to obtain genome-wide WUS binding patterns. ChIP-exo analysis by using a Dex inducible form of WUS [*35S::WUS-GR*] in the *ap1;cal1* background should help overcome the tissue limitations of our system. ChIP experiments can be carried out by using the methods and anti-WUS antibodies that have been described earlier by our laboratory (Yadav et al., 2013), which led to the discovery of the WUS-binding CRM in the *CLV3* enhancer region. Our recent study revealed a destabilization of WUS-GR within 12 hours of Dex application and nuclear translocation (Fig. 4.9) [Rodriguez et al., 2016]. Therefore, harvesting the SAMs for ChIP analysis within 6 hours of Dex application should limit the loss of WUS-GR protein and sufficiently enrich WUS protein in the nuclei. ChIP using pre-immune serum and INPUT DNA can serve as controls. Sheared DNA bound by

WUS can be pulled down by our labs WUS-specific antibodies or those commercially available that bind GR. After sequences are aligned to the genome through tools such as Bowtie, which are based around the Burrows Wheeler Transform, and can perform exceptionally fast accurate alignment (Langmead et al., 2009). The resulting mapped reads can be further processed with a peakcaller such as GEM (Guo et al., 2012) to identify areas of enriched binding from the alignments. In the case of ChIP-exo, binding events are signified by the presence of peak pairs, which flank the binding regions. The end result will provide a snapshot of WUS-bound regions across the entire genome in an *in vivo* context. ChIP-exo has been shown to improve the spatial resolution of binding events from a roughly 200 base-pair resolution of regular ChIP-seq up to nearly single bp resolution (Gua et al., 2012; Skene et al., 2015). The enhanced resolution could resolve fine details in the binding such as four binding motifs of a single TF clustered within a 57 bps region (Rhee et al., 2012). For our purposes, closely spaced cis-elements would become readily apparent. By analyzing the distance between complementary peaks (that will be obtained through forward and reverse strand sequencing), one can infer the size of the footprint, which is a reflection of the number of WUS molecules bound to a cis-element. The peak height is a readout of sequence enrichment that can be used to infer relative occupancy of each cis-element. These features are particularly important in resolving individual WUS binding cis-elements genome wide including the closely clustered cis-elements such as those present in *CLV3 CRM*.

Completion of both experiments will potentially identify three classes of genes that respond to changes in WUS levels (activated, repressed, and activation/repression switch). This classification will be a powerful tool to determine how cis-element organization, specifically in the promoters/enhancers of WUS-regulated genes encodes gene regulation. Our previous ChIP-seq, although it localized WUS binding to the *CLV3 CRM*, it was unable to resolve the individual cis-elements. The resolution of CHIP-exo will enable analysis of promoters/enhancers based on the number of neighboring cis-elements, relative affinities and cis-elements with multi-TAAT cores. Based on our experience of working with the *CLV3-CRM*, we could find clusters of low affinity cis-elements in gene promoters/enhancers that respond to WUS concentration. Our preliminary analysis reveals that WUS binds to a cis-element in *KANADI1 (KAN1)* promoter with 3 times higher affinity than the high affinity (970) cis-element in the *CLV3 CRM* (Data not shown). *KAN1* is a repressed target whose expression is restricted to lateral edges of the PZ where WUS accumulates at extremely low levels, justifying the requirement of higher affinity cis-elements (Yadav et al., 2016). Contrasting *KAN1* and *CLV3* suggests that independent/dispersed high-affinity cis elements may be sufficient to achieve repression whereas a cluster of lower-affinity cis elements may be required to mediate a concentration-dependent switch. This analysis will allow large scale comparison of cis-element organization in different classes of WUS-regulated genes leading to a better understanding of the cis-regulatory logic.

Nested Functions

Domain	Function	Function	Function
Homodimerization domain1 (HOD1)	DNA binding	Dimerization	Spatial Restriction
Homodimerization domain2 (HOD2)	Dimerization	Spatial Restriction	
Acidic Domain	Transcriptional Regulation	Destabilization	
WUS Box (WB)	Transcriptional Regulation	Nuclear Retention	Destabilization
ERF-associated amphiphilic repression (EARL)	Transcriptional Regulation	Nuclear Export	Destabilization

Opposing Functions

Domain	Function	Domain	Function
WB	Nuclear Retention	EARL	Nuclear Export

Fig. 5.1 Functions of domains within the WUS protein. Domains in the WUS protein have been characterized by various groups to determine their function. Many of the domains perform more than 1 function (Nested functions) while other domains of WUS perform counteracting function (opposing functions).

Materials and methods

Plant Growth, Genotypes, and Microscopy. *Arabidopsis* plant growth procedures for imaging and phenotypic analysis were followed as described in earlier studies (Yadav et al., 2011; Yadav et al., 2010; Reddy et al., 2005; Reddy et al., 2004). Preparation for live imaging, Dex treatment, the optics, the microscopy platform (Zeiss 510 LSM), image acquisition, and image reconstruction have been described in earlier studies (Yadav et al., 2011; Reddy et al., 2005; Reddy et al., 2004). All transgenic lines were generated in Landsberg *erecta* (Ler) background. *wus-1*, *clv3-2*, and *wus-7* have been described previously (Laux et al., 1996; Fletcher et al., 1999; Graf et al., 2010). For *35S::eGFP-WUS-GR* and *35S::eGFP-GR* analysis on Dex plates, seedlings were germinated on MS plates for 7 d containing 10 μ M Dex. Plants were germinated on MS-agar plates and allowed to grow for 10 d before they were transferred into clear plastic boxes containing MS-agar. For single time point observations, plants were grown on soil. Upon bolting, when the shoot apex emerged out of the rosette, the plants were prepared for time-lapse imaging. The MS-agar surface was overlaid with 1% (wt/vol) agarose to minimize contamination. The older floral buds were removed to expose SAMs. The rosette was stabilized by applying 1.5% (wt/vol) molten agarose onto the stem. FM4-64 (50 μ g/mL) was applied directly onto the shoot meristems 30 min before imaging. eGFP-tagged constructs were imaged with 488 nm excitation, and emission was collected between 500 nm and 550 nm by using a Zeiss 510 confocal microscope.

Vegetative SAM sections (see following section) were imaged using a Leica SP5 system fitted with an argon laser that was activated to 20%. The images were taken using a 40 \times objective and a 2.5 \times digital zoom. eGFP-tagged constructs were imaged with

excitation at 488 nm, and emission was collected between 500 and 550 nm. mYFP-tagged constructs were imaged by using either 488 nm or 514 nm excitation, and emission was collected between 550 and 600 nm. The bright-field images were captured by simultaneous scanning.

Plant Seedling Sectioning for Confocal Microscopy and RNA in Situ Hybridization. Seedlings were germinated on MS plates for 7 d, embedded in 5% agarose, hand cut with a fine razor, mounted on glass slides, and imaged as described in *Plant Growth, Genotypes, and Microscopy*. Wherever appropriate, seedlings were germinated on Murashiga and Skoog (MS) plates containing 10 μ M Dex. Tissue preparation, sectioning of plants for RNA in situ analysis, probe synthesis, hybridization, and detection were performed as described earlier (www.its.caltech.edu/~plantlab/protocols/insitu.html). The mGFP5 probe used in this study has been described in an earlier study (Reddy et al., 2005).

qRT-PCR. For qRT-PCR, RNA was isolated from SAMs expressing amiR-WUS that had been treated with Dex or mock treated for 4 or 8 d using the RNeasy kit (Qiagen). cDNA was reverse-transcribed using ThermoScript RT (Invitrogen). qRT-PCR reactions were performed using the sensiMix SYBR kit (Bioline) on a Bio-Rad iQ5 Cyclor. Analyses were performed for duplicate samples, and quantification was standardized to ubiquitin (UBQ10) mRNA levels. Primers used in this study are listed in Table 1.

Fluorescence Quantification. Image stacks (.lif files) from the Leica SP5 microscopy were imported into ImageJ software using the LOCI Bio-Formats plugin. Image stacks then were separated into individual xy .tiff images using the Image → Stacks → Stack to Images function. Fluorescent channels from these images were isolated using the Image → Color → Split Channel function. The region of interest (ROI) manager was loaded using the Analyze → Tools → ROI Manager function, and circular regions of interest were drawn around the nuclei expressing H2B-mYFP or eGFP:WUS. The measure tool in the ROI manager was used to determine the average fluorescence within each region of bounded nuclei, and these values were assigned to their respective cells as numbered by ROI selection. Cells were assigned to SAM layers as L1, L2, L3, and so forth. These values were averaged across each layer, and this process was repeated in five plants per construct to obtain the quantification values used to compare fluorescence intensity values across layers.

Phenotypic Complementation Analysis. The SAM size quantification was carried out on plants that were ~5 wk old. A minimum of nine SAMs from six independent transgenic lines for each mutant promoter were used for quantifying SAM height. The adaxial junction of the fifth primordia was used as reference to measure the SAM height (see the schematic in Fig. 2.3P for details). Height was measured from the base of the fifth primordia to the SAM tip. For multiple comparisons, statistical analysis was performed by one-way ANOVA followed by Tukey's HSD test using the soft R Project (v.3.1.2) package.

Plasmid Construct and Generation of Transgenic Lines. Deletions, mutations, and addition of an extra NES coding sequence, identified previously as a potent nuclear export signal in Rev protein from HIV-1 (Haasen et al., 1999), in *eGFP-WUS* were generated by inverse PCR using 5' phosphorylated oligos listed in Table 1, using *eGFP-WUS* in a PCR4 vector as template (Yadav et al., 2011). All mutations, deletions, and *WUS*-containing exogenous NLSs and NESs were introduced into the *WUS* promoter in pCAMBIA2300 (Yadav et al., 2011). To generate the *pCLV3::LhG4, 6XOP::eGFP-WUS* and *pCLV3::LhG4, 6XOP::NLS-eGFP-WUS* lines, the coding sequences of *eGFP-WUS* and *NLS-eGFP-WUS* were cloned into the pENTR vector (Invitrogen). The recombination reaction was carried out with the Gateway *6XOP pzp222* binary vector to create *6XOP::eGFP-WUS* and *6XOP::NLS-eGFP-WUS*, respectively. Twenty independent transgenic lines carrying these constructs were crossed to the driver lines *CLV3::LhG4* used in an earlier study (Yadav et al., 2010). The constructs *35S::eGFP-WUS-GR* and *35S::eGFP-GR* were generated by adding the *GR* sequence to the *eGFP-WUS* in the PCR4 vector. Then, the *e-WUS-GR* and *eGFP-GR* were cloned in the pENTR cloning vector. Finally, LR reaction was carried out with the pMDC32 binary vector containing the *2X35S* promoter (Curtis et al., 2003). The number of independent transgenic lines analyzed for each transgene is shown as “*n*” in parentheses at appropriate places in the paper.

The reporter construct *pCLV3::H2B-mYFP* was generated by introducing the BamH1-containing coding sequence of H2B-mYFP described in an earlier studies (Müller et al., 2006; Brand et al., 2002). The *CLV3* promoter contained the region 1,500 bp upstream and 1,200 bp downstream in the pGREEN binary vector. Mutations and

deletions of *pCLV3* were performed by inverse PCR using 5' phosphorylated oligonucleotides (Table 1). A minimum of eight plants from independent transgenic lines of each promoter mutation construct were obtained and analyzed for H2B-mYFP fluorescence in both vegetative and inflorescence SAMs. The actual number of independent transgenic plants screened for each mutant promoter is stated in parentheses at appropriate places in the text. To account for the variability across different insertion lines, fluorescence intensity was quantified from five SAMs derived from independent transgenic lines.

To generate a Dex-inducible amiRNA for silencing *WUS*, the 21-nt amiRNA sequence against *WUS* was designed based on guidelines outlined at wmd3.weigelworld.org/cgi-bin/webapp.cgi. The sequence showing no or the fewest possible off-targets was chosen for further construction of the amiRNA. For the amplification of the amiRNA precursor, several rounds of PCR were carried out using the primers listed in Table 1. The final amplification product of the overlapping PCR, coding for the amiR-*WUS* precursor, was first cloned into the pENTR vector. The LR reaction with pENTR amiR-*WUS* was set up with the *6xOP-pzp222* binary vector to create *6xOP::amiR-WUS*. The independent lines carrying this construct were crossed to the *35S::GR-LhG4* driver line to generate *35S::GR-LhG4;6xOP::amiR-WUS*. The number of independent transgenic lines and combinations tested in each case are stated in parentheses at appropriate places in the text.

EMSA. His-WUS fusion full-length protein WUS(aa1–292), truncated WUS proteins WUS(aa1–208) and WUS(aa1–134), the HOD1 single mutant WUS(aa1–208):G77E, and the HOD1/HOD2 double mutant WUS(aa1–134):G77E were generated using the oligonucleotides listed in Table 1. The amplified DNA fragments were cloned into pET28a plasmid (Novagen) for recombinant expression in *Escherichia coli* BL21 cells as described previously (Yadav et al., 2011; Yadav et al., 2013). His-WUS fusion proteins were purified as described earlier (Yadav et al., 2011; Yadav et al., 2013). All oligonucleotides used for EMSAs are listed in Table 1. Oligonucleotide radiolabeling, DNA–protein binding reactions, and electrophoresis were performed as described earlier (Yadav et al., 2011). Purified full-length His-WUS and truncated and mutated protein versions were diluted in 20 μ M Hepes-KOH at pH 7.8, 100 μ M KCl, and 1 μ M EDTA at 1 \times concentration (0.5 ng/ μ L) for binding assays. For K_d calculation, WUS binding was quantified by densitometry from three independent saturation curves using Quantity One 1-D Analysis Software (Bio-Rad), and the fraction of the oligos bound by WUS at each protein concentration was calculated. Graphical representation and nonlinear fit for a saturation-binding curve and K_d calculation were performed using GraphPad Prism 5.0 software. The data are presented as the mean \pm SE of three independent experiments.

SEC and WUS Detection and Quantification. Full-length WUS (WUS aa1–292) and the HOD1 and HOD2 double mutant [WUS (aa1–134):G77E] were expressed in *E. coli* BL21 cells, purified from soluble lysates using the his-tag protocol (Ni-NTA His-Bind Resins; Novagen), and subsequently dialyzed against 20 mM Hepes (pH 7.8) and 100 mM KCl buffer. Resin Bio-Gel P-100 (Bio-Rad) was hydrated in 20 mM Hepes (pH 7.8) and 100 mM KCl buffer and was packed on a 0.7 \times 20 cm chromatography column (Bio-

Rad) following the manufacturer's instructions. SEC was performed with the dialyzed full-length (WUS aa1–292) and the HOD1 and HOD2 double-mutant [WUS (aa1-134:G77E)] forms suspended in 20 mM Hepes (pH 7.8) and 100 mM KCl buffer at room temperature, with a flow rate of 0.05 mL/min. Elutions of 250-mL fractions were collected, and the presence of WUS protein was analyzed in each elution using the Bio-Dot system (Bio-Rad) using anti-WUS antibody (Yadav et al., 2011). To calculate the WUS dimer K_d , SEC was performed using 0.3-, 3-, and 15- μ M dialyzed full-length WUS (WUS aa1–292). Concentrations of WUS monomer and WUS dimer were measured upon pooling the eluted fractions representing the two WUS species using the BCA Protein Assay Reagent and following the manufacturer's instructions for enhanced sensitivity (Thermo Scientific Pierce). The ratio of WUS dimer/WUS monomer was determined. Graphical representation and K_d calculation were performed using GraphPad Prism 5.0 software. The data are presented as the mean \pm SE of four independent experiments.

Yeast Two-Hybrid Interaction. A Gal4-based two-hybrid system was used in this study. A WUS coding sequence was used as a template to generate truncations, deletions, and mutant versions using the oligonucleotides listed in Table 1. All WUS fragments were cloned in yeast two-hybrid vectors pGBKT7 and pGADT7 (Clontech) and cotransformed into yeast two-hybrid strain AH109 (Clontech) using standard procedures. Transformants were selected on solid synthetic drop-out (SD) medium that lacked both leucine and tryptophan, (SD-Leu-Trp). WUS–WUS protein interaction was tested on solid SD medium that lacked leucine, tryptophan, histidine, and adenine (SD-Leu-Trp-His-Ade). To perform a semiquantitative growth assay, suspensions of each cotransformed yeast cell were prepared at standardized densities. Serial dilutions (10^{-1} , 10^{-2} , 10^{-3} and 10^{-4}) were made and spotted onto solid selective media: SD-Leu-Trp and SD-Leu-Trp-His-Ade.

Bimolecular Fluorescence Complementation. For BiFC analyses in *N. benthamiana* cells, the N-terminal fragment of eGFP (N-eGFP) from nucleotides 1 to 465 (amino acids 1 to 155) and the C-terminal fragment of eGFP (C-eGFP) from nucleotides 466 to 723 (amino acids 156 to 241) were fused to a WUS coding sequence and cloned into pENTR, along with N-eGFP and C-eGFP fragments that were used as negative controls. They were then recombined with the destination vector pMDC32 under the control of a 2X35S promoter. Mutations for homodimerization were introduced with primers from Table 1. *Agrobacterium tumefaciens* GV3101 transformed with WUS BiFC constructs was introduced in leaves of 3- to 4-wk-old *Nicotiana* by agroinfiltration. In all cases, agrobacterium transformed with the corresponding two BiFC plasmids along with the p19 suppressor of silencing was introduced into *N. benthamiana* leaves in a 1:1:1 ratio. The fluorescence was monitored by using an inverted Leica TCS-SP5 confocal system.

Table 1. Primers used in study

Construct	Primer name	Primer Sequence
pCLV3:: H2b-mYFP and mutant promoters		
H2b-mYFP	H2b-mYFP-BamH-Fw	CAGGATCCATGGCGAAGGCAGATAAGAAACCAGCGG
	H2b-mYFP-BamH-Rev	GTGGATCCTTATTTGTATAGTTCATCCATGCCATGTG
pCLV3-1080M	pCLV3-1080M-Fw	CATATGATCCATTCAATTTATGTTTTTTC
	pCLV3-1080M-Rev	AGCCTTGCCGGCGCCGTATCGAGGG
pCLV3D-1200, -900	pCLV3D-1200, -900-Fw	AAGCATATAACTGTTTCCAGATTAAC
	pCLV3D-1200, -900-Rev	CAGATTCCGTTTTGCTTCGTTACTC
pCLV3 950M	pCLV3 950M –Fw	CGTACCCCCAAATTTTCCCAACGGTACATTGC
	pCLV3 950M-Rev	TTTTCAATTGTCAATGCAAATACCCCATGG
pCLV3 970M	pCLV3 970M –Fw	GGTATTTGCATTGACAATTGAAAACGTAC
	pCLV3 970M – Rev	CCATGGATGTGATAGTCACAATTAAC
pCLV3 997M	pCLV3 997M –Fw	GTGACTATCACATCCATTAATTATTTGC
	pCLV3 997M – Rev	AATGGAACATACAATAATAAAAATGATGATG
pCLV3 1007M	pCLV3 1007M – Fw	GATTCGATGATGTGGTGGGAAGG
	pCLV3 1007M – Rev	ATCATCATCATTTTTGGGGTTGTATGTT
pCLV3 1060M	pCLV3 1060M – Fw	GTCGGTCCCCTTATCCTTCCCACCACATCATC
	pCLV3 1060M – Rev	TTTGGGGCAGTGACAGGCAGTGTGTCAGTG

pCLV3 943-1067	pCLV3 1067M – Fw	CCGACTTTGGGGCAGTGACAG
	pCLV3 1043M – Rev	CCCAACGGTACATTGCTTTGG
EMSA probes		
950	950-Fw	AACGTACTAATAAATTTTCCCAACGGTA
	950-Rev	TACCGTTGGGAAAATTTATTAGTACGTT
950M	950M-Fw	AACGTACCCCAAATTTTCCCAACGGTA
	950M-Rev	TACCGTTGGGAAAATTTGGGGGTACGTT
970	970-Fw	CACATCCATTAATTATTTGCATTGACAATTG
	970-Rev	CAATTGTCAATGCAAATAATTAATGGATGTG
970M	970M-Fw	CACATCCATCCCCTATTTGCATTGACAATTG
	970M-Rev	CAATTGTCAATGCAAATAGGGGATGGATGTG
997	997-Fw	TTATTGTATGTTTAATTGTGACTAT
	997-Rev	ATAGTCACAATTAACATACAATAA
997M	997M-Fw	TTATTGTATGTTCCATTGTGACTAT
	997M-Rev	ATAGTCACAATGGAACATACAATAA
1007	1007-Fw	ACATACAATAATAAAAATGATGATGAT
	1007-Rev	ATCATCATCATTTTTATTATTGTATGT
1007M	1007M-Fw	ACATACAAGGGGAAAATGATGATGAT
	1007M-Rev	ATCATCATCATTTTTCCCCTTGTATGT
1060	1060-Fw	GTCGGTTTAATTTATCCTTCCCA
	1060-Rev	TGGGAAGGATAAATTAACCGAC
1060M	1060M-Fw	GTCGGTCCCCTTATCCTTCCCA
	1060M-Rev	TGGGAAGGATAAGGGGAACCGAC

970-M1	970-M1-Fw	CACATCCAGTAATTATTTGCATTGACAATTG
	970-M1-Rev	CAATTGTCAATGCAAATAATTACTGGATGTG
970-M2	970-M2-Fw	CACATCCATGAATTATTTGCATTGACAATTG
	970-M2-Rev	CAATTGTCAATGCAAATAATTCATGGATGTG
970-M3	970-M3-Fw	CACATCCATTGATTATTTGCATTGACAATTG
	970-M3-Rev	CAATTGTCAATGCAAATAATCAATGGATGTG
970-M4	970-M4-Fw	CACATCCATTAGTTATTTGCATTGACAATTG
	970-M4-Rev	CAATTGTCAATGCAAATAACTAATGGATGTG
970-M5	970-M5-Fw	CACATCCATTAAGTATTTGCATTGACAATTG
	970-M5-Rev	CAATTGTCAATGCAAATACTTAATGGATGTG
970-M6	970-M6-Fw	CACATCCATTAATGATTTGCATTGACAATTG
	970-M6-Rev	CAATTGTCAATGCAAATCATTAAATGGATGTG
970-M7	970-M7-Fw	CACATCCATTAATTGTTTGCATTGACAATTG
	970-M7-Rev	CAATTGTCAATGCAAACAATTAATGGATGTG
970-M8	970-M8-Fw	CACATCCATTAATTAGTTGCATTGACAATTG
	970-M8-Rev	CAATTGTCAATGCAACTAATTAATGGATGTG
970-M9	970-M9-Fw	CACATCCATTAATTATGTGCATTGACAATTG
	970-M9-Rev	CAATTGTCAATGCACATAATTAATGGATGTG

Cloning of WUS deletion and mutation in pET-28a for protein expression in *E. coli*

WUS-NDE	NdeI-WUS- Fw	CATATGATGGAGCCGCCACAGCATCA
WUS-FL-XHO	Xho-WUS- Rev	CTCGAGCTAGTTCAGACGTAGCTCA
WUS-208-XHO	Xho-WUS-208-Rev	CTCGAGTCCACCTACGTTGTTGTAATTCATAG
WUS-134-XHO	Xho-WUS-134-Rev	CTCGAGCGTGATGATGGTGAAGTAGAGGATG
WUS-7M	WUS-7M-Fw	GAGACAGTTCGAAAAGATTGAGG
	WUS-7M-Rev	AGCCTTGACAGTGATCTTC

qRT-PCR primers		
WUS	WUS-Fw	GAAGACGGGGGAATGGGATGAGATT
	WUS-Rev	GAGCTTTAATCCCGAGCGACACCGG
UBQ10	UBQ10-Fw	GATCTTTGCCGGAAAACAATTGGAGGA
	UBQ10-Rev	CGACTTGTCATTAGAAAAGAAAGAGATACA
WUS	WUS-Fw	ATCATGCAAGCTCAGGTACTGAATGT
	WUS-Rev	GAGCTTTAATCCCGAGCGACACCGG
amiRWUS Cloning		
amiRWUS precursor	WUS-I miR-s	gaTATTAATCACTAGCGAAGCGTtctctctttgtattcc
	WUS-II miR-a	gaACGCTTCGCTAGTGATTAATAtcaaagagaatcaatga
	WUS-III miR	gaACACTTCGCTAGTCATTAATTcacaggtcgtgatg
	WUS-IV miR	gaAATTAATGACTAGCGAAGTGTtctacatatattcct
amiRWUS	WUS-oligo A (GW)	CACCTGCAAGGCGATTAAGTTGGGTAAC
pENTR	WUS-oligo B	GCGGATAACAATTTACACAGGAAACAG
	NLS-eGFP-Fw-GW	CACCATGGAGCAGAAGCTGATCTCCGAGGAGGAC
	eGFP-Fw-GW	CACCATGGTGAGCAAGGGCGAGGAGCTGTTCCACC
eGFP-WUS deletion and mutation for structure-function analyse		
eGFP-NES-WUS	NES-WUS-Fw	AACGATTAACCCTCGATATGGAGCCGCCACAGCATCA GC
	NES-WUS-Rev	CTAATGGTGGTAATTGTAAGGATCCCTTGACAGCTCG TCC
Free eGFP and free NLS-eGFP	DWUS-Fw	TGAACTAGGCCTGCAAGGGCG
	DWUS-Rev	GGATCCCTTGACAGCTCGTC

eGFP-WUS (1-134)	SP/ WUS1/1-1147	CTGGCGCGCCATGGTGAGCAAGGGCGAGGAGCTGTT CA
	ASP/WUS1/1- 1147	CCAGGCCTTCAGGGAACACCGTGATGATGGTGAAGTA G
eGFP-WUS (281-292)	DEARL-Fw	CTAGGCCTGCAAGGGCGAATTCGCG
	DEARL-Rev	CGAACTTCCGATTGGCCATACTTCC
eGFP-WUS (249-265)	DWB-Fw	CACATCAACGGTGGTAGTGGTGCCATC
	DWB-Rev	TTCCAGATAAGCATCGCCACCACATTC
eGFP-WUS (230-246)	PEST Fw	GCTTATCTGGAACATCGACGTACGC
	PEST rev lg	CTTTGCTCTATCGAAGAAGTTGTAAGG
eGFP-WUS (208-227)	IFF-PEST-1 forward	GCAAAGCCTCTGTTTGGTCTAGAAGG
	IFF PEST1 rev	ACCTACGTTGTTGTAATTCATAGAACAG
eGFP-WUS (134-208)	5'pIFF-F	GGATGGGCAAACATGGATCATCATTAC
	5'pIFF-R	GGGAACACCGTGATGATGGTGAAG
EARLM	EARLM-Fw	TTCTGCTGAGGCACGTGCGAACTAG
	EARLM-Rev	GCGCAAGGGCGAACTTCCGATTGGCC
WBM	WBM-Fw	CGACGTACGGCTCCTGCCTTCCCTATGCAC
	WBM-Rev	ATGTTCCAGATAAGCATCGCCACCACATTC
BiFC cloning		
pENTR cloning	N'eGFP-Fw-GW	CACCATGGTGAGCAAGGGCGAGGAGCTGTTC
	C'eGFP-Fw-GW	CACCATGGACAAGCAGAAGAACGGCATCAAG
	WUS-5'-Rev	CTAGTTCAGACGTAGCTCAAGAGAAGC
Yeast two hybrid		
134-ECORI	134 Rev	CAATTCGTTGATGATGGTGAAGTAGAGGATG
208-ECORI	208 rev	CTGGAATTCCTATGCCCATCCTCCACCTACGTTG

250-ECORI	250 rev	GAATTCCTATTCCAGATAAGCATCGCCACCAC
FL-ECORI	FL REV	CTGGAATTCCTAGTTCAGACGTAGCTCAAGAG
134-NDE-F	134 forward	CAG CATATG CCCATGCAGAGACCTGCTAATT CCG
Cloning of WUS deletion and mutation in pET-28a for protein expression in <i>Escherichia coli</i>		
WUS-NDE	Forward	CATATGATGGAGCCGCCACAGCATCA
WUS-FL-XHO	REVERSE	CTCGAGCTAGTTCAGACGTAGCTCA
WUS-208-XHO	REVERSE	CTCGAGTCCACCTACGTTGTTGTAATTCATAG
WUS-134-XHO	REVERSE	CTCGAGCGTGATGATGGTGAAGTAGAGGATG
WUS-7M	WUS-7M-FW	GAGACAGTTCGAAAAGATTGAGG
	WUS-7M-REV	AGCCTTGCAGTGATCTTC
Expressing eGFP-WUS in L2 layer		
pHDG4	SP/At4g17710/1-3115	AAGGTACCGGATCCTGATTAGAGCAATTAGCCCGT
	ASP/At4g17710/1-3115	ATGGCGCGCCAGACAAAGAGAAGACTGAGTTTAAA

References

- Aida, M., Ishida, T., & Tasaka, M. (1999). Shoot apical meristem and cotyledon formation during Arabidopsis embryogenesis: interaction among the CUP-SHAPED COTYLEDON and SHOOT MERISTEMLESS genes. *Development*, *126*(8), 1563–1570.
- Aida, M., Ishida, T., Fukaki, H., Fujisawa, H., & Tasaka, M. (1997). Genes involved in organ separation in Arabidopsis: an analysis of the cup-shaped cotyledon mutant. *The Plant Cell Online*, *9*(6), 841–857.
- Aza-Blanc, P., Ramírez-Weber, F. A., Laget, M. P., Schwartz, C., & Kornberg, T. B. (1997). Proteolysis that is inhibited by hedgehog targets Cubitus interruptus protein to the nucleus and converts it to a repressor. *Cell*, *89*(7), 1043–1053.
- Banerji, J., Rusconi, S., & Schaffner, W. (1981). Expression of a beta-globin gene is enhanced by remote SV40 DNA sequences. *Cell*, *27*(2 Pt 1), 299–308.
- Barton, M. K. (2010). Twenty years on: The inner workings of the shoot apical meristem, a developmental dynamo. *Developmental Biology*, *341*(1), 95–113.
- Benjamins, R., & Scheres, B. (2008). Auxin: the looping star in plant development. *Annual Review of Plant Biology*, *59*, 443–465.
- Benková, E., Michniewicz, M., Sauer, M., Teichmann, T., Seifertová, D., Jürgens, G., & Friml, J. (2003). Local, Efflux-Dependent Auxin Gradients as a Common Module for Plant Organ Formation. *Cell*, *115*(5), 591–602.
- Berger, M. F., Badis, G., Gehrke, A. R., Talukder, S., Philippakis, A. A., Peña-Castillo, L., ... Hughes, T. R. (2008). Variation in homeodomain DNA binding revealed by high-resolution analysis of sequence preferences. *Cell*, *133*(7), 1266–1276.
- Berman, B. P., Nibu, Y., Pfeiffer, B. D., Tomancak, P., Celniker, S. E., Levine, M., ... Eisen, M. B. (2002). Exploiting transcription factor binding site clustering to identify cis-regulatory modules involved in pattern formation in the Drosophila genome. *Proceedings of the National Academy of Sciences of the United States of America*, *99*(2), 757–762.
- Bhalerao, R. P., & Bennett, M. J. (2003). The case for morphogens in plants. *Nature Cell Biology*, *5*(11), 939–943.

- Boisnard-Lorig, C., Colon-Carmona, A., Bauch, M., Hodge, S., Doerner, P., Bancharel, E., ... Berger, F. (2001). Dynamic analyses of the expression of the HISTONE:: YFP fusion protein in Arabidopsis show that syncytial endosperm is divided in mitotic domains. *The Plant Cell*, 13(3), 495–509.
- Bothma, J. P., Garcia, H. G., Esposito, E., Schlissel, G., Gregor, T., & Levine, M. (2014). Dynamic regulation of eve stripe 2 expression reveals transcriptional bursts in living Drosophila embryos. *Proceedings of the National Academy of Sciences of the United States of America*, 111(29), 10598–10603.
- Brand, U., Grünewald, M., Hobe, M., & Simon, R. (2002). Regulation of CLV3 expression by two homeobox genes in Arabidopsis. *Plant Physiology*, 129(2), 565–575.
- Brand, U., Fletcher, J. C., Hobe, M., Meyerowitz, E. M., & Simon, R. (2000). Dependence of Stem Cell Fate in Arabidopsis on a Feedback Loop Regulated by CLV3 Activity. *Science*, 289(5479), 617–619.
- Busch, W., Miotk, A., Ariel, F. D., Zhao, Z., Forner, J., Daum, G., ... Lohmann, J. U. (2010). Transcriptional control of a plant stem cell niche. *Developmental Cell*, 18(5), 849–861.
- Byrne, M. E., Simorowski, J., & Martienssen, R. A. (2002). ASYMMETRIC LEAVES1 reveals knox gene redundancy in Arabidopsis. *Development*, 129(8), 1957–1965.
- Byrne, M. E., Barley, R., Curtis, M., Arroyo, J. M., Dunham, M., Hudson, A., & Martienssen, R. A. (2000). Asymmetric leaves1 mediates leaf patterning and stem cell function in Arabidopsis. *Nature*, 408(6815), 967–971.
- Cheng, Y., Dai, X., & Zhao, Y. (2007). Auxin synthesized by the YUCCA flavin monooxygenases is essential for embryogenesis and leaf formation in Arabidopsis. *The Plant Cell*, 19(8), 2430–2439.
- Clark, S. E., Williams, R. W., & Meyerowitz, E. M. (1997). The CLAVATA1 gene encodes a putative receptor kinase that controls shoot and floral meristem size in Arabidopsis. *Cell*, 89(4), 575–585.
- Clark, S. E., Running, M. P., & Meyerowitz, E. M. (1995). CLAVATA3 is a specific regulator of shoot and floral meristem development affecting the same processes as CLAVATA1. *Development*, 121(7), 2057–2067.

- Crawford, K. M., & Zambryski, P. C. (2000). Subcellular localization determines the availability of non-targeted proteins to plasmodesmatal transport. *Current Biology: CB*, *10*(17), 1032–1040.
- Crocker, J., Abe, N., Rinaldi, L., McGregor, A. P., Frankel, N., Wang, S., ... Stern, D. L. (2015). Low affinity binding site clusters confer hox specificity and regulatory robustness. *Cell*, *160*(1-2), 191–203.
- Curtis, M. D., & Grossniklaus, U. (2003). A Gateway Cloning Vector Set for High-Throughput Functional Analysis of Genes in Planta. *Plant Physiology*, *133*(2), 462–469.
- Daum, G., Medzihradzky, A., Suzaki, T., & Lohmann, J. U. (2014). A mechanistic framework for noncell autonomous stem cell induction in Arabidopsis. *Proceedings of the National Academy of Sciences*, *111*(40), 14619–14624.
- Dolzblasz, A., Nardmann, J., Clerici, E., Causier, B., van der Graaff, E., Chen, J., ... Laux, T. (2016). Stem Cell Regulation by Arabidopsis WOX Genes. *Molecular Plant*, *9*(7), 1028–1039.
- Driever, W., & Nüsslein-Volhard, C. (1988). The bicoid protein determines position in the Drosophila embryo in a concentration-dependent manner. *Cell*, *54*(1), 95–104.
- Endrizzi, K., Moussian, B., Haecker, A., Levin, J. Z., & Laux, T. (1996). The SHOOT MERISTEMLESS gene is required for maintenance of undifferentiated cells in Arabidopsis shoot and floral meristems and acts at a different regulatory level than the meristem genes WUSCHEL and ZWILLE. *The Plant Journal: For Cell and Molecular Biology*, *10*(6), 967–979.
- Fiers, M., Golemiec, E., van der Schors, R., van der Geest, L., Li, K. W., Stiekema, W. J., & Liu, C.-M. (2006). The CLAVATA3/ESR motif of CLAVATA3 is functionally independent from the nonconserved flanking sequences. *Plant Physiology*, *141*(4), 1284–1292.
- Fletcher, J. C., Brand, U., Running, M. P., Simon, R., & Meyerowitz, E. M. (1999). Signaling of Cell Fate Decisions by CLAVATA3 in Arabidopsis Shoot Meristems. *Science*, *283*(5409), 1911–1914.
- Friml, J., Vieten, A., Sauer, M., Weijers, D., Schwarz, H., Hamann, T., ... Jürgens, G. (2003). Efflux-dependent auxin gradients establish the apical–basal axis of Arabidopsis. *Nature*, *426*(6963), 147–153.

- Furutani, M., Vernoux, T., Traas, J., Kato, T., Tasaka, M., & Aida, M. (2004). PIN-FORMED1 and PINOID regulate boundary formation and cotyledon development in *Arabidopsis* embryogenesis. *Development*, *131*(20), 5021–5030.
- Gaudet, J., & Mango, S. E. (2002). Regulation of organogenesis by the *Caenorhabditis elegans* FoxA protein PHA-4. *Science*, *295*(5556), 821–825.
- Giorgetti, L., Siggers, T., Tiana, G., Caprara, G., Notarbartolo, S., Corona, T., ... Natoli, G. (2010). Noncooperative interactions between transcription factors and clustered DNA binding sites enable graded transcriptional responses to environmental inputs. *Molecular Cell*, *37*(3), 418–428.
- Giulini, A., Wang, J., & Jackson, D. (2004). Control of phyllotaxy by the cytokinin-inducible response regulator homologue ABPHYL1. *Nature*, *430*(7003), 1031–1034.
- Gordon, S. P., Chickarmane, V. S., Ohno, C., & Meyerowitz, E. M. (2009). Multiple feedback loops through cytokinin signaling control stem cell number within the *Arabidopsis* shoot meristem. *Proceedings of the National Academy of Sciences of the United States of America*, *106*(38), 16529–16534.
- Govind, S., Whalen, A. M., & Steward, R. (1992). In vivo self-association of the *Drosophila* rel-protein dorsal. *Proceedings of the National Academy of Sciences of the United States of America*, *89*(17), 7861–7865.
- Graf, P., Dolzblasz, A., Würschum, T., Lenhard, M., Pfreundt, U., & Laux, T. (2010). MGOON1 Encodes an *Arabidopsis* Type IB DNA Topoisomerase Required in Stem Cell Regulation and to Maintain Developmentally Regulated Gene Silencing. *The Plant Cell*, *22*(3), 716–728.
- Gregor, T., Wieschaus, E. F., McGregor, A. P., Bialek, W., & Tank, D. W. (2007). Stability and nuclear dynamics of the bicoid morphogen gradient. *Cell*, *130*(1), 141–152.
- Guo, Y., Mahony, S., & Gifford, D. K. (2012). High Resolution Genome Wide Binding Event Finding and Motif Discovery Reveals Transcription Factor Spatial Binding Constraints. *PLoS Computational Biology*, *8*(8), e1002638.
- Haasen, D., Köhler, C., Neuhaus, G., & Merkle, T. (1999). Nuclear export of proteins in plants: AtXPO1 is the export receptor for leucine-rich nuclear export signals in *Arabidopsis thaliana*. *The Plant Journal: For Cell and Molecular Biology*, *20*(6), 695–705.

- Helliwell, C. A., Chin-Atkins, A. N., Wilson, I. W., Chapple, R., Dennis, E. S., & Chaudhury, A. (2001). The Arabidopsis AMP1 gene encodes a putative glutamate carboxypeptidase. *The Plant Cell*, 13(9), 2115–2125.
- Higuchi, M., Pischke, M. S., Mähönen, A. P., Miyawaki, K., Hashimoto, Y., Seki, M., ... Kakimoto, T. (2004). In planta functions of the Arabidopsis cytokinin receptor family. *Proceedings of the National Academy of Sciences of the United States of America*, 101(23), 8821–8826.
- Ikeda, M., Mitsuda, N., & Ohme-Takagi, M. (2009). Arabidopsis WUSCHEL is a bifunctional transcription factor that acts as a repressor in stem cell regulation and as an activator in floral patterning. *The Plant Cell*, 21(11), 3493–3505.
- Ip, T. Y., Levine, M., & Small, S. J. (1992). The bicoid and dorsal morphogens use a similar strategy to make stripes in the Drosophila embryo. *Journal of Cell Science*, 1992(Supplement 16), 33–38.
- Ip, Y. T., Park, R. E., Kosman, D., Bier, E., & Levine, M. (1992). The dorsal gradient morphogen regulates stripes of rhomboid expression in the presumptive neuroectoderm of the Drosophila embryo. *Genes & Development*, 6(9), 1728–1739.
- Jasinski, S., Piazza, P., Craft, J., Hay, A., Woolley, L., Rieu, I., ... Tsiantis, M. (2005). KNOX action in Arabidopsis is mediated by coordinate regulation of cytokinin and gibberellin activities. *Current Biology: CB*, 15(17), 1560–1565.
- Jia, S., Flores-Saaib, R. D., & Courey, A. J. (2002). The Dorsal Rel Homology Domain Plays an Active Role in Transcriptional Regulation. *Molecular and Cellular Biology*, 22(14), 5089–5099.
- Jiang, J., & Levine, M. (1993). Binding affinities and cooperative interactions with bHLH activators delimit threshold responses to the dorsal gradient morphogen. *Cell*, 72(5), 741–752.
- Jiang, J., Kosman, D., Ip, Y. T., & Levine, M. (1991). The dorsal morphogen gradient regulates the mesoderm determinant twist in early Drosophila embryos. *Genes & Development*, 5(10), 1881–1891.
- Kaufmann, K., Pajoro, A., & Angenent, G. C. (2010). Regulation of transcription in plants: mechanisms controlling developmental switches. *Nature Reviews. Genetics*, 11(12), 830–842.

- Kerstetter, R. A., Laudencia-Chingcuanco, D., Smith, L. G., & Hake, S. (1997). Loss-of-function mutations in the maize homeobox gene, *knotted1*, are defective in shoot meristem maintenance. *Development*, *124*(16), 3045–3054.
- Kieffer, M., Stern, Y., Cook, H., Clerici, E., Maulbetsch, C., Laux, T., & Davies, B. (2006). Analysis of the transcription factor WUSCHEL and its functional homologue in *Antirrhinum* reveals a potential mechanism for their roles in meristem maintenance. *The Plant Cell*, *18*(3), 560–573.
- Kim, T. K., & Maniatis, T. (1996). Regulation of interferon-gamma-activated STAT1 by the ubiquitin-proteasome pathway. *Science*, *273*(5282), 1717–1719.
- Kondo, T., Sawa, S., Kinoshita, A., Mizuno, S., Kakimoto, T., Fukuda, H., & Sakagami, Y. (2006). A plant peptide encoded by *CLV3* identified by in situ MALDI-TOF MS analysis. *Science*, *313*(5788), 845–848.
- Kurakawa, T., Ueda, N., Maekawa, M., Kobayashi, K., Kojima, M., Nagato, Y., ... Kyozuka, J. (2007). Direct control of shoot meristem activity by a cytokinin-activating enzyme. *Nature*, *445*(7128), 652–655.
- Langmead, B., Trapnell, C., Pop, M., & Salzberg, S. L. (2009). Ultrafast and memory-efficient alignment of short DNA sequences to the human genome. *Genome Biology*, *10*(3), R25.
- Laux, T., Mayer, K. F., Berger, J., & Jürgens, G. (1996). The WUSCHEL gene is required for shoot and floral meristem integrity in *Arabidopsis*. *Development*, *122*(1), 87–96.
- Laux, T., & Jurgens, G. (1997). Embryogenesis: A New Start in Life. *The Plant Cell*, *9*(7), 989–1000.
- Leibfried, A., To, J. P. C., Busch, W., Stehling, S., Kehle, A., Demar, M., ... Lohmann, J. U. (2005). WUSCHEL controls meristem function by direct regulation of cytokinin-inducible response regulators. *Nature*, *438*(7071), 1172–1175.
- Lenhard, M., & Laux, T. (2003). Stem cell homeostasis in the *Arabidopsis* shoot meristem is regulated by intercellular movement of *CLAVATA3* and its sequestration by *CLAVATA1*. *Development*, *130*(14), 3163–3173.
- Lenhard, M., & Laux, T. (1999). Shoot meristem formation and maintenance. *Current Opinion in Plant Biology*, *2*(1), 44–50.

- Levine, M. (2010). Transcriptional enhancers in animal development and evolution. *Current Biology: CB*, 20(17), R754–63.
- Liberman, L. M., Reeves, G. T., & Stathopoulos, A. (2009). Quantitative imaging of the Dorsal nuclear gradient reveals limitations to threshold-dependent patterning in *Drosophila*. *Proceedings of the National Academy of Sciences of the United States of America*, 106(52), 22317–22322.
- Lifanov, A. P., Makeev, V. J., Nazina, A. G., & Papatsenko, D. A. (2003). Homotypic regulatory clusters in *Drosophila*. *Genome Research*, 13(4), 579–588.
- Liscum, E., & Reed, J. W. (2002). Genetics of Aux/IAA and ARF action in plant growth and development. *Plant Molecular Biology*, 49(3-4), 387–400.
- Lo, R. S., & Massagué, J. (1999). Ubiquitin-dependent degradation of TGF-beta-activated smad2. *Nature Cell Biology*, 1(8), 472–478.
- Lohmann, J. U., Hong, R. L., Hobe, M., Busch, M. A., Parcy, F., Simon, R., & Weigel, D. (2001). A molecular link between stem cell regulation and floral patterning in *Arabidopsis*. *Cell*, 105(6), 793–803.
- Long, J. A., Moan, E. I., Medford, J. I., & Barton, M. K. (1996). A member of the KNOTTED class of homeodomain proteins encoded by the STM gene of *Arabidopsis*. *Nature*, 379(6560), 66–69.
- Ma, Q., & Baldwin, K. T. (2000). 2,3,7,8-tetrachlorodibenzo-p-dioxin-induced degradation of aryl hydrocarbon receptor (AhR) by the ubiquitin-proteasome pathway. Role of the transcription activator and DNA binding of AhR. *The Journal of Biological Chemistry*, 275(12), 8432–8438.
- Ma, X., Yuan, D., Diepold, K., Scarborough, T., & Ma, J. (1996). The *Drosophila* morphogenetic protein Bicoid binds DNA cooperatively. *Development*, 122(4), 1195–1206.
- Mansfield, S. G., & Briarty, L. G. (1991). Early embryogenesis in *Arabidopsis thaliana*. II. The developing embryo. *Canadian Journal of Botany. Journal Canadien de Botanique*, 69(3), 461–476.
- Mayer, K. F., Schoof, H., Haecker, A., Lenhard, M., Jürgens, G., & Laux, T. (1998). Role of WUSCHEL in regulating stem cell fate in the *Arabidopsis* shoot meristem. *Cell*, 95(6), 805–815.

Meyerowitz, E. M. (1997). Genetic control of cell division patterns in developing plants. *Cell*, 88(3), 299–308.

Mizukami, Y., & Fischer, R. L. (2000). Plant organ size control: AINTEGUMENTA regulates growth and cell numbers during organogenesis. *Proceedings of the National Academy of Sciences of the United States of America*, 97(2), 942–947.

Muratani, M., & Tansey, W. P. (2003). How the ubiquitin-proteasome system controls transcription. *Nature Reviews. Molecular Cell Biology*, 4(3), 192–201.

Méthot, N., & Basler, K. (1999). Hedgehog Controls Limb Development by Regulating the Activities of Distinct Transcriptional Activator and Repressor Forms of Cubitus interruptus. *Cell*, 96(6), 819–831.

Möller, B., & Weijers, D. (2009). Auxin control of embryo patterning. *Cold Spring Harbor Perspectives in Biology*, 1(5), a001545.

Müller, B., & Sheen, J. (2008). Cytokinin and auxin interaction in root stem-cell specification during early embryogenesis. *Nature*, 453(7198), 1094–1097.

Müller, R., Borghi, L., Kwiatkowska, D., Laufs, P., & Simon, R. (2006). Dynamic and Compensatory Responses of Arabidopsis Shoot and Floral Meristems to CLV3 Signaling. *The Plant Cell*, 18(5), 1188–1198.

Noyes, M. B., Christensen, R. G., Wakabayashi, A., Stormo, G. D., Brodsky, M. H., & Wolfe, S. A. (2008). Analysis of homeodomain specificities allows the family-wide prediction of preferred recognition sites. *Cell*, 133(7), 1277–1289.

Ogawa, M., Shinohara, H., Sakagami, Y., & Matsubayashi, Y. (2008). Arabidopsis CLV3 peptide directly binds CLV1 ectodomain. *Science*, 319(5861), 294.

Okamoto, S., Nakagawa, T., & Kawaguchi, M. (2011). Expression and functional analysis of a CLV3-like gene in the model legume *Lotus japonicus*. *Plant & Cell Physiology*, 52(7), 1211–1221.

Ong, C.-T., & Corces, V. G. (2011). Enhancer function: new insights into the regulation of tissue-specific gene expression. *Nature Reviews. Genetics*, 12(4), 283–293.

Parker, D. S., White, M. A., Ramos, A. I., Cohen, B. A., & Barolo, S. (2011). The cis-regulatory logic of Hedgehog gradient responses: key roles for gli binding affinity, competition, and cooperativity. *Science Signaling*, 4(176), ra38.

- Perales, M., Rodriguez, K., Snipes, S., Yadav, R. K., Diaz-Mendoza, M., & Reddy, G. V. (2016). Threshold-dependent transcriptional discrimination underlies stem cell homeostasis. *Proceedings of the National Academy of Sciences of the United States of America*, 113(41), E6298–E6306.
- Quint, M., & Gray, W. M. (2006). Auxin signaling. *Current Opinion in Plant Biology*, 9(5), 448–453.
- Ramos, A. I., & Barolo, S. (2013). Low-affinity transcription factor binding sites shape morphogen responses and enhancer evolution. *Philosophical Transactions of the Royal Society of London. Series B, Biological Sciences*, 368(1632), 20130018.
- Reddy, G. V., Heisler, M. G., Ehrhardt, D. W., & Meyerowitz, E. M. (2004). Real-time lineage analysis reveals oriented cell divisions associated with morphogenesis at the shoot apex of *Arabidopsis thaliana*. *Development*, 131(17), 4225–4237.
- Reddy, G. V., & Meyerowitz, E. M. (2005). Stem-cell homeostasis and growth dynamics can be uncoupled in the *Arabidopsis* shoot apex. *Science*, 310(5748), 663–667.
- Reeves, G. T., & Stathopoulos, A. (2009). Graded dorsal and differential gene regulation in the *Drosophila* embryo. *Cold Spring Harbor Perspectives in Biology*, 1(4), a000836.
- Reinhardt, D., Mandel, T., & Kuhlemeier, C. (2000). Auxin regulates the initiation and radial position of plant lateral organs. *The Plant Cell*, 12(4), 507–518.
- Reinhardt, D., Pesce, E.-R., Stieger, P., Mandel, T., Baltensperger, K., Bennett, M., ... Kuhlemeier, C. (2003). Regulation of phyllotaxis by polar auxin transport. *Nature*, 426(6964), 255–260.
- Rhee, H. S., & Pugh, B. F. (2012). ChIP-exo method for identifying genomic location of DNA-binding proteins with near-single-nucleotide accuracy. *Current Protocols in Molecular Biology / Edited by Frederick M. Ausubel... [et Al.]*, Chapter 21, Unit 21.24.
- Rodriguez, K., Perales, M., Snipes, S., Yadav, R. K., Diaz-Mendoza, M., & Reddy, G. V. (2016). DNA-dependent homodimerization, sub-cellular partitioning, and protein destabilization control WUSCHEL levels and spatial patterning. *Proceedings of the National Academy of Sciences*, 113(41), E6307–E6315.
- Rogers, K. W., & Schier, A. F. (2011). Morphogen gradients: from generation to interpretation. *Annual Review of Cell and Developmental Biology*, 27, 377–407.

- Rowan, S., Siggers, T., Lachke, S. A., Yue, Y., Bulyk, M. L., & Maas, R. L. (2010). Precise temporal control of the eye regulatory gene Pax6 via enhancer-binding site affinity. *Genes & Development*, *24*(10), 980–985.
- Rupp, H. M., Frank, M., Werner, T., Strnad, M., & Schmülling, T. (1999). Increased steady state mRNA levels of the STM and KNAT1 homeobox genes in cytokinin overproducing *Arabidopsis thaliana* indicate a role for cytokinins in the shoot apical meristem. *The Plant Journal: For Cell and Molecular Biology*, *18*(5), 557–563.
- Sayou, C., Nanao, M. H., Jamin, M., Posé, D., Thévenon, E., Grégoire, L., ... Parcy, F. (2016). A SAM oligomerization domain shapes the genomic binding landscape of the LEAFY transcription factor. *Nature Communications*, *7*, 11222.
- Schoof, H., Lenhard, M., Haecker, A., Mayer, K. F. X., Jürgens, G., & Laux, T. (2000). The Stem Cell Population of *Arabidopsis* Shoot Meristems Is Maintained by a Regulatory Loop between the CLAVATA and WUSCHEL Genes. *Cell*, *100*(6), 635–644.
- Schulze, S., Schäfer, B. N., Parizotto, E. A., Voinnet, O., & Theres, K. (2010). LOST MERISTEMS genes regulate cell differentiation of central zone descendants in *Arabidopsis* shoot meristems. *The Plant Journal: For Cell and Molecular Biology*, *64*(4), 668–678.
- Scofield, S., Dewitte, W., Nieuwland, J., & Murray, J. A. H. (2013). The *Arabidopsis* homeobox gene SHOOT MERISTEMLESS has cellular and meristem-organisational roles with differential requirements for cytokinin and CYCD3 activity. *The Plant Journal: For Cell and Molecular Biology*, *75*(1), 53–66.
- Scofield, S., Dewitte, W., & Murray, J. A. (2014). STM sustains stem cell function in the *Arabidopsis* shoot apical meristem and controls KNOX gene expression independently of the transcriptional repressor AS1. *Plant Signaling & Behavior*, *9*. Retrieved from <https://www.ncbi.nlm.nih.gov/pubmed/24776954>
- Sinha, N. R., Williams, R. E., & Hake, S. (1993). Overexpression of the maize homeobox gene, KNOTTED-1, causes a switch from determinate to indeterminate cell fates. *Genes & Development*, *7*(5), 787–795.
- Skene, P. J., & Henikoff, S. (2015). A simple method for generating high-resolution maps of genome-wide protein binding. *eLife*, *4*, e09225.
- Small, S., Blair, A., & Levine, M. (1992). Regulation of even-skipped stripe 2 in the *Drosophila* embryo. *The EMBO Journal*, *11*(11), 4047–4057.

- Spitz, F., & Furlong, E. E. M. (2012). Transcription factors: from enhancer binding to developmental control. *Nature Reviews. Genetics*, *13*(9), 613–626.
- Steeves TA, S. I. (1989). *Patterns in Plant Development: Shoot Apical Meristem Mutants of Arabidopsis thaliana*. New York: Cambridge Univ Press.
- Struhl, G., Struhl, K., & Macdonald, P. M. (1989). The gradient morphogen bicoid is a concentration-dependent transcriptional activator. *Cell*, *57*(7), 1259–1273.
- Szemenyei, H., Hannon, M., & Long, J. A. (2008). TOPLESS mediates auxin-dependent transcriptional repression during Arabidopsis embryogenesis. *Science*, *319*(5868), 1384–1386.
- ten Hove, C. A., Lu, K.-J., & Weijers, D. (2015). Building a plant: cell fate specification in the early Arabidopsis embryo. *Development*, *142*(3), 420–430.
- Tony Ip, Y., Park, R. E., Kosman, D., Bier, E., & Levine, M. (1992). The dorsal gradient morphogen regulates stripes of rhomboid expression in tile presumptive neuroectoderm of the Drosophila embryo. *Genes & Development*, *6*, 1728–1739.
- Vatén, A., Dettmer, J., Wu, S., Stierhof, Y.-D., Miyashima, S., Yadav, S. R., ... Helariutta, Y. (2011). Callose biosynthesis regulates symplastic trafficking during root development. *Developmental Cell*, *21*(6), 1144–1155.
- Vernoux, T., Besnard, F., & Traas, J. (2010). Auxin at the shoot apical meristem. *Cold Spring Harbor Perspectives in Biology*, *2*(4), a001487.
- Werner, T., Motyka, V., Laucou, V., Smets, R., Van Onckelen, H., & Schmülling, T. (2003). Cytokinin-Deficient Transgenic Arabidopsis Plants Show Multiple Developmental Alterations Indicating Opposite Functions of Cytokinins in the Regulation of Shoot and Root Meristem Activity. *The Plant Cell Online*, *15*(11), 2532–2550.
- Werner, T., & Schmülling, T. (2009). Cytokinin action in plant development. *Current Opinion in Plant Biology*, *12*(5), 527–538.
- Wolpert, L. (1969). Positional information and the spatial pattern of cellular differentiation. *Journal of Theoretical Biology*, *25*(1), 1–47.
- Wong, C. E., Singh, M. B., & Bhalla, P. L. (2013). Spatial expression of CLAVATA3 in the shoot apical meristem suggests it is not a stem cell marker in soybean. *Journal of Experimental Botany*, *64*(18), 5641–5649.

Xu, C., Liberatore, K. L., MacAlister, C. A., Huang, Z., Chu, Y.-H., Jiang, K., ... Lippman, Z. B. (2015). A cascade of arabinosyltransferases controls shoot meristem size in tomato. *Nature Genetics*, *47*(7), 784–792.

Yadav, R. K., Perales, M., Gruel, J., Girke, T., Jönsson, H., & Reddy, G. V. (2011). WUSCHEL protein movement mediates stem cell homeostasis in the Arabidopsis shoot apex. *Genes & Development*, *25*(19), 2025–2030.

Yadav, R. K., Perales, M., Gruel, J., Ohno, C., Heisler, M., Girke, T., ... Reddy, G. V. (2013). Plant stem cell maintenance involves direct transcriptional repression of differentiation program. *Molecular Systems Biology*, *9*, 654.

Yadav, R. K., Tavakkoli, M., & Venugopala Reddy, G. (2010). WUSCHEL mediates stem cell homeostasis by regulating stem cell number and patterns of cell division and differentiation of stem cell progenitors. *Development*, *137*(21), 3581–3589.

Yanai, O., Shani, E., Dolezal, K., Tarkowski, P., Sablowski, R., Sandberg, G., ... Ori, N. (2005). Arabidopsis KNOXI proteins activate cytokinin biosynthesis. *Current Biology: CB*, *15*(17), 1566–1571.

Zhao, Y. (2008). The role of local biosynthesis of auxin and cytokinin in plant development. *Current Opinion in Plant Biology*, *11*(1), 16–22.

Zhao, Z., Andersen, S. U., Ljung, K., Dolezal, K., Miotk, A., Schultheiss, S. J., & Lohmann, J. U. (2010). Hormonal control of the shoot stem-cell niche. *Nature*, *465*(7301), 1089–1092.

Zhou, Y., Liu, X., Engstrom, E. M., Nimchuk, Z. L., Pruneda-Paz, J. L., Tarr, P. T., ... Meyerowitz, E. M. (2014). Control of plant stem cell function by conserved interacting transcriptional regulators. *Nature*, *517*(7534), 377–380.